A Strong Motion Network in the city of Chania: Analysis and presentation of results in a GIS environment.

Ένα δίκτυο επιταχυνσιογράφων στην πόλη των Χανίων: Ανάλυση και παρουσίαση των αποτελεσμάτων σε περιβάλλον GIS.

By

Georgios Chatzopoulos

Student ID: MTF4

Dissertation submitted in partial fulfilment for the degree of

Master of Science

2018

Abstract

Crete Island (Greece), located in the front of the Hellenic subduction zone, is in continuous need of seismic monitoring. Aiming increasing seismic readiness and provide more knowledge-information to citizens and civil protection authorities, the Hellenic Seismological Network of Crete (HSNC) started operating a permanent strong ground motion (SGM) network in the urban environment of Chania and its southern basin. The network is equipped with sensors as that of Trimble's Reftek 130 along with the Satways' GSense 16bit ones aiming to build a dense network with increased spatial resolution in the monitoring area. The SGM sensors monitoring capabilities, the network topology and the geological characteristics in the installation sites are presented. In the test period 2015-2017, one of our intentions was to investigate the seismic amplification in Chania basin which covers the contemporary part of the city, the Venetian old town and the fast-developing southern basin. Spectral ratio techniques have been used on ambient noise (H/V) and seismic signal (RF) to provide supplementary information for the local site conditions in station locations. Analysis of the strong motion data enables us to calculate the peak ground acceleration and present it in a GIS environment. Different interpolation techniques have been tested. The results support the importance of use of low cost Urban SGM sensors to enhance civil protection activities.

Περίληψη

Η Νήσος Κρήτη (Ελλάδα) που βρίσκεται στο μέτωπο της Ελληνικής ζώνης υποβύθισης, είναι υπό την ανάγκη για συνεχώς σεισμική παρακολούθηση . Το Ελληνικό σεισμολογικό δίκτυο της Κρήτης έχοντας ως στόχο να αύξηση την σεισμική ετοιμότητα και να παρέχει γνώση -πληροφορία στην πολιτική προστασία και τους πολίτες, ξεκίνησε να λειτουργεί ένα μόνιμο δίκτυο επιταχυνσιογράφων στο αστικό περιβάλλον των Χανίων και στην νότια ιζηματογενές λεκάνη. Δίκτυο είναι εξοπλισμένο με αισθητήρες Reftek 130 της Trimble καθώς και τους 16bit GSense της Satways με στόχο να δημιουργηθεί για την περιοχή ερευνάς ένα πυκνό δίκτυο με αυξημένη διακριτική ικανότητα. Παρουσιάζονται οι δυνατότητες καταγραφής των επιταχυνσιογράφων, η τοπολογία του δικτύου και τα γεωλογικά χαρακτηριστικά στις θέσεις των σταθμών. Στην δοκιμαστική περίοδο 2015-2017, μια από τις προθέσεις μας ήταν να μελετηθεί η σεισμική απόκριση του εδάφους στην λεκάνη των Χανίων η οποία καλύπτει το σύγχρονο αστικό κομμάτι, την Βενετσιάνικη παλιά πόλη και την ταχέως αναπαυόμενη νοτιά λεκάνη. Τεχνικές βασισμένες σε φασικούς λογούς χρησιμοποιήθηκαν σε μικροθορύβου (H/V) και σεισμικό σήμα (RF) με σκοπό να παρέχουν πληροφορίες για τις τοπικές εδαφικές συνθήκες στις θέσεις των σταθμών. Η ανάλυση των δεδομένων των επιταχυνσιογράφων επιτρέπει των υπολογισμό την μέγιστης εδαφικής επιτάχυνσης καθώς και την παρουσίαση της σε περιβάλλον GIS. Δοκιμάστηκαν διάφορες τεχνικές παρεμβολής. Τα αποτελέσματα υποστηρίζουν την χρήση του χαμηλού κόστους επιταχυνσιογράφων στο αστικό δίκτυο επιταχυνσιογράφων τα με σκοπό την ενίσχυση των δραστηριοτήτων για την προστασία του πολίτη.

Acknowledgment

We acknowledge support of this thesis by the project “HELPOS - Hellenic Plate Observing System” (MIS 5002697) which is implemented under the Action “Reinforcement of the Research and Innovation Infrastructure”, funded by the Operational Programme "Competitiveness, Entrepreneurship and Innovation" (NSRF 2014-2020) and co-financed by Greece and the European Union (European Regional Development Fund)

To Be Pleased

I would like to thank my supervisor Professor of Technical Institute of Crete and UNESCO Chair holder in “Solid Earth Physics and Geohazards Risk Reduction F. Vallianatos for the knowledge, experience, time and the financial support in my research. My second supervisor Dr. Ilias Papadopoulos from university of West Indies, who had the original idea to create a SGM network in Chania urban environment, for his knowledge, time, ideas and advices in this project. Dr. Maria Kouli from Technical Institute of Crete for her help, knowledge in the interpolation procedures. The research director from Institute of Geodynamics of National Observatory of Athens Dr. Georgios Drakatos for accepting to become my external examiner. Last but not least my family member Despoina and Menelaos as well as my friends for being always there for me.

Table of Contents

1 Introduction

1.1 Motivation and development of SGM network

The city of Chania (Crete, Greece) is an area with an attractive natural environment along with plenty cultural monuments. Due to its unique geotectonic setting, located at the seismically active front of Hellenic subduction zone, it is in continuous need of seismic monitoring. The broader tectonic active area of South Aegean has been a study case for subduction seismicity with significant results (McKenzie 1972, Le Pichon and Angelie, 1979, Papazachos B 1990, Papazachos C and Nolet G 1997 for eg.). Aiming to increase seismic readiness and provide more knowledge-information to civil protection authorities, the Hellenic Seismological Network of Crete (HSNC) started operating a permanent Strong Ground Motion (SGM) network in the urban environment of Chania and its southern basin. The main idea of this research was to create a dense grid of accelerometers that will record the ground motion in different geological formations during an earthquake. After a short analysis, the results of ground shaking are going to be presented in easy to understand peak ground acceleration maps (the color scale indicates the increase of ground shaking so that people who are not familiar with the subject could interpret the map) constructed with an interpolation technique. The sensors record the ground motion in continuous mode and the full waveforms and metadata are stored in servers back in HSNC headquarters. The first six SGM sensors (ATEI, LENT, PASK, PERI, G0LD, ABEA) were fully installed in 2015, initially as an experimental project, aiming to set up a dense SGM network to monitor the ground motion in a thick sedimentary basin with different stiffness materials. In the beginning, there was a period with no significant events or events located far from Chania and the network didn't record any satisfactory data set. In a second phase started early in 2016, a considerable number of events near the vicinity of the SGM network produced some satisfying results which motivated us to maintain the network, increase spatial resolution and expand it. Gradually, more sensors were added to provide better spatial resolution reaching the number of 14 stations. During the expansion of the SGM network the necessity to monitor locations of high economic impact arose. Examples are the Souda Harbor and areas with cultural monuments such as the Grand Arsenal in Venetian old port in the northern part of Chania. In addition, during the test period 2015-2017, one of the intentions was to investigate the site amplification in the location of SGM stations in Chania basin which covers the contemporary part of the city, the Venetian old town and the fast-developing Southern basin.

1.2 Types of monitoring instruments

In Geophysics, Civil Engineering and other earth related studies there are many ways to measure, report and describe the ground motion. Aiming to satisfy the monitoring needs, a variety of different types of sensors has been designed for the various seismological applications. The ground shaking analysis depends on the recording capabilities of the sensor and the provided raw information is reported with different units. Most of the modern seismological instruments use electromagnetic sensors, relay on Faraday's Law of electromagnetic induction: "*whenever a conductor is placed in a varying magnetic field an electromotive force is induced*" to measure the ground motion and through a digitizer the produced EMF (electrical voltage) is translated into the appropriate records. For example, if the recording instrument is a seismometer (figure 1.1a) the reported units are shown as meter per second because this device is measuring the ground velocity, if the sensor is an accelerometer (figure 1.1b) then it records the changes in ground velocity and the output values are in meter per square second or in units of $\boldsymbol{g}$ where 1 $\boldsymbol{g}$ = 9.81 m/s².

Figure 1.1. Some common used seismological sensors: a)broadband seismometer (Guralp 3ESPC - http://www.guralp.com/products/instruments/guralp-3-series), b) accelerometer with digitizer (Ref Tek 130SM - http://www.reftek.com/ref-tek-130-smhr-24-bit-strong-motion-accelerograph/)

There are other types of seismological sensors, such as the creepmeters used for monitoring the crustal deformation by measuring the changes in the distance on opposite sides of a fault. Another type of instruments are the strainmeters which monitor the stain changes inside boreholes. Reguarding the sensors report units, it is possible to use differentiation or integration equations to change the raw data from one form into another but usually it is avoided due to the possible errors that could occurr during the signal conversion processing, especially in cases

where high noise values exist. In this thesis, the main instruments that have been used are accelerometers installed permanently in various locations in the city of Chania. In some cases seismometers are used for supplamentary information.

1.3 Ground Parameters

Historically the measurement of earthquake parameters, such as magnitude and intensity, started in the end of 19th century where the Italian Michele Stefano Conte de Rossi and Swiss François-Alphonse Forel developed the first earthquake intensity scale based on perceptiveness of earthquakes by humans. The scale was used to measure the impact of earthquakes on humans and buildings, and for the same earthquake varies depending on the distance from the earthquake. In 1902, the Italian volcanologist Giuseppe Mercalli modified the Rossi–Forel scale and added two intensity levels to make the well-known Mercalli intensity scale (Tiedemann,1992) which was later modified by Harry O. Wood and Frank Neumann (Wood and Neumann, 1931) to the Modified Mercalli Intensity scale (MMI). In 1935 the American seismologist Charles Francis Richter along with the contribution of the American seismologist Harry O. Wood presented the very well-known (and still in use today) local magnitude scale (Richter, 1935). This scale is intended to measure the energy released by an earthquake and assigns a unique value to an earthquake. The main aspect of the new instrumental scale is that it uses the recorded values of the seismic wave amplitudes at stations in different distances to express the magnitude of an earthquake while the existing intensity scales were related to the description of the macroseismic phenomena. Although the new proposed Richter scale is a quantitative scale determining the magnitude of an earthquake, there is no direct relationship connecting it with ground acceleration, while the existing empirical scales oriented by the earthquake effects, such as the Mercalli can empirically correlated with ground acceleration.

Modern ground motion sensors are equipped with 3 components to record the complete movement of the ground in a tri-axial orthogonal system. For convenience usually, we align and orientate the sensor in a way that one component is vertical to the ground, and the two horizontal components are aligned with the true North-South and East-West direction. One of the most widely used parameters in earthquake signal processing is the **Peak Ground Acceleration (PGA**), which is simply defined as the largest absolute value of acceleration of an earthquake (figure 1.2), recorder in one of the three components at the specific location of observation (Douglas, 2003).

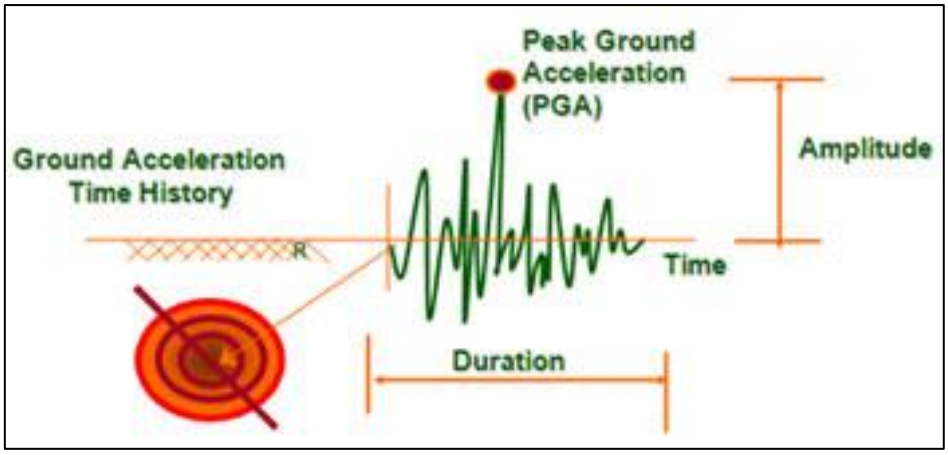

Figure 1.2 The peak ground acceleration is the largest absolute acceleration amplitude.
Image from: https://www.geospatialworld.net/article/earthquake-disaster-management-using-gis-and-probabilistic-risk-assessment/

If the reported acceleration is the mean value of the two horizontal dimensions then the results is known as **Peak Horizontal Acceleration (PHA).** In case the recorder is a seismometer the aforesaid parameter described is the **Peak Ground Velocity (PGV)** and the **Peak Horizontal Velocity (PHV**) Two very commonly used parameters especially by civil engineers, are the **Arias intensity (I_A)** which is the time-integral of the square of the ground acceleration proposed by Arturo Arias (1970) and the **Vs30** proposed by Borcherdt and Glassmoyer (1992) which is the average **shear** wave velocity of the top 30m.

In the beginning of the 21st century, U.S. Geological Survey Earthquake Hazards Program, developed a software known as **ShakeMap** to create automated PGA distribution maps in near real time after significant events, in order to rapid estimate the potential damage, help civil protection agencies quick respond and start the recovery procedures as well as for public information. Generating shakemaps requires some ground motion parameters such as the PGA and PGV values. Additionally, the USGS' software combines the ground motion parameters with information as that of geological formations, site amplification, empirical ground-motion prediction relations to estimate the ground motion values in areas without measurements. In the present thesis the shakemaps that are presented have been created with the ArcGIS software (https://www.esri.com/en-us/home) following a similar philosophy with USGS' ShakeMap. There are some anthropogenic or atmospheric disturbances cause some very low amplitude vibrations known as **ambient noise or microtremors.** Although this small-scale shaking exists continuously, it is not perceptive by living organisms and seismological instruments are required to record it. There are a lot of possible sources responsible for these microtremors, a simple categorization is to separate them in non-anthropogenic such as the sea waves, tides,

atmospheric processes, small earthquakes and other geological motions and anthropogenic oriented, including all human made motion. The nature of ambient noise was a debate for many years, a considerable number of researchers hypothesized that the microtremors are from body while other support the idea that they are mainly consisted by surface waves which is probably the most acceptable theory (Aki, 1957, Akamatsu, 1961, Nogoroshi and Igarashi, 1970, 1971, Udwadia and Trifunac, 1973, Irikura and Kawanaka, 1980 and others). Long term ambient noise monitoring in the three gulfs of Tokyo (Kamura, 1997), Kobe (Seo et al., 1996, Seo, 1997), and Fukui (Seo, 1998) has shown that:

- The low frequencies ambient noise (from 0.3 up to 0.5 Hz), is generated by distant sea waves possibly correlated to meteorological disturbances in oceans.
- The moderate frequencies (from 0.3-0.5 up to 1 Hz), where the ambient noise is produced by near sea waves and the wind.
- Above 1 Hz where the ambient noise is mainly created by human activities.

The microtremor recordings are commonly used for microzonation surveys and site geotechnical characterization. The two common defined parameters with this method, using spectral ratio techniques are the ground's predominant **frequency f_0** and the respective **amplitude A_0** (or the frequencies f_1, f_2… and the corresponding amplitudes A_1, A_2… if there are more than one (Sesame 2004)). A considerable group of scientists (Field and Jacob, 1993, Lachet και Bard, 1994, Lermo and Chavez-Garcia, 1994a, Dravinski et al., 1996, Wakamatsu and Yasui, 1996, Al Yuncha and Luzon, 2000, Fah et al,. 2001, Maresca et al., 2003 and others) have proved that the microtremors can be used to accurately obtain the resonance frequency of the geological formation while amplitude can be considered as the lowest threshold of site amplification (Haghshenas et al. 2008). In this research project the resonance frequency and amplitude of the different geological formations at the station locations have been examined with different spectral ratio techniques.

1.4 Area of Study

1.4.1 Geology of Crete

The Crete Island is located in the southern part of Greece, covering an area about 8336 km^2, which makes it one of the largest islands in the Mediterranean Sea. The island's main morphological features are the wide coastlines and the high mountain range with East-west

direction. The area of interest is the city of Chania in the northwestern part of Crete. It is possible to consider Crete Island as one of the most important geological museum of Europe, because it has tectonic, geologic and morphologic features which are considered as historical reflections of the Hellenic orogenetic process. The geology of Crete, can be characterized as a complex structure consisted by continuous nappe units (figure 1.3), developed from different stress fields that acted since upper Oligocene-Miocene. The driving forces that formed Crete's geological structure are the tectonic plates collision, more specific the subduction of the Mediterranean plate under the Aegean plate (McKenzie, 1972; Le Pichon and Angelier, 1979) which placed the extensive tectonic nappes on Plattenkalk limestone of the Talea Ori unit (Mountrakis, 1986; Kilias, et al., 1999). and is considered as the lowest tectonic unit. A synoptic description of the tectonic units of Crete from lower to upper formations:

1. Plattenkalk unit (PK), consisted by a sequence with schist type rocks on the base followed by thick and fine grained shallow sea carbonates such as limestones and dolomites, with clastic silicate layers while in some cases, there are thin layers of phyllite. The age of the whole unit is estimated upper Paleozoic (Permian) on base and Eocene/Oligocene to the top of the unit, where there is a meta-flysch layer (Epting, et al., 1972; Fytrolakis, 1980).

2. Tripalion unit (Trp) is a heterogenous recrystallized geological formation mainly exposed in western part of Crete. In the lower part of this unit there are white marbles, recrystallized limestones from Jurassic period while in the upper part there is a breccia mix of limestones and dolomites (Kopp, & Ott, 1977).

3. Phyllite- Quartzite (Ph-Q) tectonic nappes, are composed with Paleozoic to Triassic age rocks such as phyllites, quartzites metasandstone, metabreccia, recrystallized limestones and metabasites with various thickness from few meters to hundreds of meters (Creutzburg & Seidel, 1975; Seidel, 1978; Krahl, et al., 1983).

4. Gavrovo-Tripoli unit (Tr), mainly consisted by carbonate sediments, limestones and sometimes dolomites. The sediments are dated from upper Triassic to Eocene and the last layer of this unit is an Oligocene flysch. (Zager, 1972; Creutzburg & Seidel, 1975).

5. Pindos tectonic nappes (Pi) can be found over Tripolis unit, usually with tectonic contact but sometimes it is possible to find it on Ph-Q unit. The nappes typically have deep sea sediments (marine limestones, radiolarites, clays and flysch) formed during the period between Triassic to Paleogene – Eocene without signs of metamorphosis. (Siedel, 1971; Bonneau & Fleury, 1971)

6. Series of three tectonic nappes of Arvi, Miamou, Vatou (Ar, Mia, Va) are deep sea sediments dated Jurassic to Cretaceous age (Bonneau, et al., 1974; Bonneau & Lys, 1978) as well ophiolitic crystalline type rocks such as basalts diabases (Siedel, et al., 1977; Bonneau & Lys, 1978)

7. Asterousia (Ast) tectonic nappe is a mix of metamorphic rocks such as amphibolites, gneisses, quartzites, marbles and schists (Creutzburg & Seidel, 1975; Siedel, et al., 1981).

8. Ophiolites tectonic nappes (Oph), they are mostly serpentinized peridotites with the relative sediments which are remains of an old ocean floor (Siedel, et al., 1981)

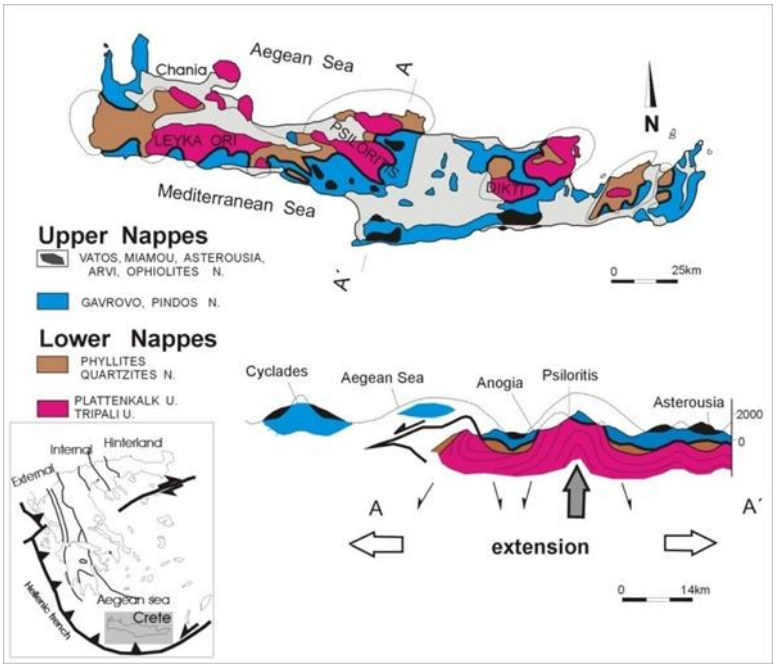

Figure 1.3 Depict of geologic units of Crete island (Killias et al.,1994, Mountrakis et al., 2004)

1.4.2 Geological formations of Chania

The research area, Chania city and its southern basin, as it is illustrated in Mountrakis (2004) geological map (figure 1.4), has as bedrock formations the thick dark grey color Plattenkalk limestones and the Tripalion white-grey thick recrystallized limestones and marbles. Both of these bedrock formations can be found either south of Chania basin on the Lefka Ori mountain range reviled as geological window or in the northeast part of Chania in Akrotiri peninsula. In the middle area between the bedrock outcrops there are Neogene and Quaternary deposits. The Neogene sediments, from east to west, are visible in a wide part in the Akrotiri peninsula up to the east part of Chania city and in the foot of Lefka Ori mountain range, mainly consisting of marles, sandstones and limestones. In the Neogene limestones in Akrotiri, there are places with

karstic weathering that forms terra rossa soils. Within the city limits there are Neogene sediments, in the east part marles and in the most west part are marles with sandstones and white-yellow limestones. The final and the wider part of the research area, is the Chania southern basin which is covered with Quaternary alluvial loose deposits such as sands clays and gravels with considerable thickness (discussed on next chapter).

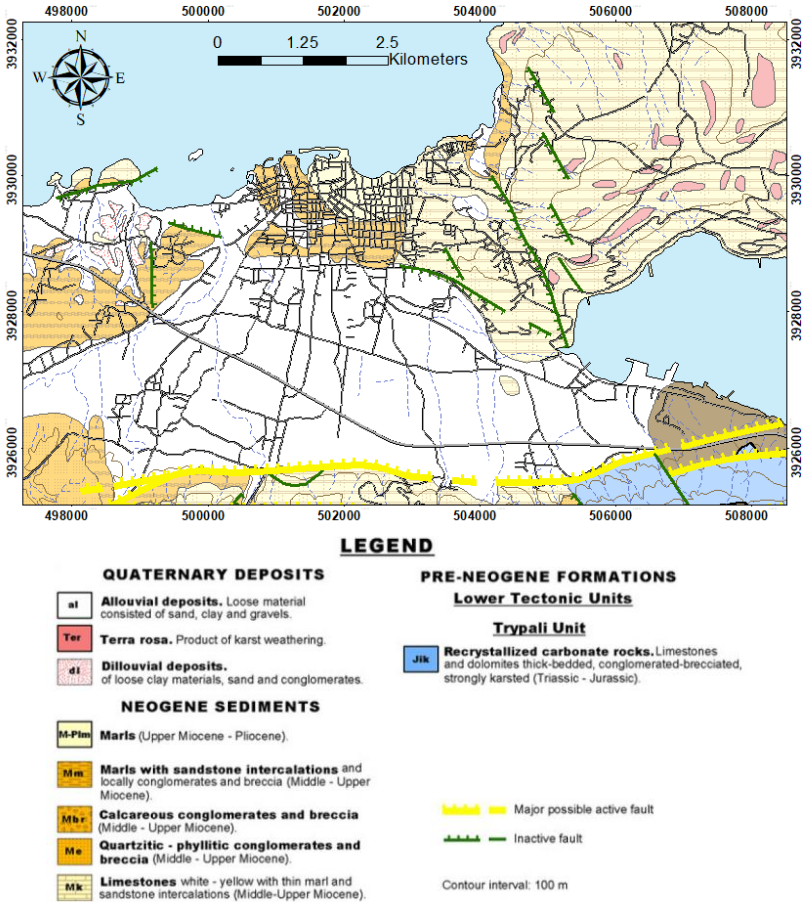

Figure 1.4 The geological formation of Chania city and the southern basin(up) as well as the corresponding legend(bottom) (Mountrakis, 2012).

2 The Strong Ground Motion Network

2.1 Monitoring instruments

Studies in the complex geological setting of the Chania basin (Athanasopoulos and Pelekis 2000, Bastelli 2002, Mastrolorenzo 2004, Sarris et al. 2005, Mountrakis et al. 2012, Papadopoulos et al. 2017), where the Neogene and Quaternary sediments have been deposited on the recrystallized carbonates of Tripalion unit, as well as the information provided by 24 water boreholes (maximum drill depth 150m) show that there is an extensive thickness of alluvial sediments, with a maximum estimated thickness of 144 meters on the Quaternary

deposits (Papadopoulos et al. 2017). Aiming to monitor the different geological formations, a dense strong ground motion network started operating in the Chania broader basin area as well as the crucial parts of the urban area and the old Venetian town. Initially the HSNC had in its disposal two types of accelerometers with similar recording capabilities, the Trimble's Ref Tek 130 ANSS/02 and the 130 SM (http://www.reftek.com/ref-tek-130-smhr-24-bit-strong-motion-accelerograph/). The available sensors were utilized in the area of interest, with sampling rate at 250Hz, aiming to provide a detailed information about the ground motion during earthquakes. The initial results of the SGM network, since the first phase with only six stations, suggested that the sensor grid should be denser to provide better spatial resolution. Aiming to enhance the resolution of the results, the HSNC installed all the available REF TEK accelerometers and afterwards it started using the low-cost Satways' GSense micro electro-mechanical systems (MEMS) sensors. This cost-effective choice made the SGM network capable to provide better spatial resolution. Additionally, the GSense sensors have some advantages that helped solve several installation problems. An example is the Grand Arsenal building in old Venetian port area, where the installation of an exterior GPS antenna would disrupt the appearance of the monument so the choice of using a GSense sensor with GPS antenna that can work indoors, was the best solution. Here follows a short presentation of the accelerometers and their specifications:

2.1.1 Trimble's Ref Tek 130-ANSS/02

The first type of instrument used in strong ground motion network is a reliable 24bit integrated tri-axial accelerometer which is a robust and compact recorder for collecting seismological data used for monitoring local, regional and global scale earthquakes. This accelerometer is used in three of the SGM network stations (DEYA, MULT and PERI). The REF TEK 130- ANSS/02 is presented in figure 2.1a, the instrument has the tri-axial sensor 0131 – 02/03/I on the bottom lid that works with ±6.9V full scale voltage and has ±3.5g clip level. On the upper lid it is equipped with four boards, each one assigned for different module: connectivity, A/D convert, data process and storage. The available cable connectors for power, GPS cable, internet and serial port are placed on the top of the upper lid along with an informative LCD screen. The case is made of anodized aluminum and it is water sealed with IP 67 rating. The recorder offers many configurable options on data acquisition, e.g. channel selection, sample rate, trigger mode, storage destination among others. The configuration of the accelerometer can be managed with a palm computer on site through the control port (serial) or it can be done

remotely with the Reftek's software RTCC (REF TEK Command and Control suite) if there is an internet connection.

2.1.2 Trimble's Ref Tek 130-SM

The majority of SGM network is equipped with the next generation model of ANSS/02, the REF TEK 130 SM which has the same features with previous model and some improvements. One of the important upgrades of 130 SM is the use of the REF TEK 130-01 digitizer board, which is used on the REF TEK 130 DAS, the third-generation seismic recorders produced by the aforesaid company (http://www.reftek.com/). At the same time, a new improved tri-axial sensor is equipped which is a low-noise force-feedback model, the 131-8019 that works on full scale in range >±3.5g with ±10V full scale voltage. The available connectors on the top of accelerometer's lid are the same with the ANSS/02, the only addition is an extra connector that provides 3 relays for external alarm notifications. The body material and inner structure of the instrument remains unchanged. A noticeable change is in the size of 130 SM outer protective case, which is considerably taller than the previous model, almost double the height. The reason behind this change is so it can keep an internal 12V battery inside (figure 2.1b). The extra battery is used for back up purposes, if for some reason the standard power supply fails the sensor will keep working for more than 48 hours. An alternative use for the internal battery feature is to use the accelerometer as portable device for monitoring aftershock sequences or to be used on similar studies.

2.1.3 Satways' GSense

The GSense are the Satways Ltd. (http://www.satways.net/) low cost 16bit tri-axial accelerometer installed in stations ATIK, ARSN and MAIC. The outside case material is made by hard metal and in the lid, there is a rubber flange to make it water-humid resistant with IP 65 rate (figure 2c). The internal MEMS accelerometer works on full scale range ±2g with typical 3.3V. The G-sense works with Raspberry Pi Linux board, it has some basic tools and options such as configure the sampling rate. The time accuracy is achieved through NTP server or/and with an external GPS antenna, which is very small compared to REF TEK's one, and it can also work indoors in some cases with very good results (accuracy error <0.02msec). The system sent mSEED data through a Seiscomp 3 seedlink service and there is OpenVPN option for cases where the network IP is dynamic.

Figure 2.1 a, b, c. The three types of accelerometer installed for the SGM network, the Ref Tek 130 ANSS/02(left) the 130 SM (middle) and the GSense (right)

2.2 The Strong Ground Motion Stations

Installing the strong motion network in the urban environment of Chania meant facing several difficulties and make some important decisions based on the available location options. Each station should comply with certain specifications e.g. to be placed on the different geological formations in Chania basin as well as the crucial part of old town. Areas with low anthropogenic noise were preferred. Other important criteria are the constant power supply, internet access and the existence of good and undisrupted GPS signal. Choosing buildings that belong to municipality such as schools, museums and health centers ensured that there is a constant power supply and in most cases internet connection exists and is used to transmit the data. Additionally, installing the accelerographs inside the city buildings help to protect the sensors from the various weather conditions, although the instruments are closed watertight with IP65 and IP 67 waterproof factor. However, common practice and experience shows it is better to operate in relative stable environment. On the negative side, someone can argue that the city environment could affect the noise levels of the recorders and change the output of this process. The answer to these assumptions is that the SGM sensors are not as sensitive as the seismometers and so far, the obtained results show that the anthropogenic noise could mislead the analysis only in small magnitude earthquakes which is not the focus of this network. Upon completion of a station's installation, there was a testing phase, a period where the sensor was constantly monitored, aiming to check if the station was working as expected, with good signal to noise ratio and undisrupted data transfer. In some cases, there are some small pauses due to internet temporal problems, but all instruments are set to keep data in their internal memory, so the sensor sends the buffered data when connection is restored. All stations that pass the test period, are registered in the International Seismological Center (ISC) as permanent accelerometric stations of HSNC. A short description in alphabetical order of the SGM stations and location characteristics is presented below in Table 2.1 and in Figure 2.2. In the SGM

presentation below, the information related with the sediment thickness for the stations located in Quaternary deposits, has been extracted from the research of Papadopoulos et al. 2017.

Table 2.1 SGM station parameters.

Station	Latitude	Longitude	Sensor	Registered
ABEA	35.5162	24.0113	130-SM	YES
ARSN	35.5181	24.0206	GSENSE	NO
ATEI	35.5193	24.0431	130-SM	YES
ATIK	35.5144	24.0312	GSENSE	NO
DEYA	35.4825	24.014	ANSS/02	YES
G0LD	35.4955	24.0306	130-SM	YES
LENT	35.5074	24.0403	130-SM	YES
MAIC	35.4943	24.0491	GSENSE	NO
MULT	35.5091	24.0118	ANSS/02	YES
NERO	35.4739	24.0423	130-SM	YES
PASK	35.4996	24.0121	130-SM	YES
PERI	35.4825	23.9928	ANSS/02	YES
POLY	35.5226	24.0602	130-SM	YES
SOUD	35.4878	24.0678	130-SM	YES

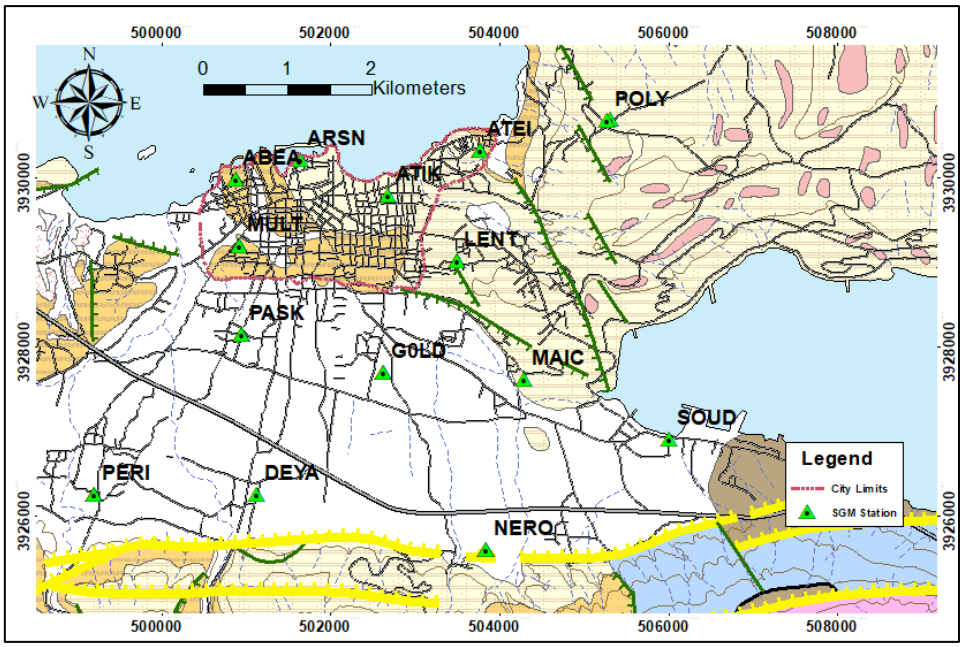

Figure 2.2 The SGM station locations in the different geological formation

2.2.1 SGM station ABEA

The accelerometer is installed on the relative new high school, inside the main theater-exhibition room which has a lot of free space and it is not used frequently (Figure 2.3). In this location, there was an old factory of olive oil and soap products named "*ABEA*". After the factory relocated out of the town, a portion of the soft soil materials such as marles with sandstones has been removed and substituted with concrete to reinforce the floor of the new school.

Figure 2.3 The ABEA station, the REF TEK 130-SM(left) and the GPS antenna (right)in the relative new high school building.

2.2.2 SGM station ARSN

The Grand Arsenal is the largest of the 17 shipping yards that were built during the Venetian occupation (1205–1669), its construction completed in 1600. (http://www.keppedih-cam.gr/politismos/xoroi-politsmoi/kentro-arxitektonikis-mesogeiou/184-ypodomes/kam/79-megalo-arsenali). In this area, the material is upper Neogene marles and a GSense (Figure 2.4) was placed in this location due to the advantage of installing the GPS antenna inside the building, which would not disrupt the external appearance of the monument.

Figure 2.4 The ARSN GSense sensor (left) in the Grand Arsenal (right).

2.2.3 SGM station ATEI

The instrument has been installed on the basement of the new building of the Chania Branch of the Technological Educational Institute of Crete, where UNESCO Chair on Solid Earth Physics & Geohazards Risk Reduction, Laboratory of Geophysics is located. The geological formation in this area is Neogene limestone and in the same location HSNCs CHAN station is installed, equipped with a broadband Guralp ESP 120 seconds seismometer.

Figure 2.5 The ATEI SGM station, the REF TEK 130-SM as well as the CHAN Guralp seismometer(left) and their GPS antennas(right).

2.2.4 SGM station ATIK

The station is installed in the basement of a Neoclassic historically listed as “Work of Art”, that belongs to the prefecture of Crete and nowadays is used as offices for public health directorate.(http://www.chania.eu/nax/old.nax.gr/indexdb5d.html?option=com_content&view=section&id=18&Itemid=133&lang=en). In this case a GSense sensor was considered as the best solution (figure 2.6), like ARSN station, to prevent the deterioration of the monument appearance. The geological formation in this location is consisted by marles.

Figure 2.6 The GSense sensor (left) of the ATIK SGM station in the Neoclassic building (right).

2.2.5 SGM station DEYA

Near small town Mournies, south of Chania and at the southern border of the Chania basin, are the offices of ΔΕΥΑΧ (DEYACH) which is the local water management authority. The accelerometer has been placed in the basement of the building in a not-very often used storeroom (figure 2.7). The surrounding area has 50-70m thick quaternary deposits

Figure 2.7 The DEYA station, the REF TEK 130-ANSS/02(left) and the GPS antenna(right).

2.2.6 SGM station G0LD

Very near to the Monastery of Chrissopigi, on a middle school building, a 130-SM sensor has been installed in the personal computer lab (figure 2.8) which was the quietest area in the school. Geologically, the materials in this location are quaternary deposits with an estimated thickness between 50 to 70m and the microtremor surveys in this area shows the largest amplitude values (will discussed in next chapter)

Figure 2.8 The G0LD SGM station, the installed REF TEK 130-SM (left)and the external GPS antenna(right).

2.2.7 SGM station LENT

Near the artificial water reservoir of Chania city which is in Lentariana -Agios Ioannis area, inside a state kindergarten a Ref Tek 130 SM sensor was installed. The SGM station in this area is placed on Neogene limestone sediments.

Figure 2.9 The LENT SGM station, the REF TEK 130-SM(left) and the GPS antenna(right).

2.2.8 SGM station MAIC

Aiming to enhance the spatial resolution in the central-eastern part of SGM network, between the stations LENT, G0LD and SOUD an instrument was installed in the Mediterranean Agronomic Institute of Chania (MAICH). The formation in this area is Neogene limestone and a Gsense sensor (figure 2.10) was placed in a non-often used storage room.

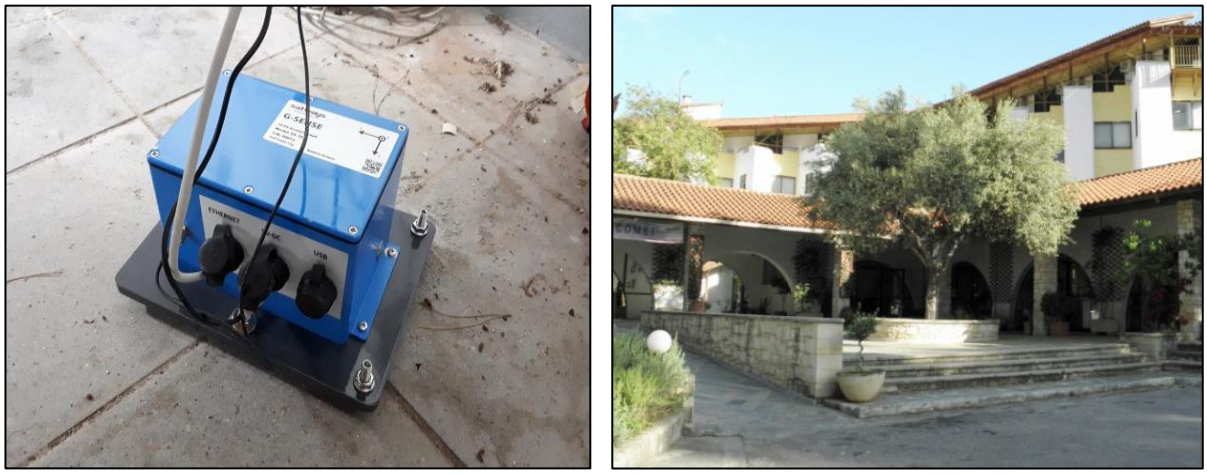

Figure 2.11 The installed GSense sensor (left) and the main entrance of Mediterranean Agronomic Institute of Chania (right).

2.2.9 SGM station MULT

A sensor 130-ANSS/02 has been placed in a school in Pachiana area in the main theatre room. The materials in this location are Neogene marles, marle-limestones and quaternary deposits. This school location is suitable cause the ground materials are similar with the ABEA station so the MULT sensor will provide additional information for the ground shaking of this formation as well as better spatial resolution near the city limits.

Figure 2.11 The MULT SGM station, the REF TEK 130-ANSS/02 and the GPS antenna

2.2.10 SGM station NERO

In Nerokourou village, near to the General Hospital of Chania, is the Museum of School Life, a contemporary museum with artifacts of school life from previous decades. The station is equipped with a 130-SM which is “hidden” inside a municipality banner so it will not interfere with the theme of the museum (figure 2.12). This building is in the edge of the quaternary basin with relative small alluvial deposits thickness. The outcrops in the museum yard and the geological map indicates that the bellow rock formation is Neogene limestones.

Figure 2.12. NERO station, the REF TEK 130-SM and the GPS antenna

2.2.11 SGM station PASK

In the Pasakaki area just a few minutes outside of the city limits, there is a school where a REF TEK 130-SM sensor was installed aiming to enhance the spatial resolution between the stations MULT and PERI. The whole area is in quaternary deposits with a considerable thickness.

Figure 2.13 The PASK station, the REF TEK 130-SM and the GPS antenna

2.2.12 SGM station PERI

The southwestern station of the SGM network is located on Perivolia village. The accelerometer is in the municipality building that is used for providing aid at home to people with special needs. The whole village is established on quaternary deposits with an estimated thickness between 40 to 50 meters.

Figure 2.14 The PERI SGM station, the REF TEK 130-ANSS/02 and the GPS antenna

2.2.13 SGM station POLY

In the beginning of the Akrotiri peninsula at the north side of Chania there is a high school which is built on Neogene limestones. A REF TEK 130-SM sensor is installed in this location. The school building is slightly outside the city limits and was chosen to be the northeast end of the SGM network.

Figure 2.15 The POLY SGM station, the REF TEK 130-SM and the GPS antenna

2.2.14 SGM station SOUD

Near to the natural harbor of Souda, which is used for passenger-ferry boats and the Crete Naval Base for Hellenic Navy and NATO forces, is a state kindergarten where a Ref TEK 130-SM was installed. This is an area with high economic impact for the Chania city. The surrounding materials in the southeastern SGM sensors are loose quaternary deposits.

Figure 2.16 The SOUD SGM station, the REF TEK 130-SM and the GPS antenna

2.4 Instrument installation and remote management

Most of the accelerometers are lightweight instruments, equipped with sensitive sensors aiming to monitor the ground velocity changes to the desired area. The first step to install an accelerometer in a "new" geologically suitable location is to check the power supply and the internet connection. The next step is to ensure that the sensors are recording accurately during an earthquake and they do not measure a tremor produced during an earthquake from the instruments shaking, so it is important to stabilize the accelerometers with the ground. The most common way to consolidate these instruments is to fasten them in the floor with a specialized concrete anchor bolt. Often at the bottom of the instrument there is an opening or a base designed for the stabilization. The instruments installed for SGM network have different kind of anchors but the principals are the same, a hole with appropriate diameter must be drilled on the ground in order to fit the wedge bolt (figure 2.17a). The accelerometers that have different sensors for each component (N-S, E-W, V) should be aligned appropriately with a GPS or a compass to always face the north direction. The last step before connecting the power cable, is to calibrate the accelerometer to be parallel with the ground with the help of an alignment bubble (figure 2.17b) and by adjusting the leveling screws (figure 2.17c).

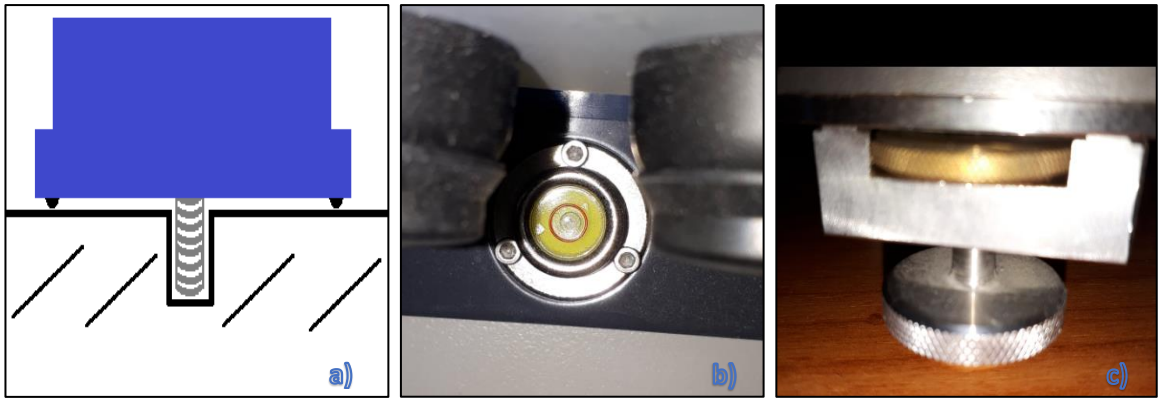

Figure 2.17 Securing the accelerometer to the ground through an anchor bolt (left) and the alignment blister (right) used for calibrating the sensor to be parallel with ground.

The sensor recording parameters can be set on site, with a Palm computer for REF TEK instruments and with a laptop for GSense ones, or it can be done remotely using internet connection if the instrument has the appropriate IP settings. All accelerometers are connected remotely to servers that gather the continuous recording of the ground motion. The REF TEK sensors must connect through UDP port 2543 to a workstation computer that has installed the Reftek Protocol Daemon (RTPD) software package. With a few words, the RTPD software provides communication with the DAS units (Ref TEK digitizers), data error-correction and

storage in archives. There are data clients for executing different jobs, inspecting the waveforms, setting the instrument parameters (figure 2.18) or connecting the RTPD with other servers with other software such as Seiscomp3 (http://www.seiscomp3.org/) and Earthworm (http://www.isti.com/products/earthworm/). Comparing the data transferring methods of two accelerometers, it is necessary for the Ref TEK sensors to send the packages to a specific RTPD server before the data could be shared to other different servers or applications. In a different manner, the GSense sensors broadcast the data with the use of the seedlink protocol to an assigned IP making the data available to all seedlink servers that are able to connect to the specific TCP IP, usually in port 18000 to gather the data. Also changing the parameters remotely in a GSense can achieved with a direct IP connection to the instrument (figure 2.19) rather than connect to the RTPD server and then to the instrument. An advantage of Ref Tek ones is that they don't require static IP and the GSense must use the OpenVPN service to broadcast the data to a virtual IP which is set in port 1194 in a workstation. For the needs of the SGM network, a new Seiscomp3 server with OpenVPN was built to collect the mSEED data from the GSense sensors.

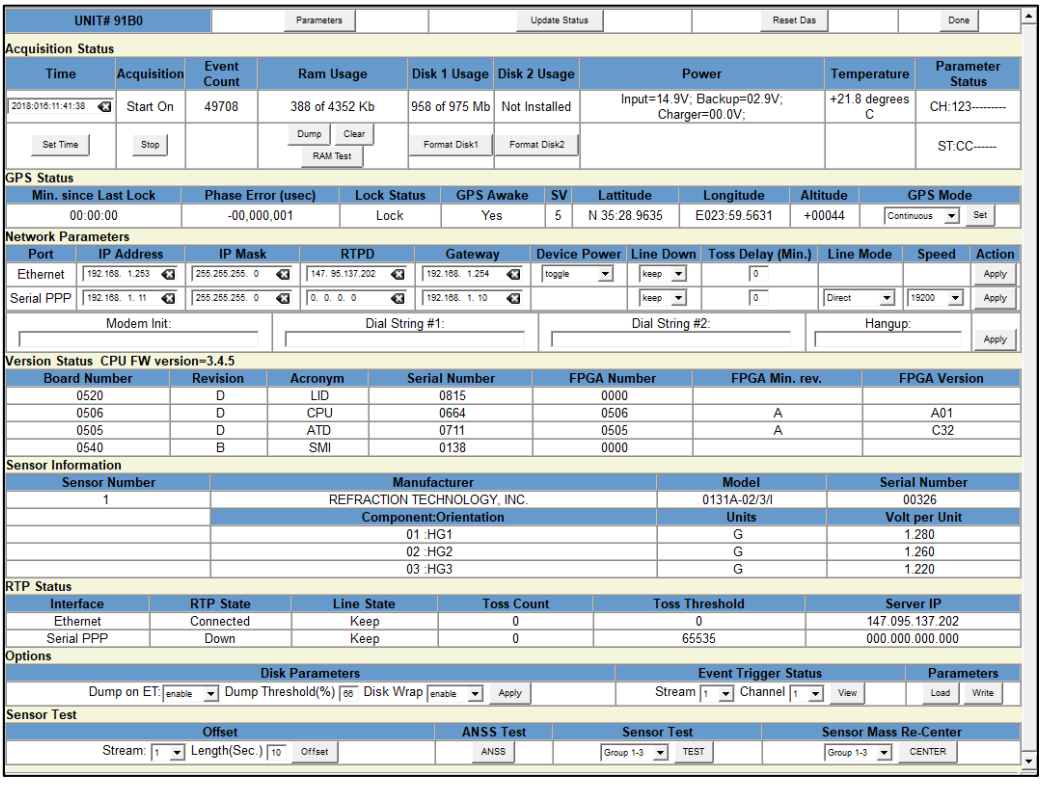

Figure 2.18 The RTCC data client that allows to change the Ref Tek sensor parameters through internet

Figure 2.19 The Gsense remote configuration software.

3 Site characterization using spectral ratio techniques

3.1 The HVSR method in ambient noise

A popular and easy to use technique in passive sources survey is the well-known single station Horizontal versus Vertical Spectral Ratio (HVSR) of ambient noise, proposed by Nakamura (1989). Although the microtremor surveys have been used for many years, a common procedure for data collection was not existed until lately. In 1998 Mucciarelli proposed a number of suggestions for taking optimal ambient noise measurements and two year later (2000) the European research project SESAME (Site EffectS assessment using AMbient Excitations, European Commission – Research Directorate-General, Contract No: EVG1-CT-2000-00026) started a series of experiments to test the different aspects of microtremors survey, such as the appropriate sensors, the suitable location for measurements and the influence of various parameters (weather, anthropogenic noise etc.). Papadopoulos et al. (2017) has performed a very detailed study of HVSR in most of the area of interest for this study. For comparison purposes we chose to perform new measurements at all locations of the strong ground motion network stations.

3.1.1 Microtremor recording instruments

Typically, the data collection can be achieved with a broadband seismometer, the choice of the sensor is depending on the resonance frequency of geological formation and the desired frequency band someone want to survey. Very broadband sensors need more time to reach equilibrium state while short period seismometers and accelerometers should be avoided in areas with resonance frequency less than 1 Hz (SESAME, 2004). The microtremor measurements in this study have been carried out with a *Lennartz Le3D/5s* seismometer (figure 3.1) (http://www.lennartz-electronic.de) which is suitable for this study since it has a natural period of five seconds, that is enough for the sediment thickness in the Chania basin and a damping factor between 0.707 and 1 (70.7–100% of critical damping) and flat response in velocity from 0.2 to 100Hz. The seismic signal is recorded with the lightweight and compact digitizer Leas City Shark II which is specially designed for ambient noise recordings (figure 3.2). The digitizer is inside a small case and the data are stored in a compact flash card. The LCD screen allows the user to customize the measurements and change available recording parameters in situ.

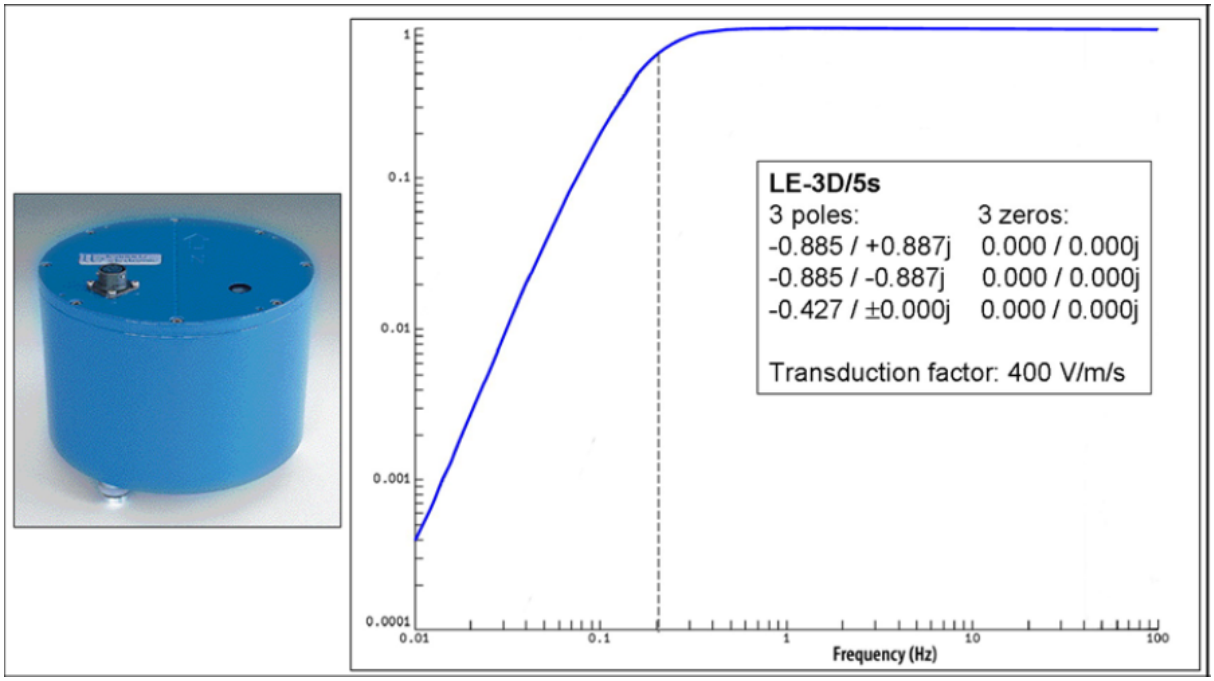

Figure 3.1 The Lennartz Le3D/5s sensor (left) and the frequency response curve (right)(http://www.lennartz-electronic.de).

Figure 3.2 The Leas City Shark II compact digitizer

3.1.2 Microtremor data recording and processing

Aiming to investigate the local site conditions of the strong ground motion station, every sensor location was considered as single site and as the SESAME H/V manual suggests, to derive an f_0 value for single site at least three different point measurements were performed at close distance (15-20 meters) from the installed accelerometer. In figure 3.3 is presented the microtremor single site survey for six different SGM stations (ABEA, DEYA, G0LD, NERO, PASK and SOUD), the blue diamond shape indicates the accelerometer location and with red circles are each of three measurement point. The same pattern for single site survey have been followed for the rest of SGM stations. The recording duration for every point was varying from 45 minutes to 1 hour and all measurements were performed during the night hours with low anthropogenic noise and with good weather conditions (no wind or rain). In most places, the measurements were repeated after a time of 3-4 months to verify the obtained results.

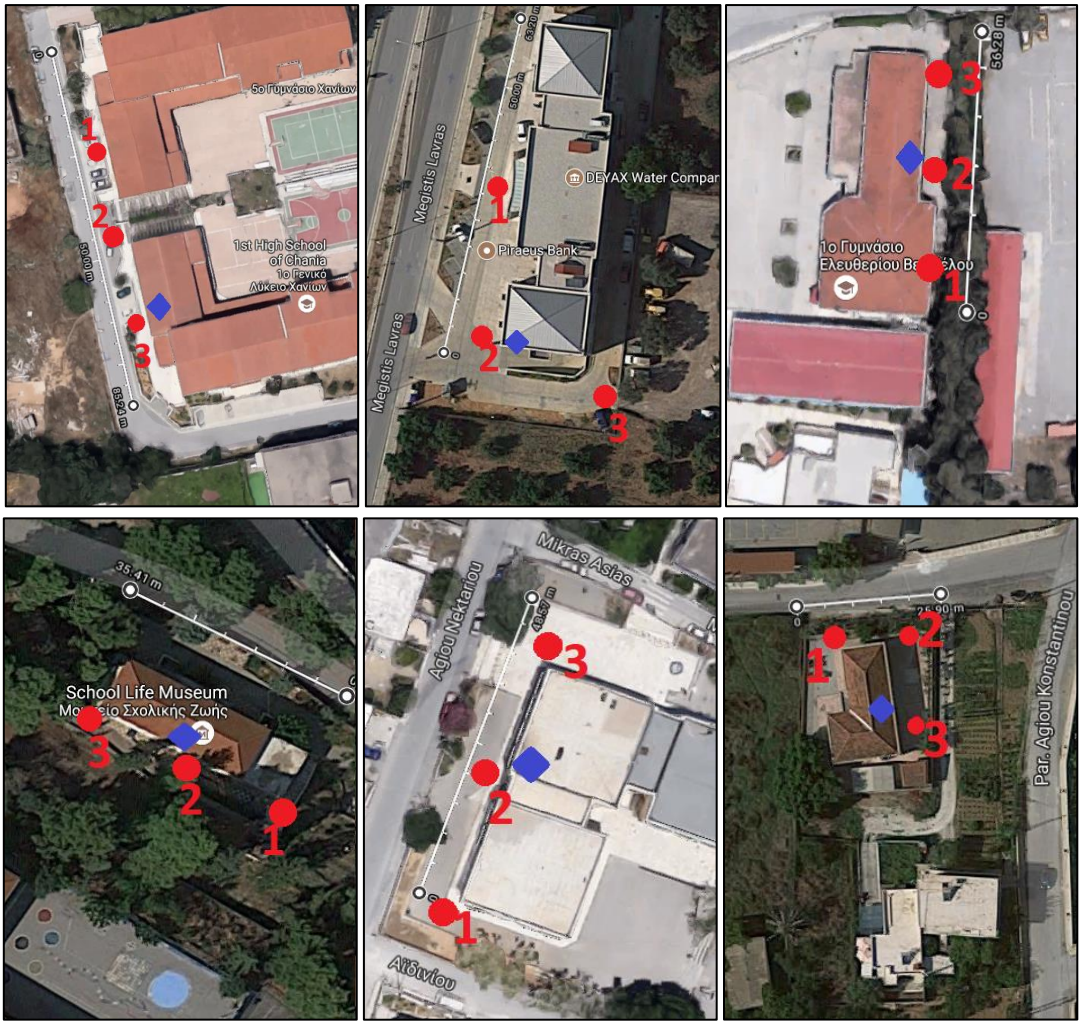

Figure 3.3 Six examples (ABEA, DEYA, G0LD, NERO, PASK and SOUD) for the single site microtremor survey.

The collected microtremor data have been processed with the Geopsy (http://geopsy.org) software which is mainly designed for ambient noise signal proceeding. The reasons choosing this software is that the developers continuously release updated versions, most procedures are automated, all the parameters are adjustable and it is friendly for users. Geopsy can load recordings with various signal formats. For this project the files that were imported was in SAC format, an example from ATEI singe station measurement is illustrated in figure 3.4. The signal processing begins with a mean value base correction and then a filter is applied to remove the geotechnical unnecessary frequencies, for these analyses a typical second order Butterworth bandpass filter between 0.2 and 20 Hz was selected (figure 3.5).

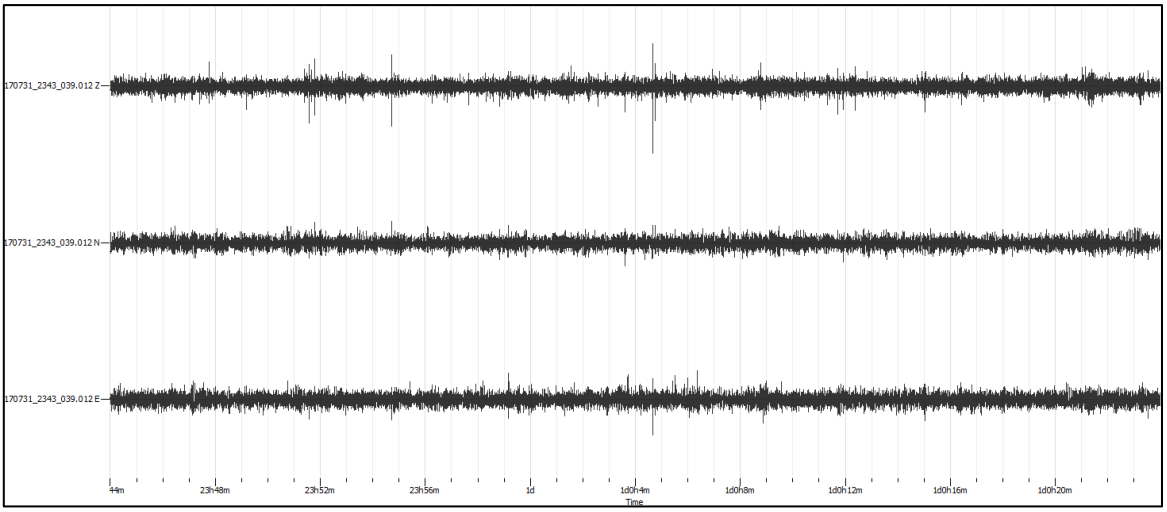

Figure 3.4 The three components of the ambient noise signal from ATEI single station measurement

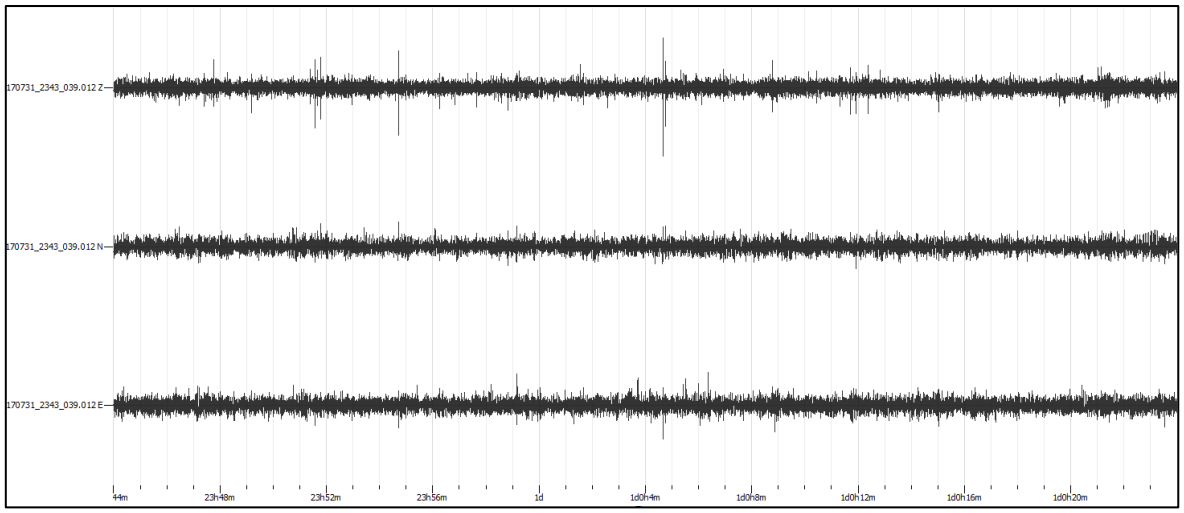

Figure 3.5 The three components after applying baseline correction and bandpass filter order 2, in the frequency band between 0.2 and 20Hz

The lowest frequency obtained from the Le3D/5s sensor is 0.2 Hz which satisfies the needs for the Chania sedimentary basin soft formations. According to SESAME manual, a reliable measurement should satisfy the minimum number of significant cycles, $n_c \geq 200$ that requires 20-time windows with minimum length at least 50 seconds, for this reason all recordings have a window length equal to 60 seconds with no overlapping windows. The Geopsy has an option to choose from the time series the desired window length (figure 3.6).

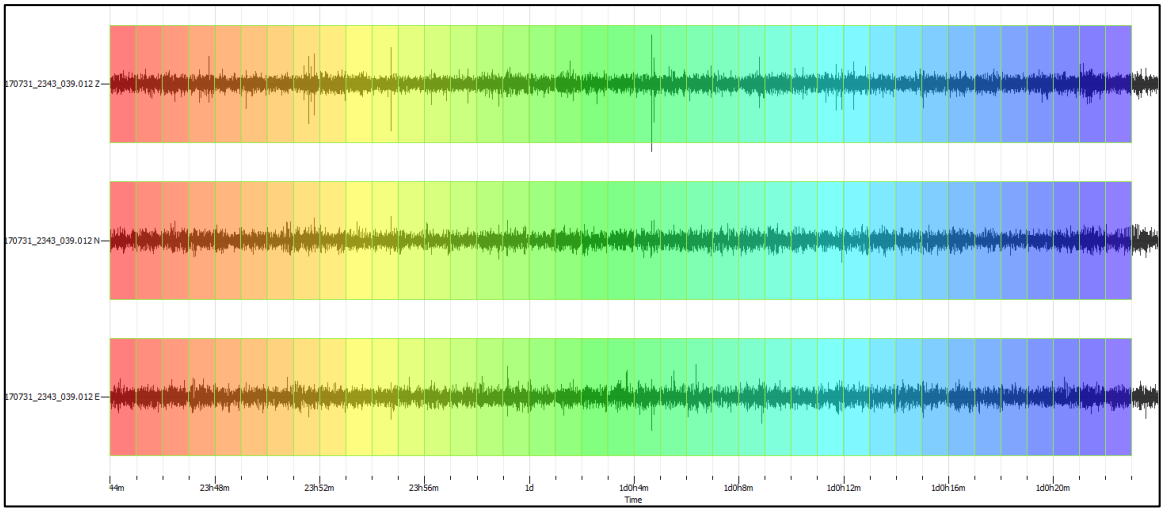

Figure 3.6 The automated procedure that select time windows, in this example the window length is equal with 60 seconds.

From the 45-60 minutes signal, some windows were manually removed cause the recorded information was not in agreement with the rest of the time windows and in most of the times was transient noise (figure 3.7).

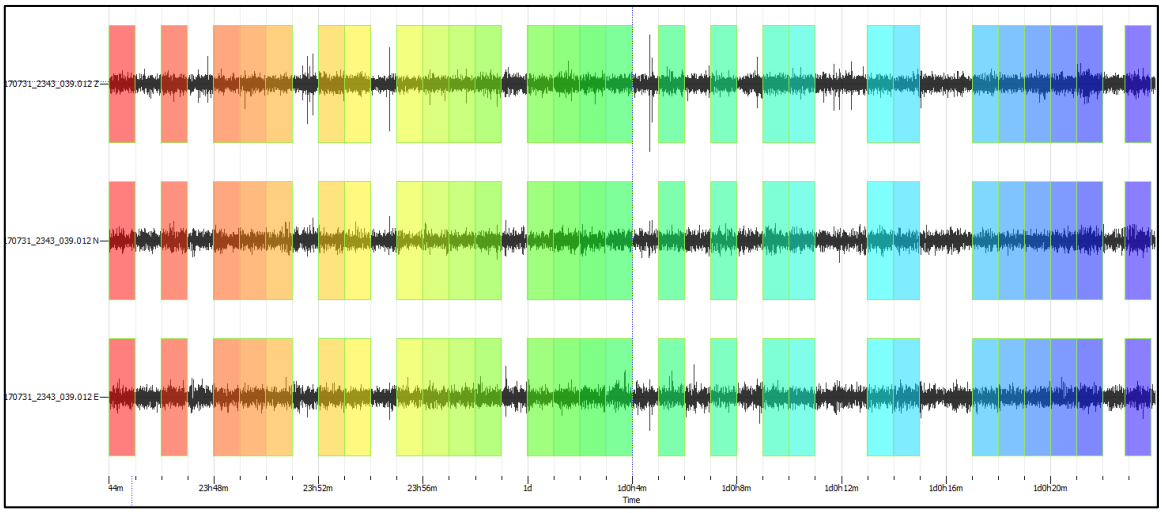

Figure 3.7 After manual inspection, the windows with transient noise are removed.

The number of windows kept after removing the transient noise were always more than 25. The last step before the calculation of the H/V spectral ratio, is to set the variables such as the output sample rate, in this case is 100Hz and the smoothing constant. Konno & Ohmachi (1998) showed that the amplitude of the H/V peak is related with the Poisson ratio and a typical value for soft saturated soils is approximately 0.5 but it decreases with the increase of the material

stiffness (Ishihara, 1996). For this reason, a smoothing constant (b-value) equal to 40 was selected with window type "Tukey" which is cosine tapered in both ends with 5% width named after John W. Tukey. The calculated H/V ratio before and after removing the time windows that have anthropogenic noise for the ATEI example is presented in figure 3.8. The predominant frequency f_0 in this study case is shifted to a lower value after the processing, while the amplitude of the highest peak remains unchanged because the bad data extermination process affected the peak in 0.6Hz.

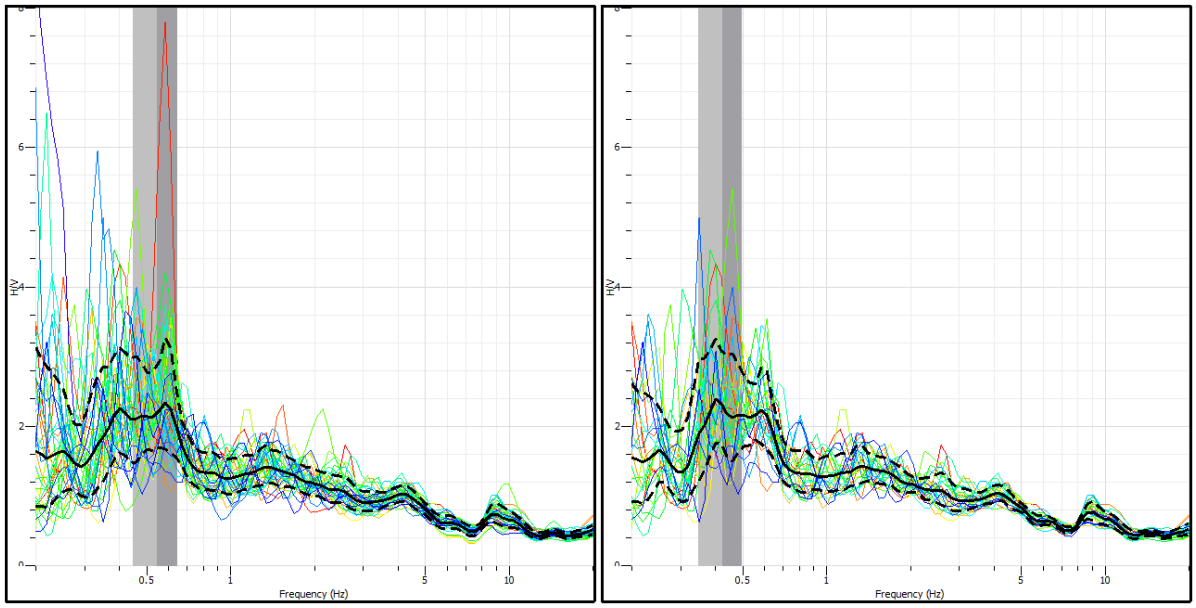

Figure 3.8 The H/V ratio before(left) and after (right) removing the transient noise windows.

Following the same steps, filters and options, the analysis to derive the H/V spectral ratio, has been carried out for each of three measurement points that have been performed on SGM' stations. The final HVSR curve for every single site, is the mean value of the three measurements (figure 3.9). The results of the H/V microtremor survey with City Shark II and Lennartz seismometer in SGM's stations are presented in figure 3.10, with red color line is the mean value of the three single station measurements and with light and dark gray color dashed line are the ± 1 standard deviations of the H/V ratios results.

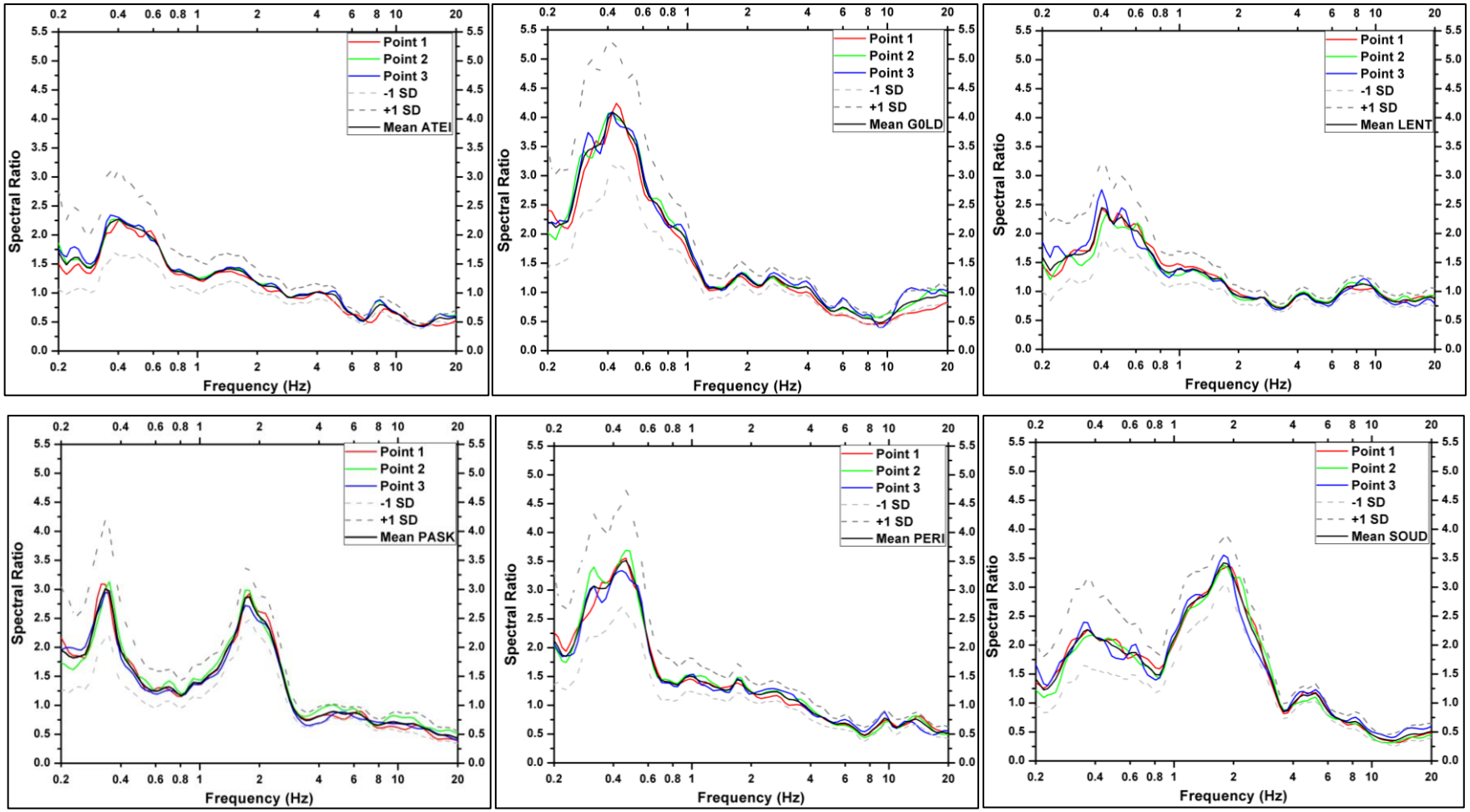

Figure 3.9 Six examples with the H/V point measurements as well as the mean values and the ±1 standard deviations for the SGM' stations (ATEI, G0LD, LENT, PASK, PERI, SOUD).

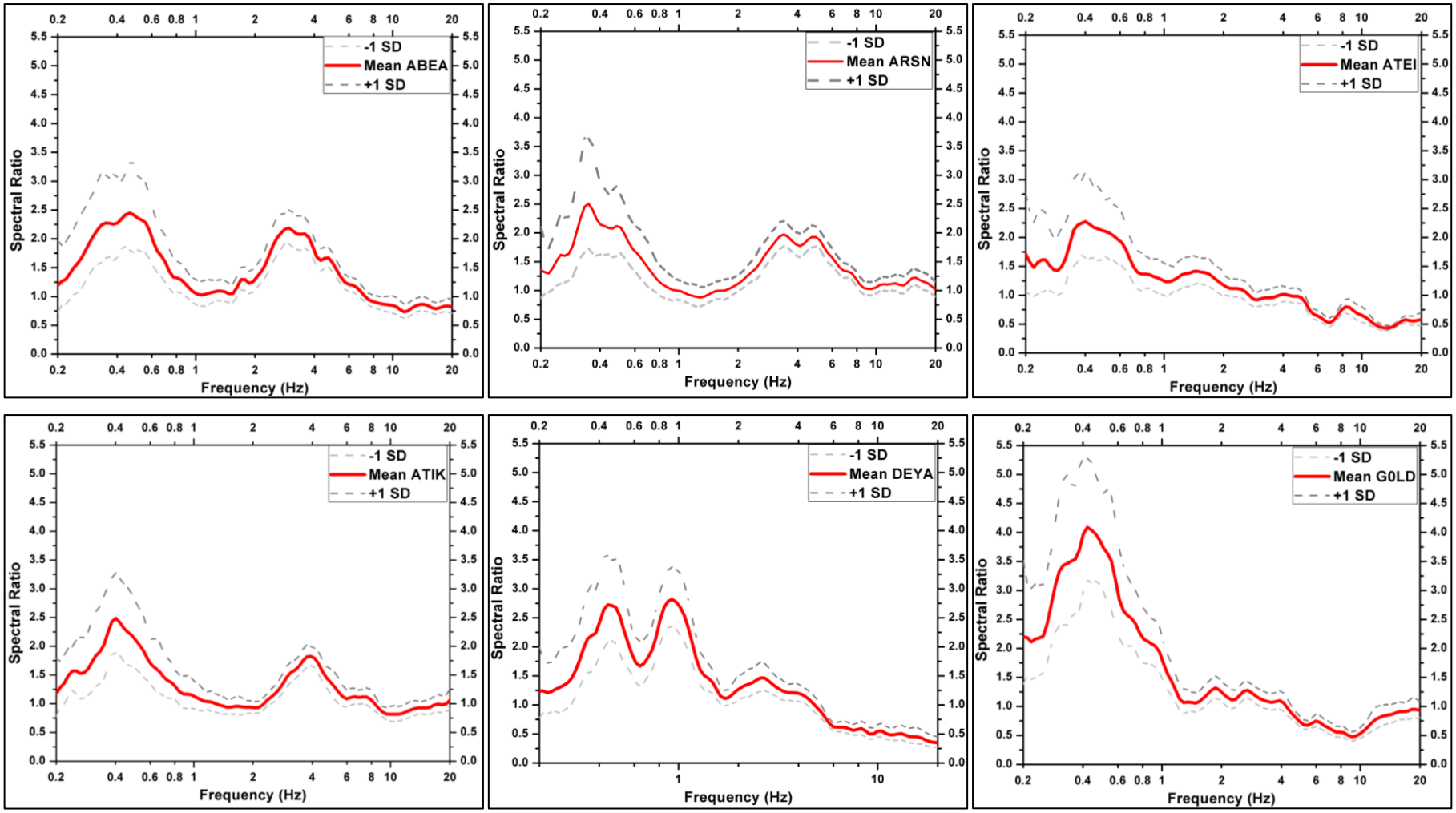
-1 SD
Mean ABEA
+1 SD
Spectral Ratio
Frequency (Hz)
-1 SD
Mean ARSN
+1 SD
Spectral Ratio
Frequency (Hz)
-1 SD
Mean ATEI
+1 SD
Spectral Ratio
Frequency (Hz)
-1 SD
Mean ATIK
+1 SD
Spectral Ratio
Frequency (Hz)
-1 SD
Mean DEYA
+1 SD
Spectral Ratio
Frequency (Hz)
-1 SD
Mean G0LD
+1 SD
Spectral Ratio
Frequency (Hz)

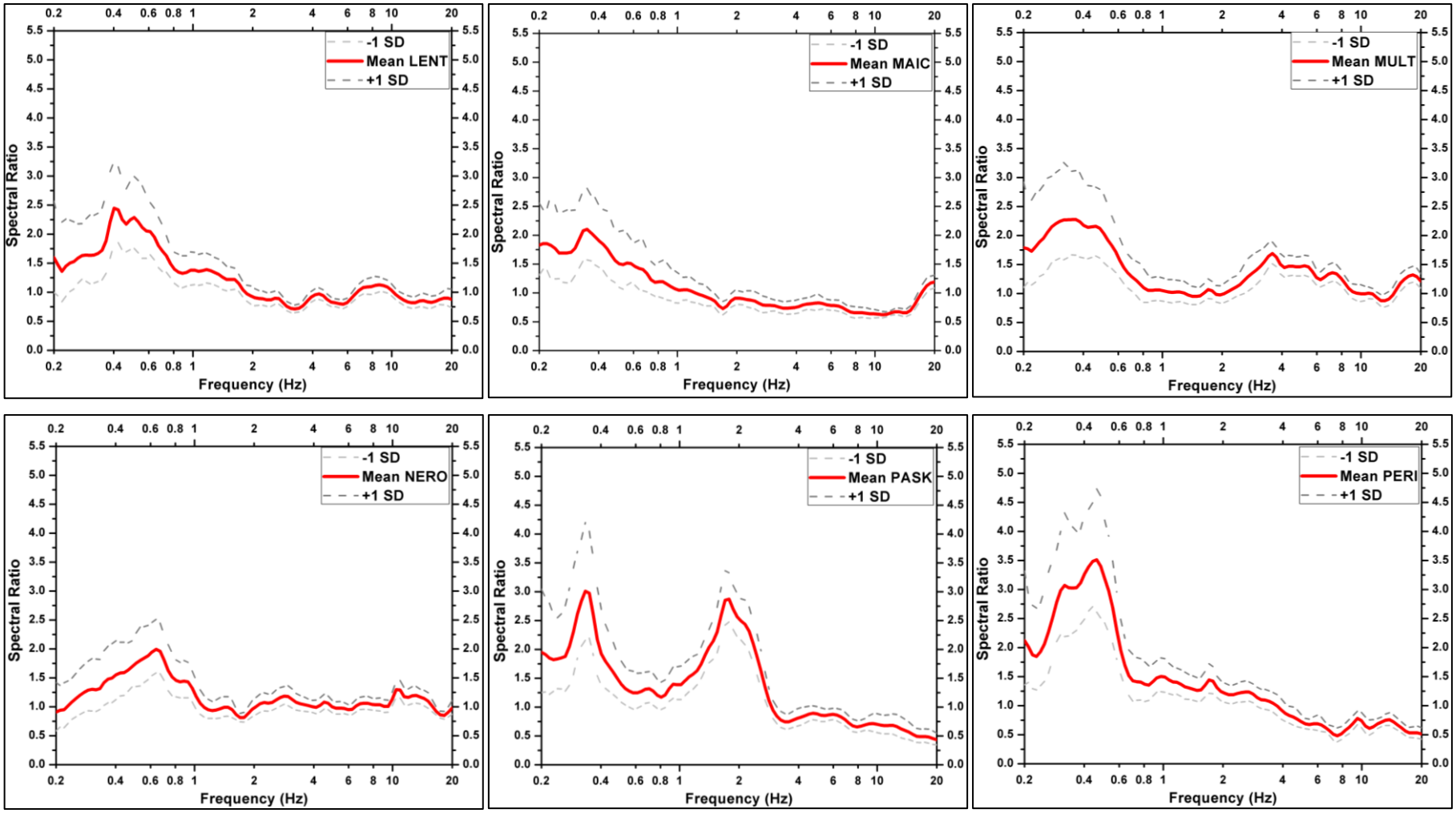
-1 SD
Mean LENT
+1 SD
Mean MAIC
Mean MULT
Mean NERO
Mean PASK
Mean PERI
Spectral Ratio
Frequency (Hz)

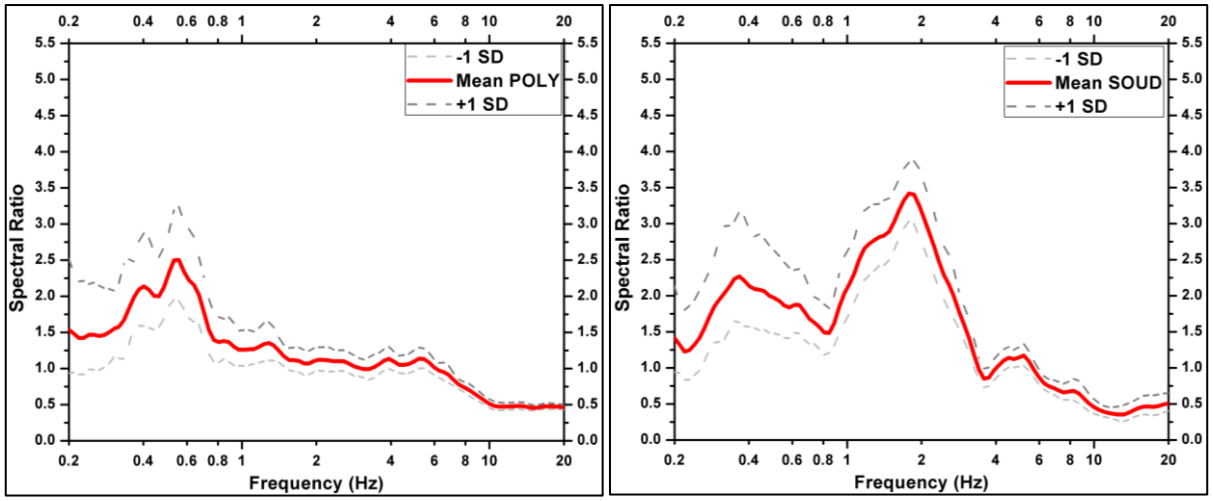

Figure 3.10 The mean H/V as well as with ±1 standard deviation from the 3-single station measurement for the SGM' station.

The numerical results from the H/V ambient noise measurements in each station location are presented in table 3.1. The predominant frequency and amplitude values (f_0, A_0) as well as the secondary peak values (f_1, A_1) in some cases, are similar with the results obtained from the extensive research of Papadopoulos et al. 2017 in the broader Chania city and its southern basin. The predominant frequency values f_0 are interpolated with simple kriging method to construct an approximation f_0 values map which has good correlation with the map from Papadopoulos et al. 2017 (figure 3.10).

Table 3.1 The predominant frequency and the corresponding amplitude peaks as well as the secondary peak for the SGM station locations.

Station	**f_0**	**A_0**	**f_1**	**A_1**
ABEA	0.46	2.44	2.96	2.18
ARSN	0.34	2.5	3.41	1.97
ATEI	0.4	2.27	-	-
ATIK	0.4	2.49	3.92	1.82
DEYA	0.44	2.72	0.92	2.81
G0LD	0.42	4.08	-	-
LENT	0.4	2.44	-	-
MAIC	0.35	2.1	-	-
MULT	0.36	2.27	3.57	1.68
NERO	0.63	1.99	-	-
PASK	0.33	3	1.78	2.87
PERI	0.46	3.51	-	-
POLY	0.55	2.5	-	-
SOUD	0.36	2.26	1.78	3.41

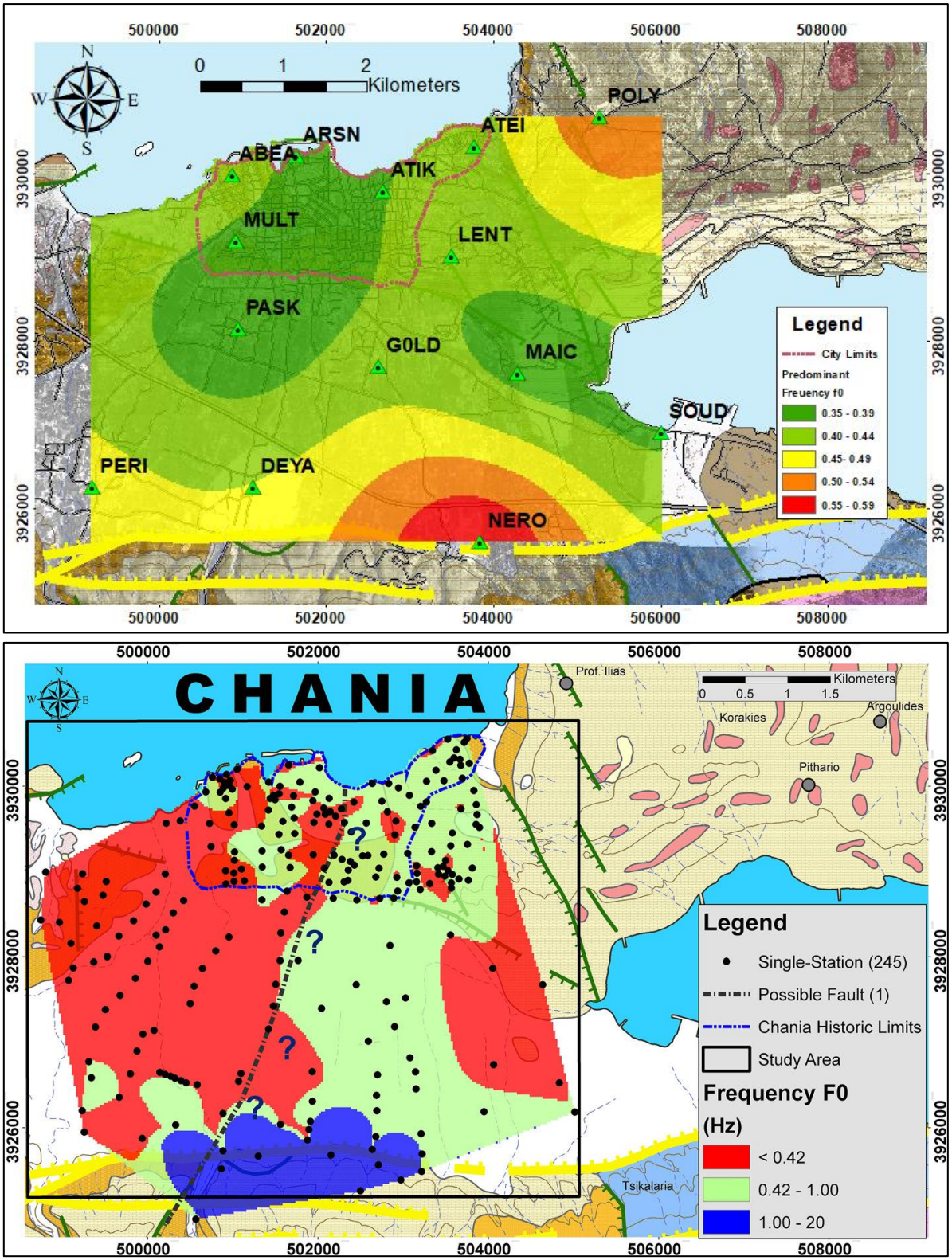

Figure 3.10 (Top) The rough estimation from interpolated results from the H/V measurements in stations location compared to the detailed results from Papadopoulos et al. 2017 (bottom).

3.2 The HVSR method using earthquake recordings

Lermo and Chavez-Garcia (1993) used spectral ratio on earthquakes to estimate the site effects in three cities in Mexico. They called their method "Receiver Function" (RF), other authors refer to the same method as Horizontal to Vertical Spectral Ratio on Earthquakes (HVSRE) (e.g. Haghshenas et al., 2008). The analysis procedure and options of the RF methods is the same as the microtremors one, with the only difference that it is applied in seismic signal. Some investigators are applying this method in whole waveform while others in specific parts such the S waves alone or from S arrival up to the end of coda. In 1995 the Field and Jacob study, of the aftershocks from the 1989 Loma Prieta earthquake, shown that HVSRE amplitudes obtained only from S waves can be correlated with the local site effects. The same approach to estimate the site response has been used by other researchers (Lachet et al., 1996; Parolai et al., 2004), have been adopted for this framework. The RF technique has been test from other research groups (Chavez-Garcia et al. 1996, Lachet et al. 1996, Riepl et al. 1998, Bonilla et al. 1997, Yamazaki and Ansary, 1997, Zare et al. 1999), leading to the following conclusions:

- The RF curve shape is stable for experimental data for the same station
- The results from this method are correlated with local site effects-surface geology and they are not affected by the source parameters or the path of wave propagation (except large or very close to sensor events with high directivity)
- The method produces results that are in good comparison with Standard Spectral Ratio (SSR) (even for measurements where the reference station is inside borehole (Lachet και Bard, 1994).

The RF method has been applied to local and regional events recorded by the accelerometer network. The first two years of the operation of our SGM network there have been several earthquake events in the vicinity of South Aegean but none of them was large and near the city of Chania. The earthquakes contributed to the RF ratio method were selected with a few criteria, one of them was to have good Signal-to-Noise Ratio (SNR). The procedure to estimate if an event has satisfying SNR (>3) is to subtract the Fast Fourier Transform (FFT) obtained from seismic signal by the FFT from ambient noise. The REF TEK's commercial software for earthquake analysis has a tool to inspect the FFT of the waveform and cut the desired windows in ASCII or SAC file format (figure 3.11). Two same size windows (approximately 8-12 sec) have been selected and saved in ASCII files, one with seismic signal beginning from the S arrival and one with noise. The two files are inserted in MATLAB programming language (https://www.mathworks.com). An algorithm to calculate the FFT of the two signals and

subtract them has been designed for this framework:

```
%Get two file with noise and signal of one component and find the SNR
clear all; close all; clc;

[FileName1,PathName1]=uigetfile ({'*.txt;*.dat;*.asc'}); % Get noise file
file1=[PathName1,FileName1]; fid = fopen(file1);
Data1 = textscan(fid, '%f', 'headerLines', 7, 'CollectOutput', true);
fclose(fid); fl1= cell2mat( Data1);

[FileName2,PathName2]=uigetfile ({'*.txt;*.dat;*.asc'}); % Get signal file
file2=[PathName2,FileName2]; fid1 = fopen(file2);
Data2 = textscan(fid1, '%f', 'headerLines', 7, 'CollectOutput', true);
fclose(fid1); fl2= cell2mat( Data2);


FS=250;                 % Sampling frequency
T=1/FS;                 % Sampling period
L=length(fl1);          % Length of signal
t=(0:L-1)*T;            % Time vector
t=t';
noise=(fl1(8:end,1));   %state where is ambient noise column
signal=(fl2(8:end,1));  %state where is seismic signal column

Y=fft(noise);           %computes a fast Fourier transform for noise
P2 = abs(Y/L);          %Compute the two-sided spectrum P2

P0 = P2(1:L/2+1);       %compute the single-sided spectrum
P0(2:end-1)=2*P0(2:end-1);
f = FS*(0:(L/2))/L;     %define the frequency domain

Y1=fft(signal);
P3 = abs(Y1/L);         %compute the single-sided spectrum
P1 = P3(1:L/2+1);
P1(2:end-1) = 2*P1(2:end-1);
f1 = FS*(0:(L/2))/L;

P=(P1./P0);   %subtract the two signals
freq=f';    %get frequency axis from columns to rows
A_result = [freq,P];  %put x,y together
A_result= A_result(freq>= 0.9 & freq<=20,:); %keep values between 0.9 -20Hz

semilogy(A_result(:,1),A_result(:,2),[0.9 20], [3 3],'r') % plot in semilog
```

Aiming to have a considerable number of waveforms for the RF method, all recorded events that occurred in the two years of the operation of SGM network have been tested for good SNR. In figure 3.12 is illustrated the East-West component of each station for four cases with the weakest SNR for the examined frequency band that have been accepted to contribute to the RF method, as the SNR was >3. Additionally, with SNR test we compare the H/V curves obtain from seismic signal recorded by an accelerometer and the same signal recorded from a close by broadband seismometer. The closest broadband sensor of the HSNC in the area is the station

CHAN (Guralp ESPC 120sec combined with REF TEK 130 digitizer), installed alongside with ATEI sensor. The HVSRE curves have been limited from 0.9 to 20Hz as the accelerometers are not sensitive below that frequency. Six examples of the H/V comparison between the ATEI accelerometer and the CHAN broadband seismometer are illustrated in figure 3.13; three of them are from close distance epicenters (30-50km) while the rest are from events with moderate up to the maximum epicentral distance (220km) that has been used in the RF method.

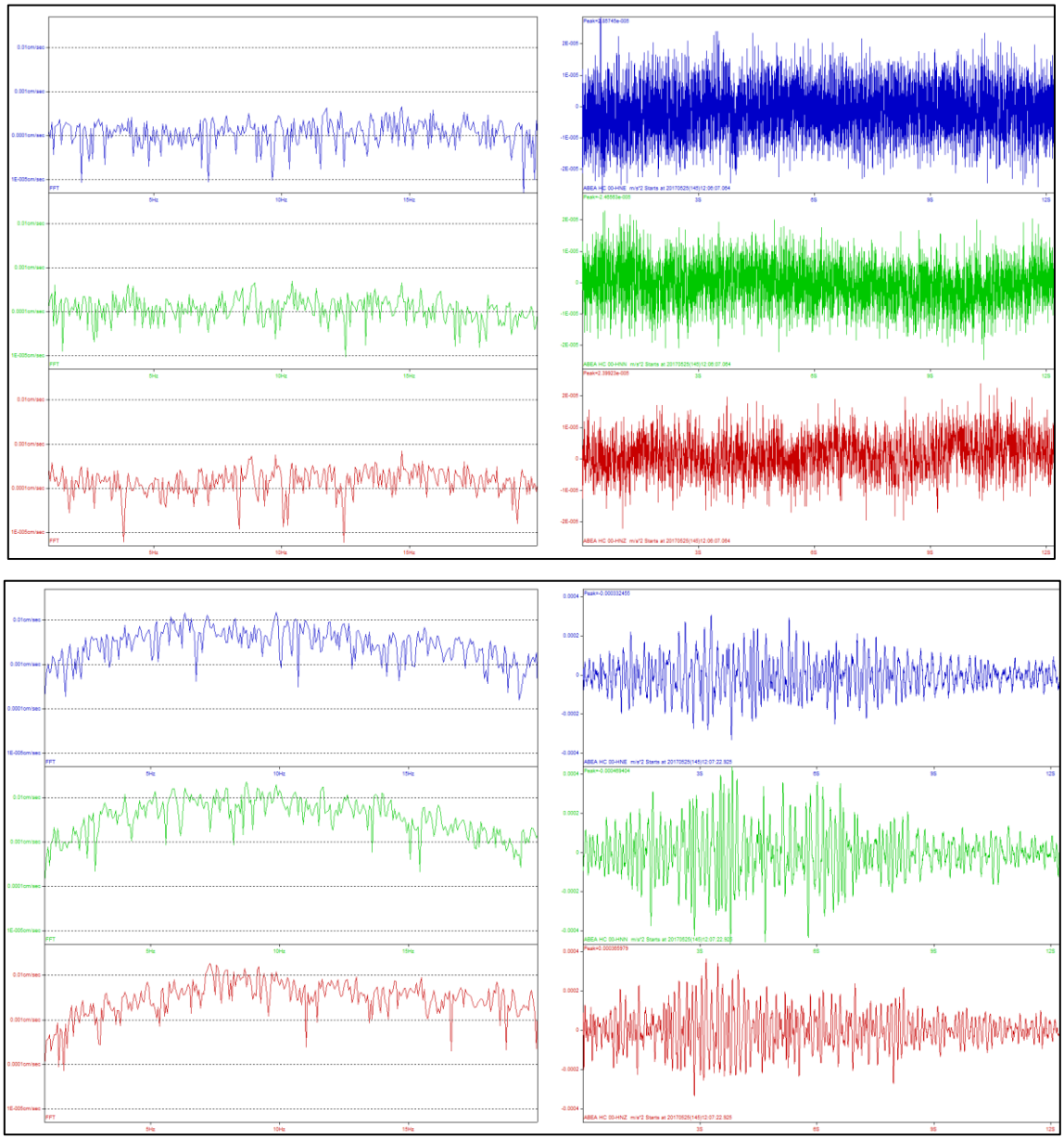

Figure 3.11 The FFT obtained from ambient noise (up) and the FFT from seismic signal on the S wave part (down). The images are acquired from REF TEK's commercial software. This example is showing an event that participated in RF technique with local magnitude 3.3 and epicentral distance from Chania 82 km.

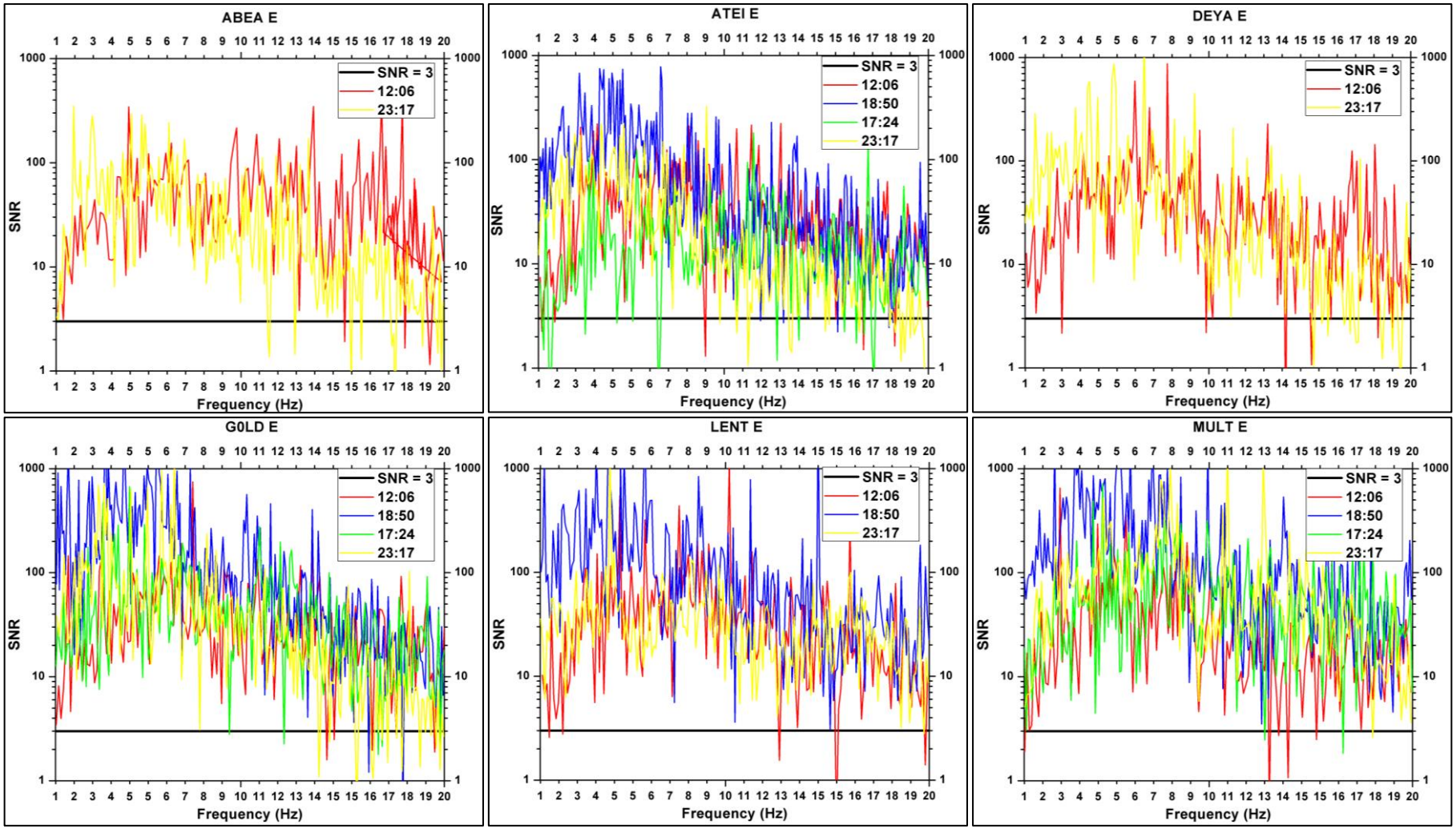
ABEA E
SNR = 3
12:06
23:17
ATEI E
SNR = 3
12:06
18:50
17:24
23:17
DEYA E
SNR = 3
12:06
23:17
G0LD E
SNR = 3
12:06
18:50
17:24
23:17
LENT E
SNR = 3
12:06
18:50
23:17
MULT E
SNR = 3
12:06
18:50
17:24
23:17
SNR
Frequency (Hz)

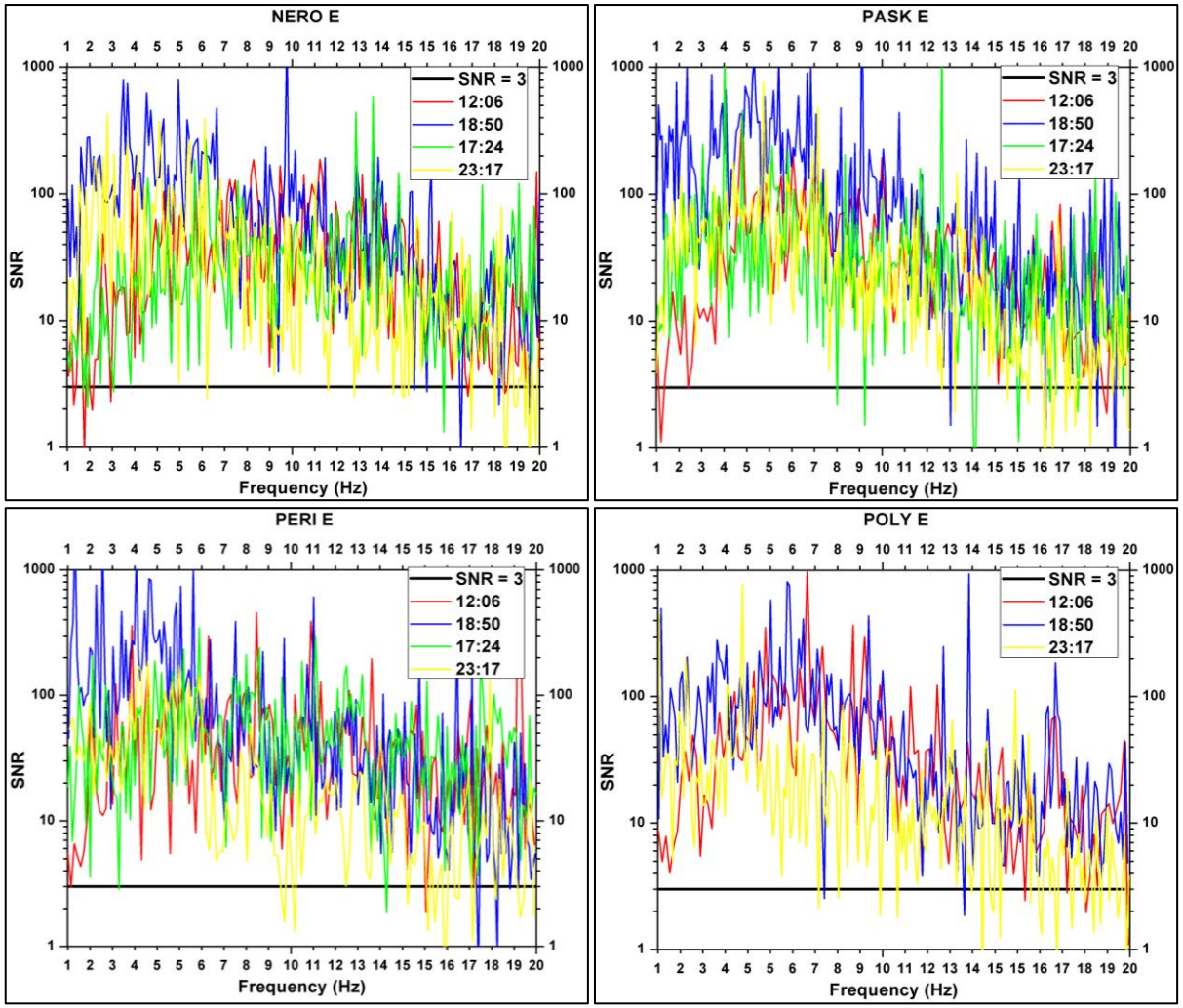

Figure 3.12 The SNR in each SGM station from the east-west component, the four cases have weak but acceptable SNR (>3).
The events used are detailly presented in catalogue below (25/05/2017 12:06, 25/01/2017 18:50, 09/09/2016 17:24 and 03/03/2017 23:17)

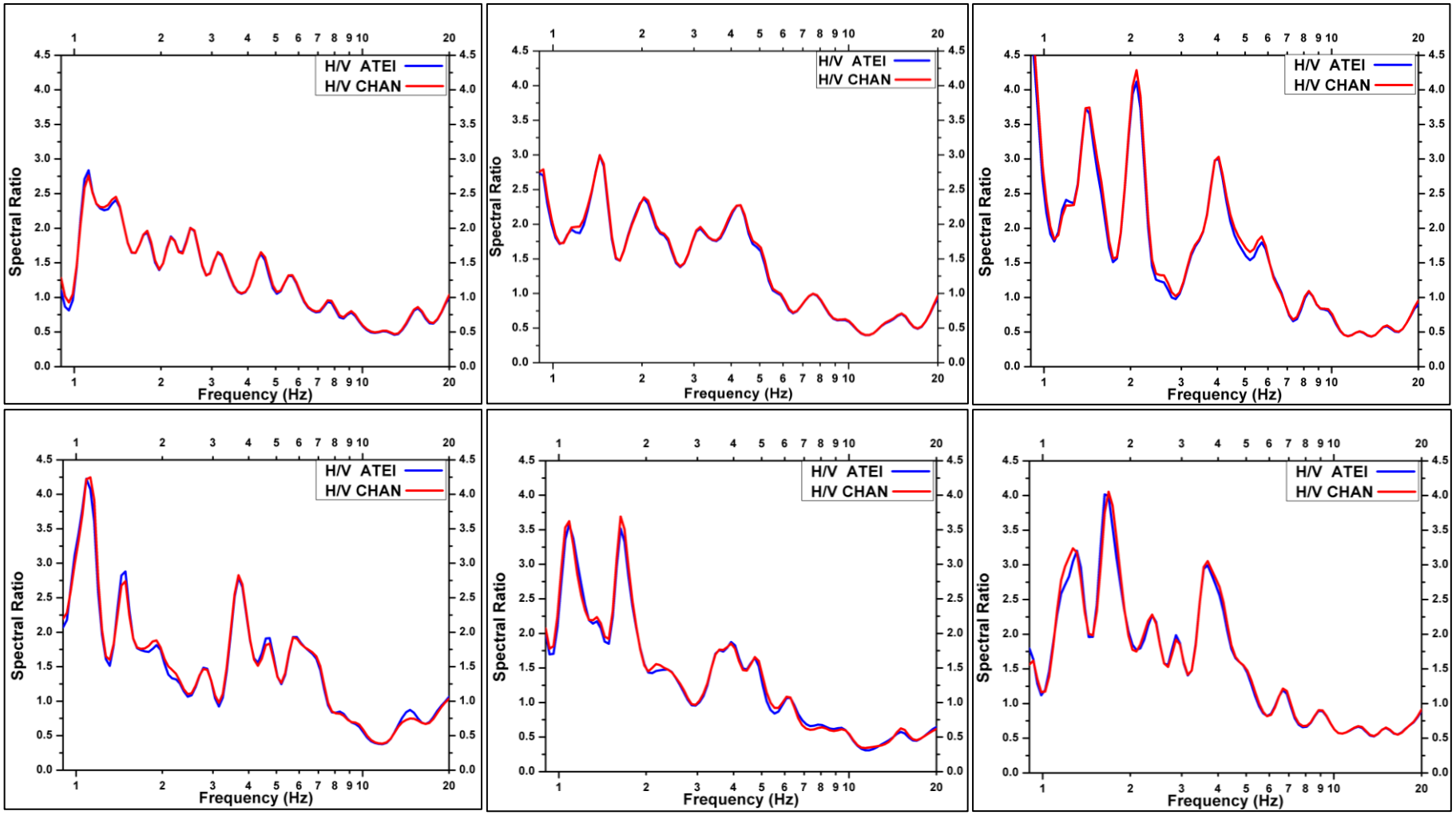

Figure 3.13 Signal comparison using the H/V ratio obtain from ATEI accelerometer (blue) and CHAN seismometer (red).
a) 2016/03/07 14:25 UTC, b) 2017/01/25 18:50 UTC, c) 2017/06/12 12:46 UTC d)2016/03/12 12:40 UTC e)2017/12/13 07:30 UTC f)2017/08/16 15:53 UTC

Other criteria to reduce the number of the possible events have been applied such us to search for events with minimum local magnitude ML=3.3; below that the SGM network didn't have recordings with good SNR and it was difficult to examine the waveform. A final criterion is to use earthquakes with maximum distance 220 km, this option is applied for excluding events that have weak signal. Although the 220 km is a considerable epicentral distance, there were some earthquakes with moderate magnitude capable to produce small acceleration values in Chania city and their waveforms had good SNR so they have contributed to the RF method. In ambient noise method, the window length was fixed to 60 second while in the RF technique, it varies from 12 to 30 second for the selected events (figure 3.14). The window length is depended on the event distance, for local earthquakes the length is small while for regional events is larger. The processing window is applied only on S-waves part, from the S-phase arrival to the beginning of coda waves. After applying the above criteria, 31 earthquakes have been identified (presented in Table 2 and figure 3.15) and have been used to produce the mean RF ratio of the SGM station locations.

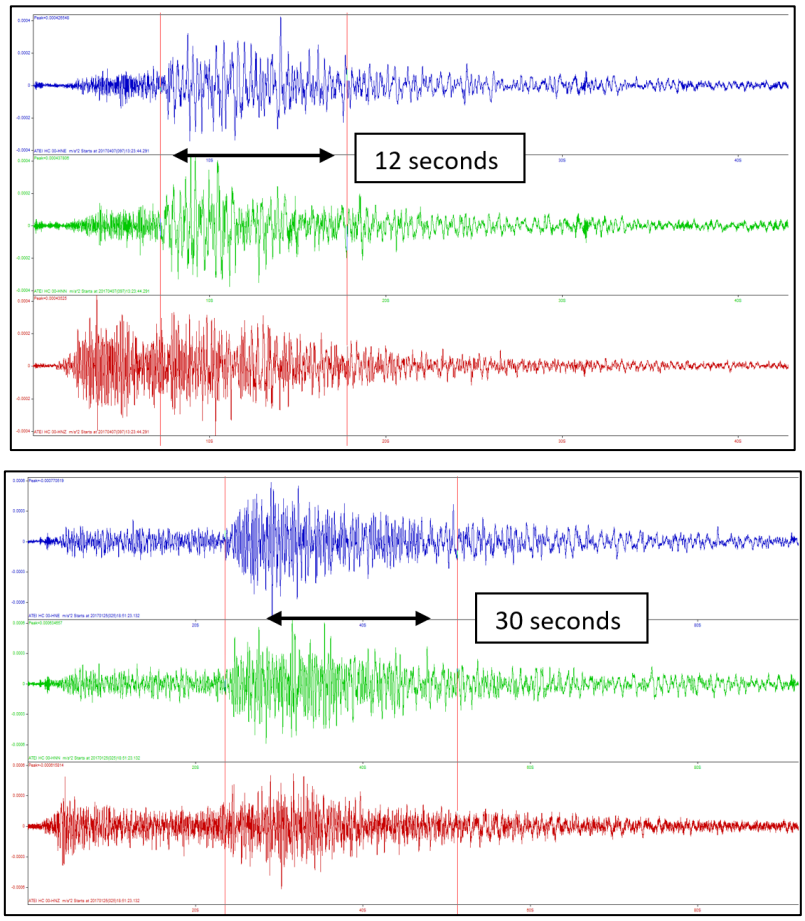

Figure 3.14 Different window length (inside the red vertical lines) for a local (left) and a regional (right) event.

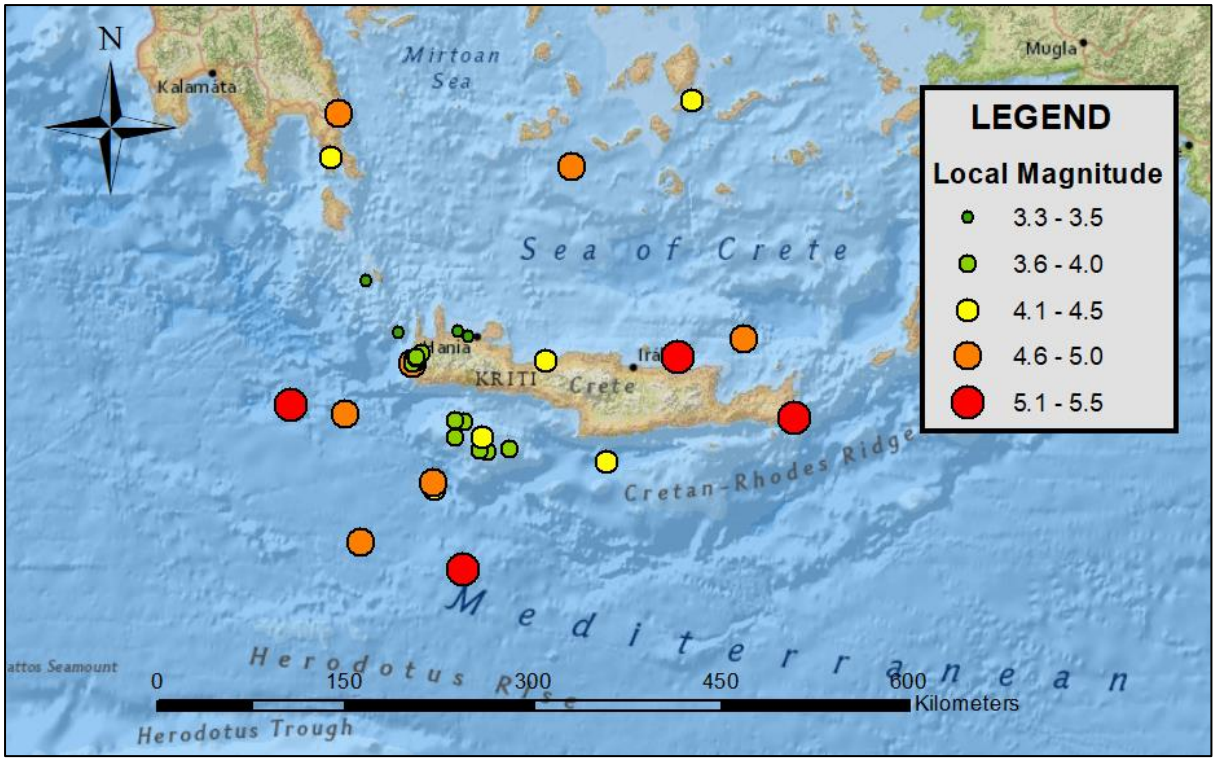

Figure 3.15 A map with the epicenters and the magnitude of the events that participated in the RF method

The frequency range for RF method is also narrowed to the 0.9-20 Hz as the installed strong motion sensors are not sensitive in frequencies lower than 1. Additionally, the accelerometers as not suitable for ambient noise surveys as they are not sensitive enough for this order of magnitude vibrations (SESAME 2004). The ambient noise H/V ratio we use in RF -H/V comparison is one obtained from the microtremor surveys with Lennartz seismometer and City Shark II. The estimation of earthquake parameter, origin time, location, depth and magnitude of the participated to RF method events, have been carried out using the data obtain by the HSNC stations (HC) as well as waveforms from other seismological networks operating in the South Aegean region like the National Observatory of Athens Seismic Network (HL) and Aristotle University of Thessaloniki Seismological Network (HT). The analysis of the events has been carried out with REF TEK commercial software. Almost all manual solution has been completed by the author of this thesis while some of them are from the HSNC manual solutions. The catalogue results are preliminary, the events have not relocated with a suitable crust model for the geotectonic setting and the use of this catalogue is only to indicate which events that have been used in RF method. We haven't included SOUD station in the RF process, due to its later installation and lack of available data. The same occurs for all stations equipped with GSense accelerometer, the16bit sensors are working on full range scale ±2g which means that

they are not so sensitive as the REF TEK ones (but still can provide the PGA), besides that they cannot record the waveform with the same accuracy as the 65,536 (2^16) steps of resolution is much more inferior than the 24-bit resolution 16,777,216 (2^24). The results from the combined RF-HV plots are shown in figures 3.15 and 3.16. According to the similarity of the results, in figure 3.16 the result with near the same shape in RF-HV curves are presented while in figure 3.17, the four stations on quaternary deposits with noticeable differences in spectral ratio curves are illustrated.

Table 3.2. Catalogue of the 31 earthquakes used for RF ratio.

Date	Time (UTC)	Latitude	Longitude	Depth (km)	Magnitude (ML)	Distance (km)
06/03/2016	23:17	35.446	23.681	20	4.0	30
07/03/2016	14:25	35.416	23.670	16	3.8	32
12/03/2016	12:40	35.413	23.672	17	4.8	32
12/03/2016	15:22	35.412	23.696	16	3.9	30
12/03/2016	7:50	35.464	23.676	23	3.9	30
13/03/2016	13:23	35.470	23.686	21	3.6	29
25/05/2016	8:36	35.036	26.288	20	5.5	210
30/07/2016	17:26	35.114	22.671	10	5.1	130
09/09/2016	17:24	36.878	25.556	150	4.2	205
18/12/2016	4:01	35.014	23.914	5	3.9	57
27/12/2016	19:31	36.555	22.965	10	4.4	150
29/12/2016	19:23	35.540	23.448	8	3.5	52
15/01/2017	3:37	35.063	23.064	21	4.6	100
16/01/2017	2:45	34.928	23.850	10	3.8	67
22/01/2017	9:22	35.515	23.945	12	3.3	12
25/01/2017	18:50	35.397	25.449	60	5.4	220
15/02/2017	23:01	34.783	24.940	12	4.5	117
03/03/2017	23:17	35.498	25.922	13	4.6	173
07/04/2017	13:23	35.387	23.577	13	3.8	46
08/04/2017	12:26	35.396	23.576	3	3.6	46
29/04/2017	22:39	35.547	23.868	18	3.3	19
25/05/2017	12:06	35.780	23.090	16	3.4	88
14/06/2017	7:10	34.620	23.707	16	4.2	103
16/06/2017	23:42	36.809	23.018	59	4.8	170
21/06/2017	12:46	35.371	24.505	65	4.3	47
31/07/2017	21:29	34.143	23.906	8	5.5	152
16/08/2017	15:53	36.498	24.691	103	4.8	124
18/08/2017	3:46	34.925	24.045	8	4.1	65
13/12/2017	07:30	34.657	23.692	30	4.8	155
20/12/2017	04:18	34.305	23.179	8	4.7	150
2018/01/26	22:09	36.056	24.246	43	4.1	64

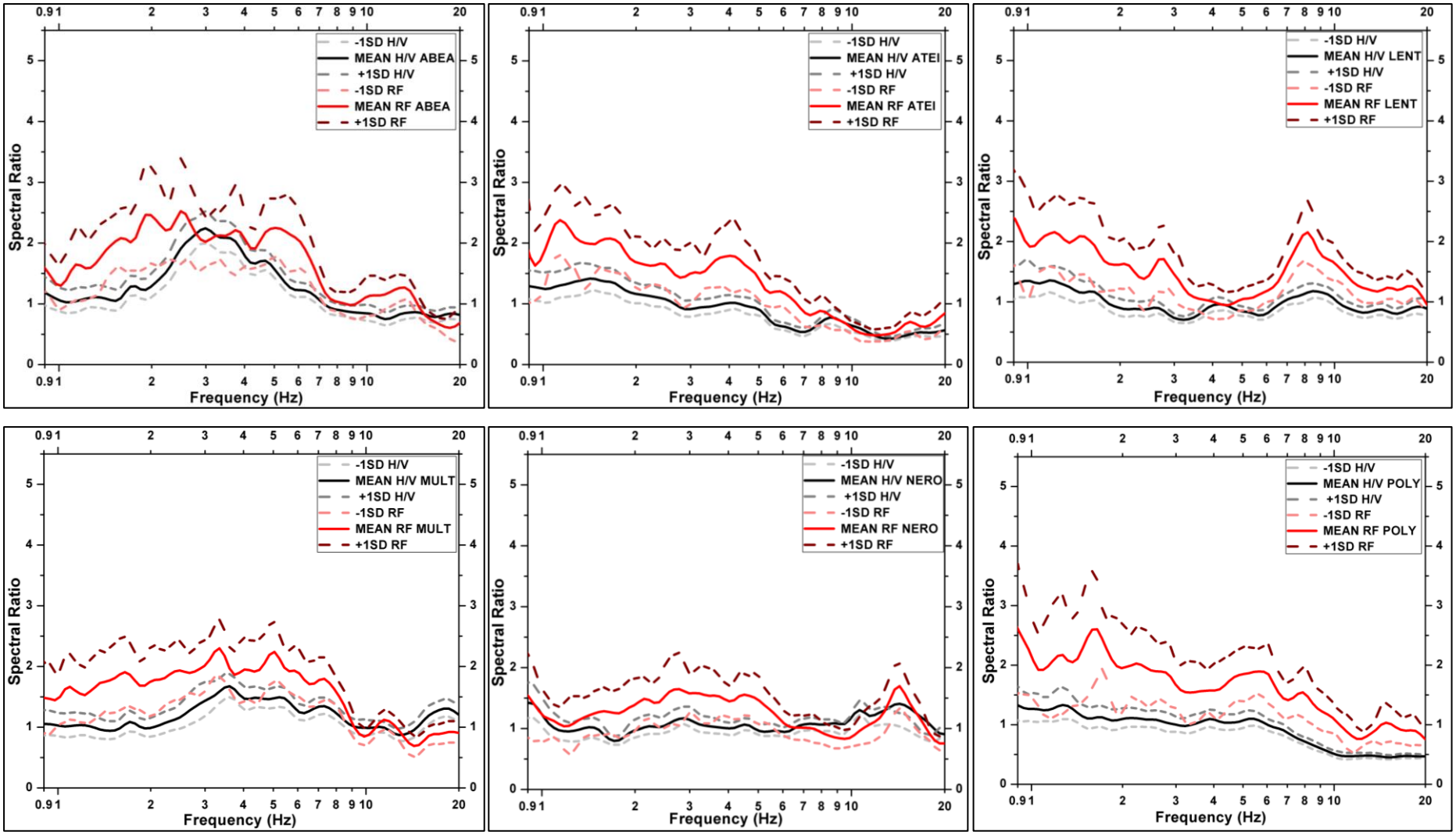

Figure 3.16 The RF-HV method results with good similarity obtained from stations located the Neogene or Quartenary-Neogene formations.

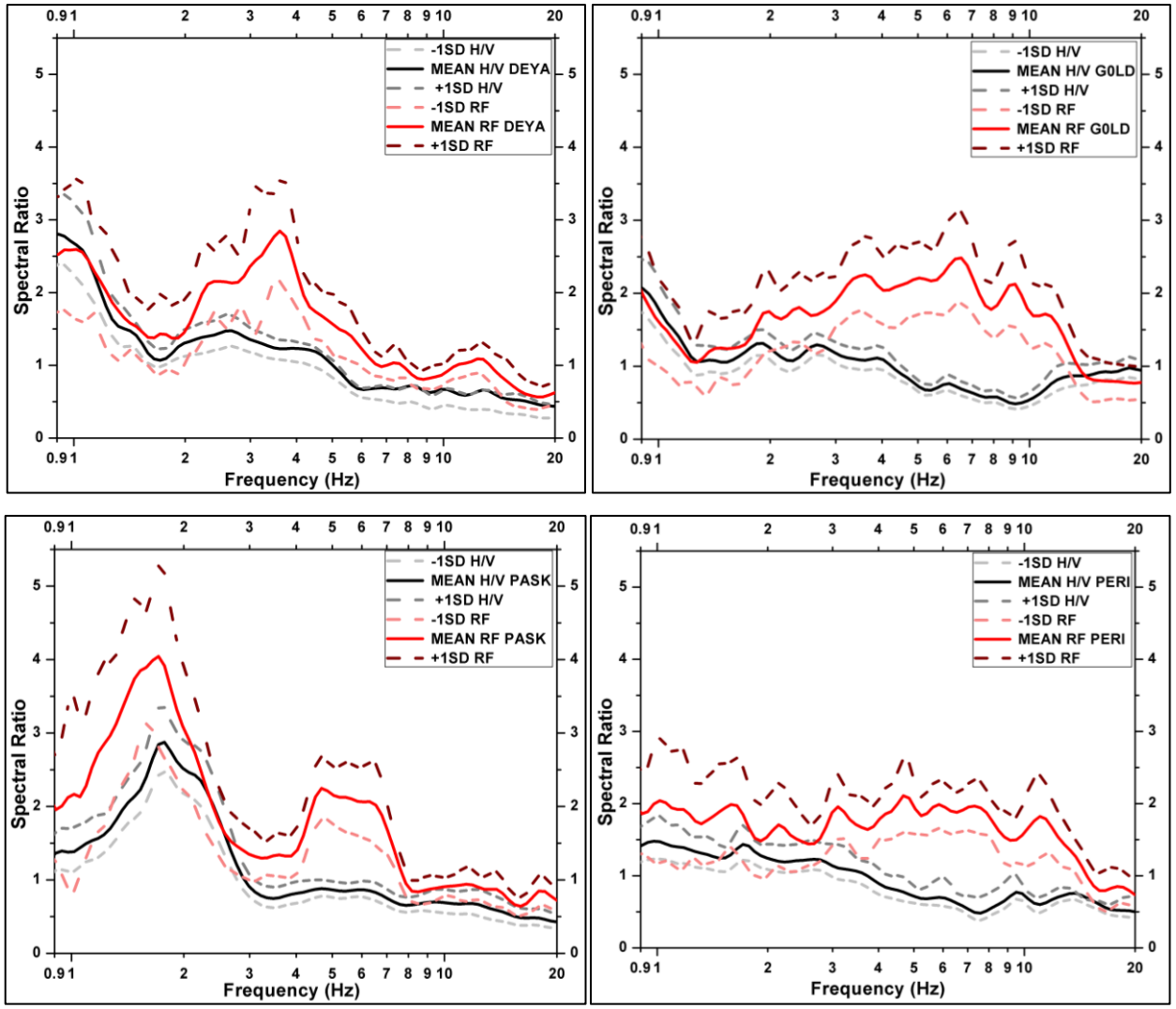

Figure 3.17 The RF-HV method results with different spectral ratio amplitude peaks obtained from stations located in the thick part of Quartenary formations.

4. SHAKE MAPS

4.1 Data extraction

In the operation of HSNC dedicated servers is used to store and distribute the seismic waveforms while other are designed to carry out the automatic signal analysis to calculate the earthquake parameters. When an earthquake triggers the monitoring workstations (Seiscomp3 and Earthworm), an email notifies the users of seismic network and several scripts are sending the catted raw waveform files to the analysts' computers so the manual solution can be achieved. Although, both automatic systems are capable to compute the PGA values of a seismic event, in this research, the acceleration values are extracted manually. The main reason for using a time-consuming procedure to calculate the necessary data in this project, is that in some of the participated events has low SNR and the automatic calculation process could be misled. The signal analysis has been carried out with the Ref Tek commercial software, which is a user-friendly Windows Graphical User Interface (GUI) and by following a few simple steps, it does calculate all the required parameters. The first task is to insert the waveforms in the software, which supports a large list of compatible formats (Reftek, SEED, Segy, SAC, ASCII, Wav and many other). Then, from the whole waveform (usually it is four minutes length around the seismic event, cut from the preliminary alert system) a focus is made on the earthquake signal, starting from P wave arrival up to the coda waves (figure 4.1).

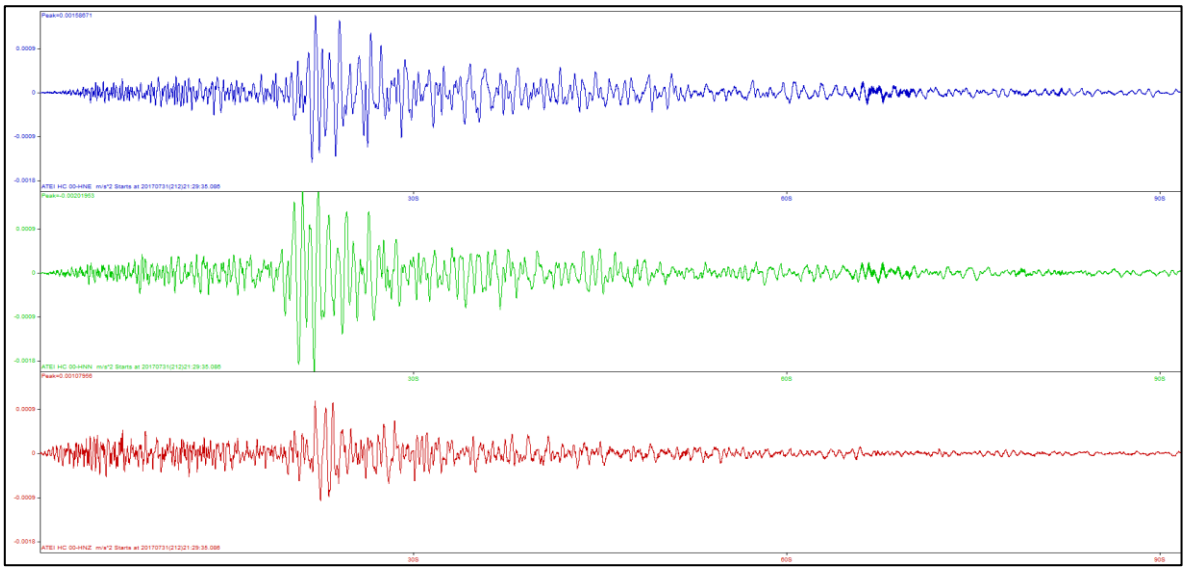

Figure 4.1 Seismic signal from P arrival up to coda waves for the analysis.

On the REF TEK (SMP) menu, it is possible enter to the SM processing only if you have accelerometer data (figure 4.2). This enables the seismic signal the manipulation such as

applying some filters to remove the unnecessary frequencies. Other possible options are: the use or not of response files for instrument correction, apply a baseline correction method (mean value has been used for this project) to the waveform if it is needed, and there are some choices regarding the response spectrum analysis such as function damping ratio and period range. Although the manual analysis is not as fast as the automatic, it has few important advantages, such as the possible inspection of many time series plot related with seismic signal (figure 4.3) and instantly produces a report, with many useful parameters such as Arias Intensity, Cumulative Absolute Velocity, Maximum Displacement to name but a few (figure 4.4).

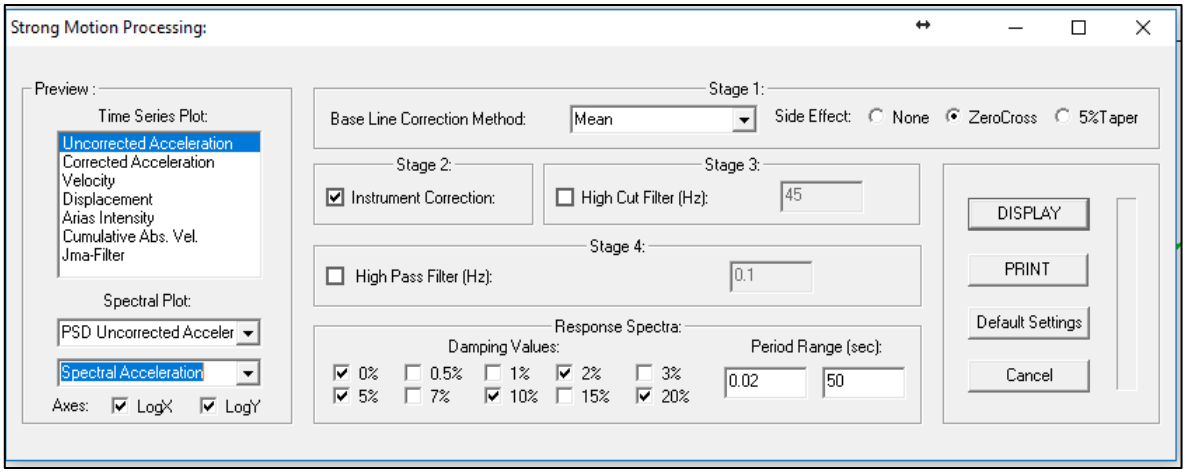

Figure 4.2 The Strong Motion Analysis (SMA) available filters and options.

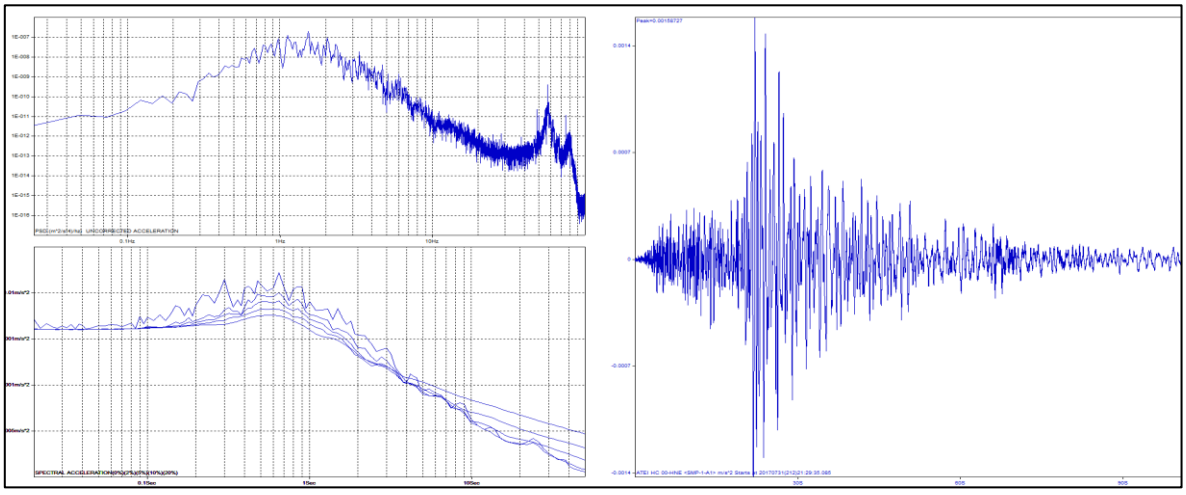

Figure 4.3 Few plots (Power Spectral Density and Spectral Acceleration) produced in SMA.

I. Instrumental	II. Feeble	III. Slight	IV. Moderate	V. Rather Strong	VI. Strong	VII. Very Strong	VIII. Destructive

Station: ATEI	**Channel: HC 00-HNE:**
Maximum Acceleration	0.00158782 m/s^2 at Time=2017.07.31 21:29:57.230
Spectral Intensity	0.000304199 cm
Predominant Period	0.650159 sec
Mean Period	0.69548 sec
2PI*Vmax/Amax	2PI*0.109099=0.685492 sec
Maximum Velocity	0.00017323 m/s at Time=2017.07.31 21:29:57.100
Maximum Displacement	0.000115697 m at Time=2017.07.31 21:31:16.660
Cum. Abs. Velocity	0.0122626 m/s
Arias Intensity	7.4515e-007 m/s
Arias Duration (5-75)	14.89 sec
Arias Duration (5-95)	33.485 sec
JMA Intensity	0
MMI Intensity	0
Station: ATEI	**Channel: HC 00-HNN:**
Maximum Acceleration	0.00201901 m/s^2 at Time=2017.07.31 21:29:57.120
Spectral Intensity	0.000398137 cm
Predominant Period	0.706207 sec
Mean Period	0.75831 sec
2PI*Vmax/Amax	2PI*0.115193=0.723782 sec
Maximum Velocity	0.000232577 m/s at Time=2017.07.31 21:29:56.050
Maximum Displacement	0.00266394 m at Time=2017.07.31 21:31:12.540
Cum. Abs. Velocity	0.014109 m/s
Arias Intensity	1.12013e-006 m/s
Arias Duration (5-75)	9.58 sec
Arias Duration (5-95)	27.665 sec
JMA Intensity	0
MMI Intensity	0
Station: ATEI	**Channel: HC 00-HNZ:**
Maximum Acceleration	0.00107983 m/s^2 at Time=2017.07.31 21:29:57.210
Spectral Intensity	0.00020207 cm
Predominant Period	0.712348 sec
Mean Period	0.628347 sec
2PI*Vmax/Amax	2PI*0.11517=0.723637 sec
Maximum Velocity	0.000124365 m/s at Time=2017.07.31 21:29:57.395
Maximum Displacement	0.00092128 4 m at Time=2017.07.31 21:31:08.160
Cum. Abs. Velocity	0.00879503 m/s
Arias Intensity	3.49941e-007 m/s
Arias Duration (5-75)	23.225 sec
Arias Duration (5-95)	40.075 sec
JMA Intensity	0
MMI Intensity	0

Figure 4.4 The various parameters calculated for a station in the SMA.

4.2 Data interpolation

4.2.1 Reasons to apply interpolation

One of the important aspects of the research is the data collection process. A common problem in an analysis is the lack of complete data or large gaps between the measurements. Most of the times the solution to the bad data problem is to use an **interpolation method** which is a procedure that predict the missing values or completes the samples between some grid points. The SGM network started operating in a test phase with six stations. After an earthquake it was possible to obtain the PGA values in the measurement point. The approach to operate a dense network with a great number of sensors, spread them in whole research area was not cost efficient. Aiming to examine the acceleration values between the first stations, it was necessary to apply an interpolation method. The first results obtained by this procedure were encouraging but the number of the stations wasn't sufficient to validate the outcome due to the fact that the interpolation methods are depended on the grid of samples. The most promising way to overcome the small grid obstacle was to expand the SGM network by adding more stations in selected locations. Following this idea, with primary target to have an appropriate number of samples from all the geological formations, the number of stations gradually increased with the use of GSense accelerometers, reaching the fourteen sensors in an area about 18 km^2. The station location tried to be distributed evenly to cover most of the geologic formations but also a focus has been set to the urban environment and the included monuments.

4.2.2 Interpolation methods

Choosing the appropriate interpolation technique to represent the spatial distribution of the samples and predict the missing values is an important job that is much depended on the dataset. The available measurements can be classified in different surfaces based on the provided information structure, two examples are the isolines which have constant values along a specific line like an isotherm or an isobar and the second paradigm is the grids that are 2.5D functional surfaces cause for any x, y location there is only one Z value (Childs 2004). In this framework, the mainly used interpolation software is the ArcGIS which uses as native format the grids that can be easily inserted with a typical excel or ASCII file. The mechanisms behind the interpolation process can be divided in two approaches. The first group has deterministic methods (Thiessen polygons, inverse distance method, splines) which is controlled by empirical or mathematical functions that take the similarity of the cells into account without considering the possible errors of the model. The other approach is the geostatistical (Kriging, Bayesian models), the predictions are based on statistics that are applied on the dataset values. These techniques assume that the variables are following the probability theory and the variance is used as a measure of the uncertainty, which is the squared deviation of a random variable from its mean (Hengl 2007). The square root of the variance is the Standard Deviation. In geostatistics, half of the variance of the differences between neighbor samples is known as semivariance. Plotting the average semivariance values in a graph produces the semivariogram. The relation describing such a plot at a distance d for a pair of samples i, j is: $Semivariogram(d) = \frac{1}{2*N(d)} \sum (sample_i - sample_j)^2$ where $N(d)$ are all the available pairs with Euclidean distances $i - j = d$ (Matheron 1962, Gandin 1963). The most common used interpolation methods in ArcGIS environment are:

- Inverse Distance Weight (IDW), a method that is working better with dense grids (at least 14 points) and determines the missing values by using the distance as a linear weight and assumes that the points that are closer to each other, have better correlation The equation for the prediction point is $Z_j = \frac{\sum_i^N z_i d_{ij}^{-p}}{\sum_i^N d_{ij}^{-p}}$ where N, i are the number of neighbors and the search points, p is the power that controls the significance of points (high values assigns to the nearest points more influence and vice versa), d_{ij} the distance from sample point i to the estimated point j, z_i is the sample value at point i (Setianto and Triandini 2013).

- Spline, is using polynomials passing from t defined points of a dataset, aiming to achieve the best curve fitting to approximate the dataset's missing values (Schoenberg 1946). The formula for the interpolation in point $S(x,y) = T(x,y) + \sum_i^N \lambda_i R(r_{(i)})$ where i=1,2,3,…,N, N is the number of points, λ_i are coefficients found by linear equation, $r_{(i)}$ is the distance from the point (x,y) to the ith point, $T(x,y)$ and are $R(r_{(i)})$ defined differently, depending on the selected option.

- Natural Neighbor (NN), a method that works better for scatter sample points, suitable for categorical data that are included in homogeneous value Voronoi polygons (Voronoi 1908). It has the same equation with IDW for constructing polygons. In this method a new Voronoi diagram is designed around the interpolation point, the weights that are applied to the prediction value are relative to the overlap area of the neighbor polygons (Sibson 1981).

- Kriging, a geostatistical technique that is based on autocorrelation, takes the relations between the grid points such as distance or direction into account and tries to correlate them to predict the missing data. The prediction model at a point is defined: $Z(s) = \mu + \varepsilon(s)$ where s are the coordinates of a sample location, μ is the deterministic trend and ε the autocorrelation errors (Johnston et al. 2003). More specifically, in order to estimate a point without measurement, it calculates the linear weighted average values of the neighbor's measurements. The prediction equation as a summary of weighted samples is $Z(s_0) = \sum_i^n \lambda_i z(s_i)$ where n, i are the number of neighbors and the search points, λ are the weights and z the measured values at location s. The summary of the weights must be $\sum_i^n \lambda_i = 1$. The weight of each point is derived by a matrix $C = A^{-1}b$ where A is a matrix of a semivariance between the points and b is a vector estimated from the semivariance between the measured and the predicted points (Setianto and Triandini 2013). The most common types of Kriging are the Universal, the Ordinary and the Simple. The Universal Kriging variation is predicting values with a trend which is controlled only by the dataset's coordinates. The Ordinary Kriging is a variation of the original method with one main difference, the assumption that the mean value μ is unknown and constant only for local areas while for Simple Kriging the μ is known and constant (Johnston et al. 2003)

All the aforesaid methods have been tested with various examples to examine the interpolation output. While the results have strong similarities, especially between NN and Kriging, the final decision was not to use the deterministic models such as the IDW and adopt for the analysis the Kriging geostatistical method. The main reason for taking this choice, was the fact that the mathematic formulas in techniques such as IDW and Spine are not able to consider the possible inhomogeneities due to the geology and the local site effects that could affect the results. Having two SGM stations at a close distance doesn't mean that they have the same geological material and the same site effects. Additionally, in the Kriging technique there is the possibility to use specific parameters to give a trend to the predicted values. Moreover, the research of Yasrebi et al. (2009), which compared different interpolation methods aiming to examine the variations of chemical properties such as pH, electrical conductivity and others, has proven that the predictive capabilities of Ordinary Kriging are better compared to the IDW method, especially in cases where there is a distribution of the different quantities in a non-uniform media such as soil. The validation method for their results was based on Jackknife resampling method which was developed by Quenouille (1949) and refined by Tukey (1958). In this technique, a number of iterations is performed, on every loop a measurement is removed from the dataset and the interpolation is completed with the remaining values.

4.2.3 Interpolation procedure

Aiming to present the ground acceleration values recorded from the SGM network, PGA distribution maps were created in ArcGIS environment. The interpolation process first step, is to insect to the ArcGIS software the dataset with the PGA values and the corresponding stations coordinates to create a grid surface layer on a map. The Geostatistical Analyst Toolbox has an option that is used to explore the dataset with statistics such as mean, standard deviation, skewness, kurtosis to name a few. The toolbox produces histograms that can be used to examine the dataset if it belongs to a normal distribution (kurtosis near 3) or another type of distribution (figure 4.5). Although Kriging does not require data to be normally distributed, it works better and unbiassed if there are. Additionally, Kriging assumes that the random interpolation errors have zero mean value, the covariance (the measure of how much two random variables vary together) between errors is controlled only by the distance and the direction between them and it also assumes the multivariate (a number of independent variables) that are used for constructing probability maps have normal distribution (Johnston et al. 2003). If the samples

are not normally distributed, a data transformation is applied to make them normal. In this research, the log transformation was used in cases that a transformation was necessary (for positive skewed data, the log transformation equation is $Y(s) = \ln(Z(s))$ where $Z(s)$ are the observed data and ln the natural logarithm).

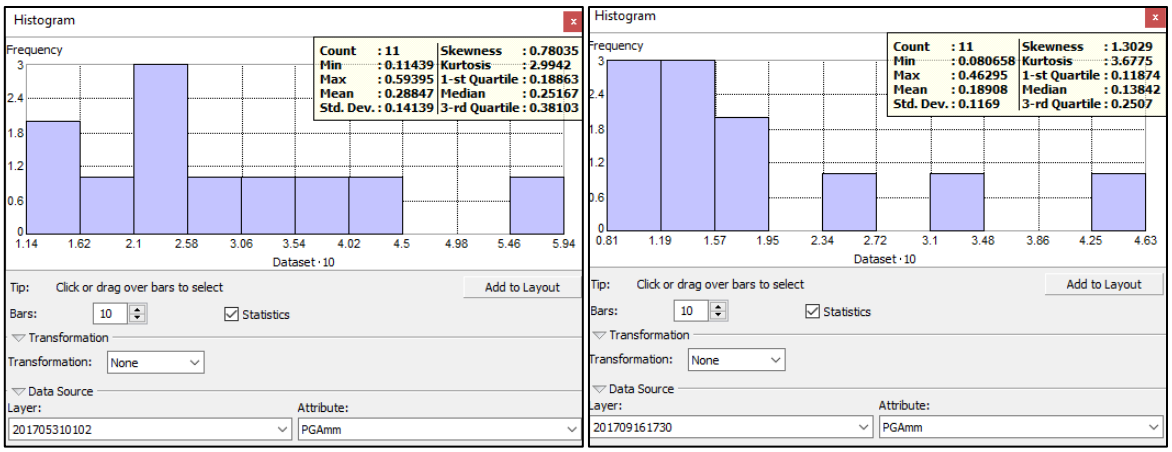

Figure 4.5 Two dataset examples, left one has normal distribution.

The next step after examining the dataset, is to choose the interpolation method. In the Geostatistical Analyst Toolbox, the Geostatistical wizard menu which have a list with the available interpolation methods, among the various interpolators are the variations of Kriging and Cokriging (universal, ordinary, simple and other types). The Cokriging method is similar with Kriging but it also incorporates additional covariates (variables that are well-sampled) and it tries to do the correlations among the poor with the well-sampled variables, it is more effective for data with significant intervariable correlation (Hong and Liu, 2012) At the first experimental stage of the SGM network, the interpolation images were produced with Ordinary Kriging method. In the next phase, the increase in the number of stations provided better spatial resolution maps and it permitted the use of more sophisticated interpolation methods, the Ordinary Cokriging method have been utilized. The Ordinary Cokriging equation to estimate a missing value is $Z(s_0) = \sum_i^n \left((\lambda_i z_1(s_i) + (\mu_i z_2(s_i)) \right)$ where n, i are the number of neighbors and the search points, λ, μ are the weights of the variables and z_1, z_2 the measured values at location s.The predominant frequency f_0 and amplitude A_0 values (the largest peak) obtained from the microtremors H/V spectral ratio in SGM stations' locations, are used as variables for Ordinary Cokriging for different case studies. The PGA along with f_0 and A_0 variables are fitted in empirical semivariograms which are used to examine the statistical correlation of the

PGA values versus the distance between all location pairs. Different semivariogram model equations (stable, spherical, tetraspherical, exponential to name a few) are used, aiming to find the optimal fitting between observed and empirical values (Isaaks and Srivastava 1989) (figure 4.6). Every single semivariogram model has been tested for each case, the ones that didn't have a good fitting were immediately rejected while the models that presented a good fitting were examined. There were two criteria for the selecting the best semivariogram model for each study case. First of all, the model must have the smallest interpolation errors between predicted and measured values. Secondly, the measured PGA values at the sample locations should remain as unchanged from the interpolation procedure as possible. The second criterion was applied because in some cases it was noticed that between two models with good fitting and similar errors, one of them presented significant reduced PGA values. An example is the 29/04/2017 22:39 event, the maximum measured value at PERI station from 21.17 was reduced to 16 mm/sec^2 with one model while for the same case with another model it remained unchanged.

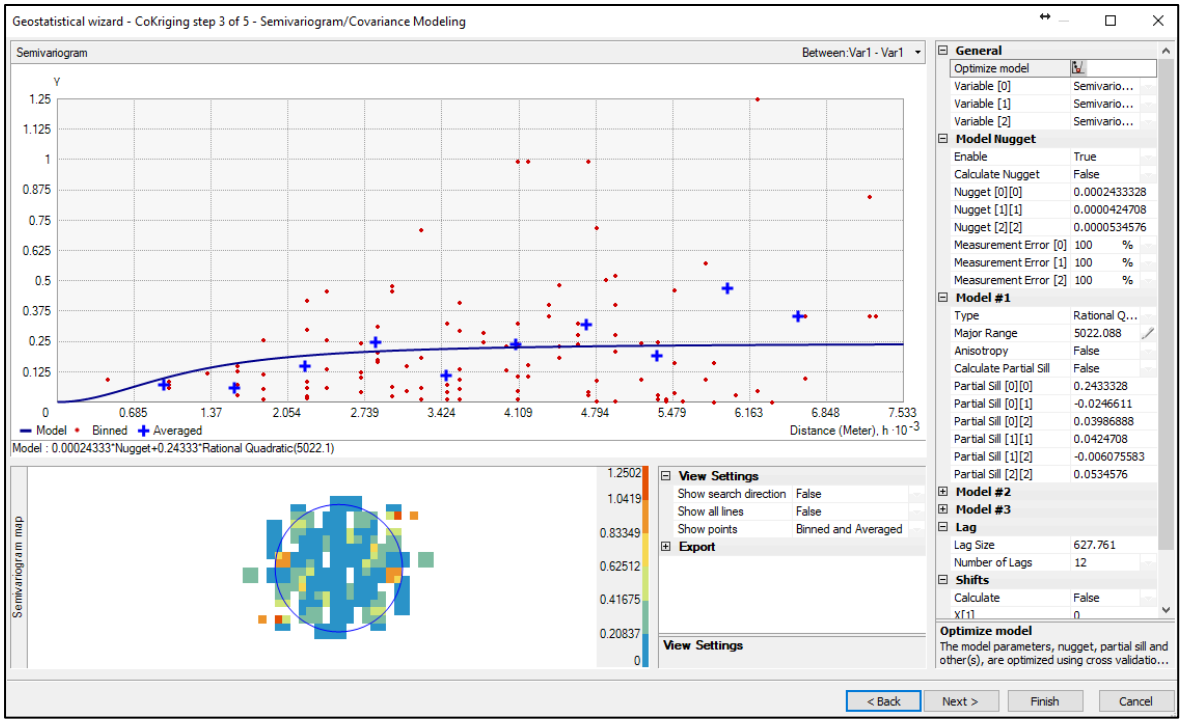

Figure 4.6 The observed average values (blue cross) are fitted in an empirical semivariogram (blue line), optimized with a model (Rational Quadratic in this case) to examine the statistical correlation.

Proceeding to the next part, there are some choices related with the neighborhood sampling area. For this work the maximum number of neighbors was set to 12, while the minimum was set to 6 to ensure that the interpolation has enough data to make the prediction. At the same time, another option regarding the research area around a point was selected to divide the area in 8 search sectors. These options were selected after trying several cases as they produced the smoother image results (figure 4.7) without altering the output values of the PGA.

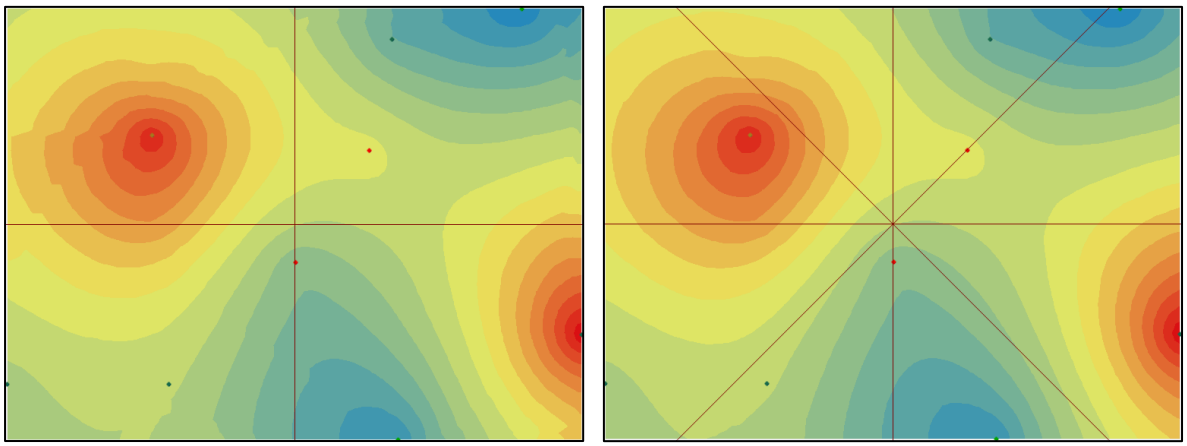

Figure 4.7 The image produced by selecting neighbors' values maximum 5 and minimum 2 in a 4-sector area (left) is rough and edgy. Setting for the same case the neighbors values to 12 and 6 and area type to 8-sector, is generating a smoother image (right).

In order to have a first classification of the events based on the azimuth of the earthquake locations, the Chania city was defined as the center of a circle, dividing the investigation area in four quartiles (SW, SE, NW and NE). In figures 4.8 to 4.15 are presented four cases, one of each quartile, with noticeable visual different result obtained using the f_0 and A_0 variables in cokriging. As it is mentioned in legends, on the upper part of the figures are the results interpolated with Ordinary Kriging and on the lower, are the ones with the Ordinary Cokriging method. The blue color areas are denoting low values of PGA while as the acceleration values gradually increases as the color change to red. In ArcGIS there is an option to do cross-validation analysis which can compare the results from two different prediction methods. The cross-validation analysis has been used to demonstrate the fitting results between Ordinary Kriging and Ordinary Cokriging. Examples from cross-validation analysis with numerical results which suggest that the use of f_0 and A_0 is improving the interpolation are illustrated in figures 4.16 to 4.23. In each of the comparing diagrams, the predicted against the measured values and the related fitting errors are presented. Details will be presented in the next chapter.

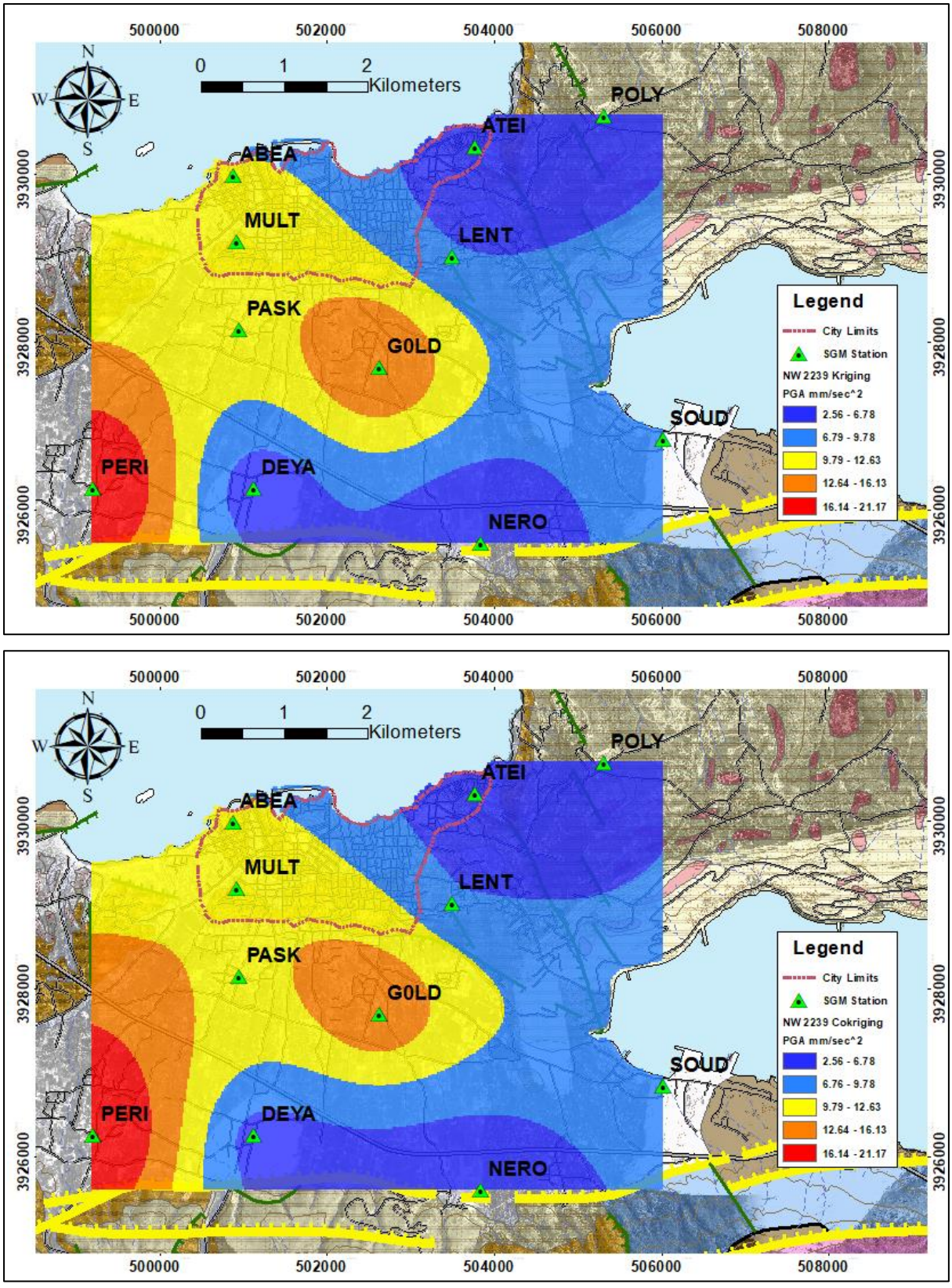

Figure 4.8 The PGA distribution as it presented from interpolation Ordinary Kriging (up) and Ordinary Cokriging, the epicenter is 18 km away northwest of Chania with local magnitude 3.3 (29/04/2017 22:39 UTC).

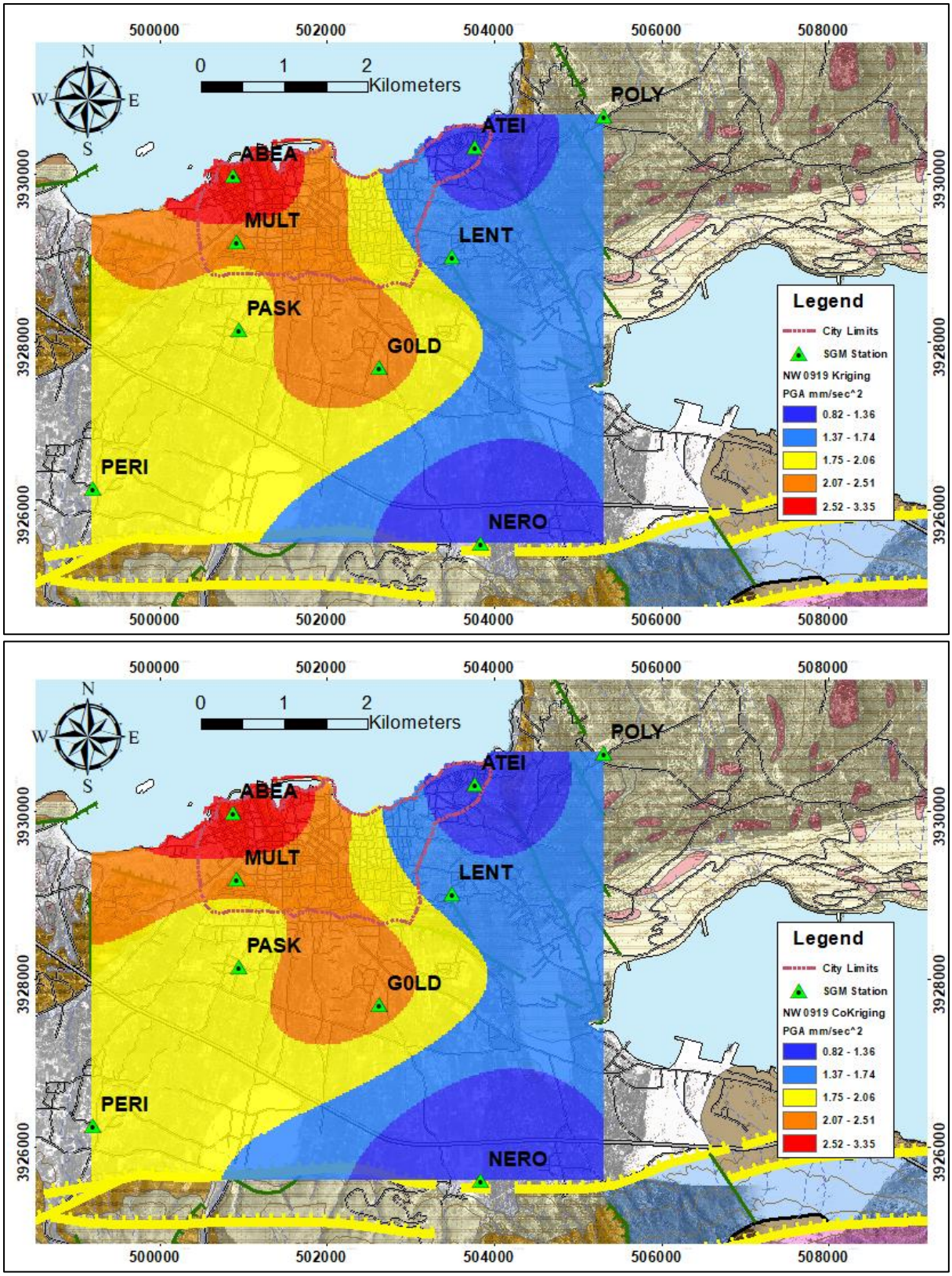

Figure 4.9 The PGA distribution as it presented from interpolation with Ordinary Kriging (up) and Ordinary Cokriging, the epicenter is 13 km away northwest of Chania with local magnitude 2.4 (22/01/2017 09:19 UTC).

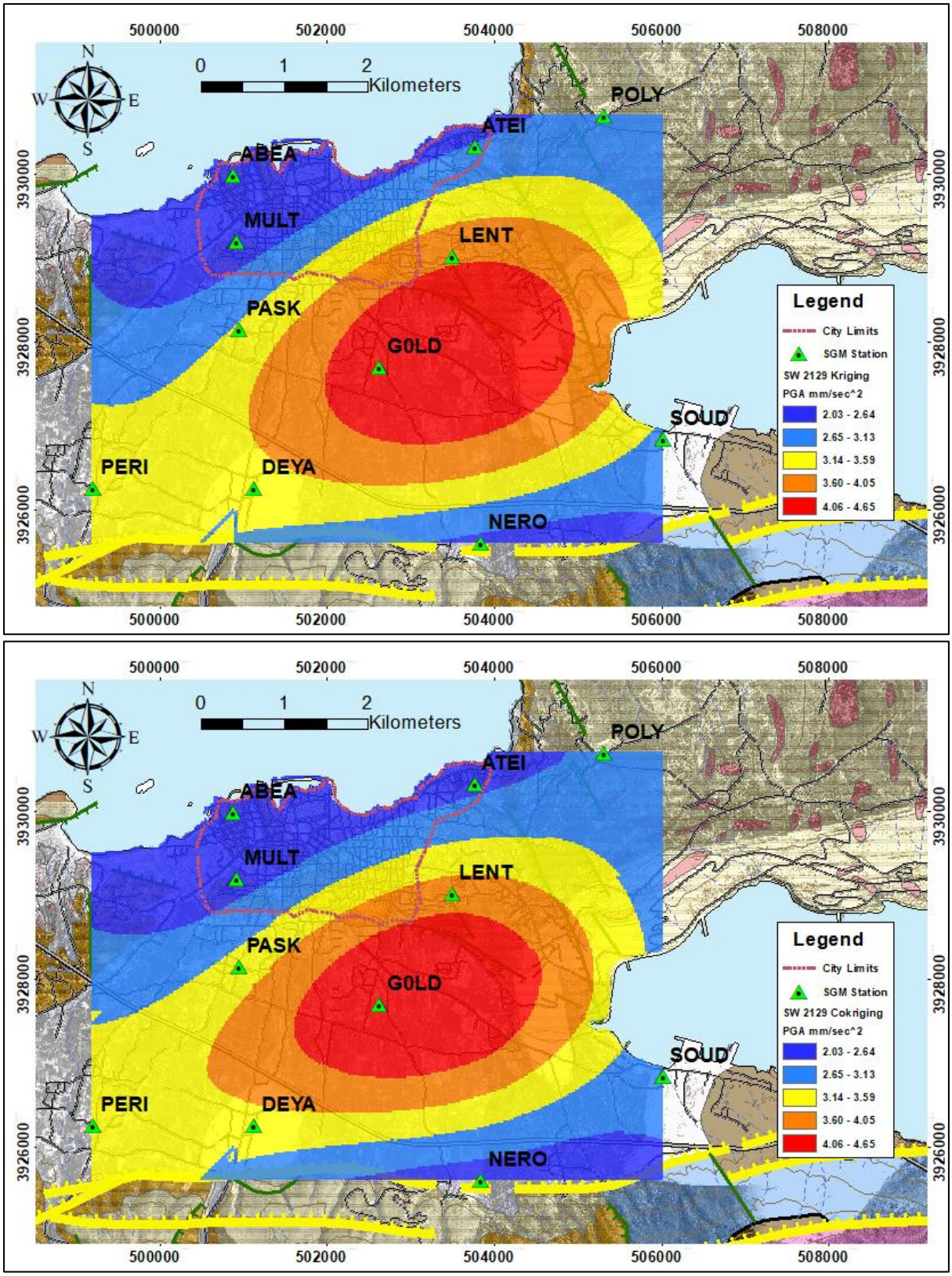

Figure 4.10 The PGA distribution as it presented from interpolation with Ordinary Kriging (up) and Ordinary Cokriging, the epicenter is 152 km away southwest of Chania with local magnitude 5.5 (31/07/2017 21:29 UTC).

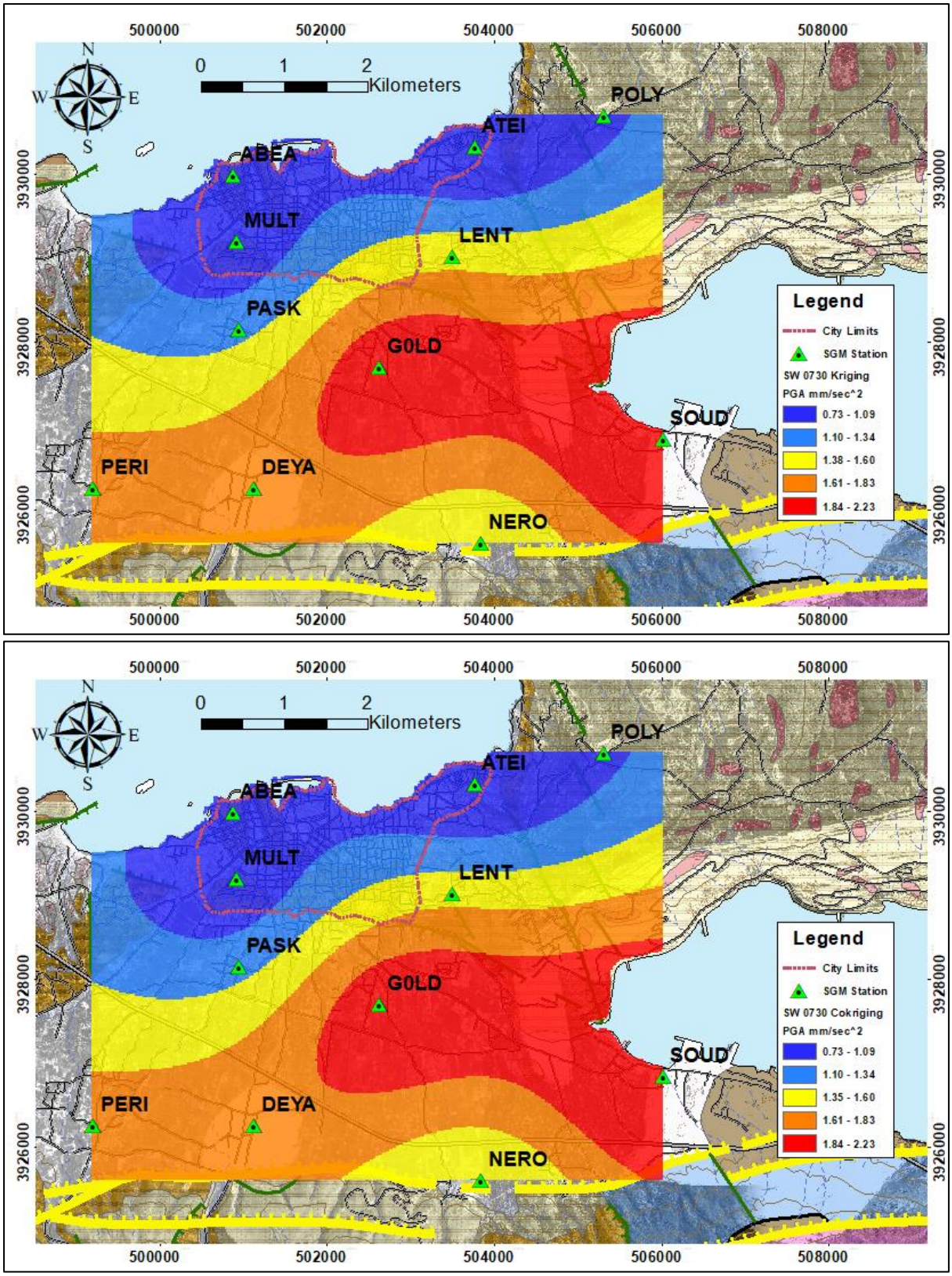

Figure 4.11 The PGA distribution as it presented from interpolation with Ordinary Kriging (up) and Ordinary Cokriging methods, the epicenter is 155 km away southwest of Chania with local magnitude 4.8(13/12/2017 07:30 UTC).

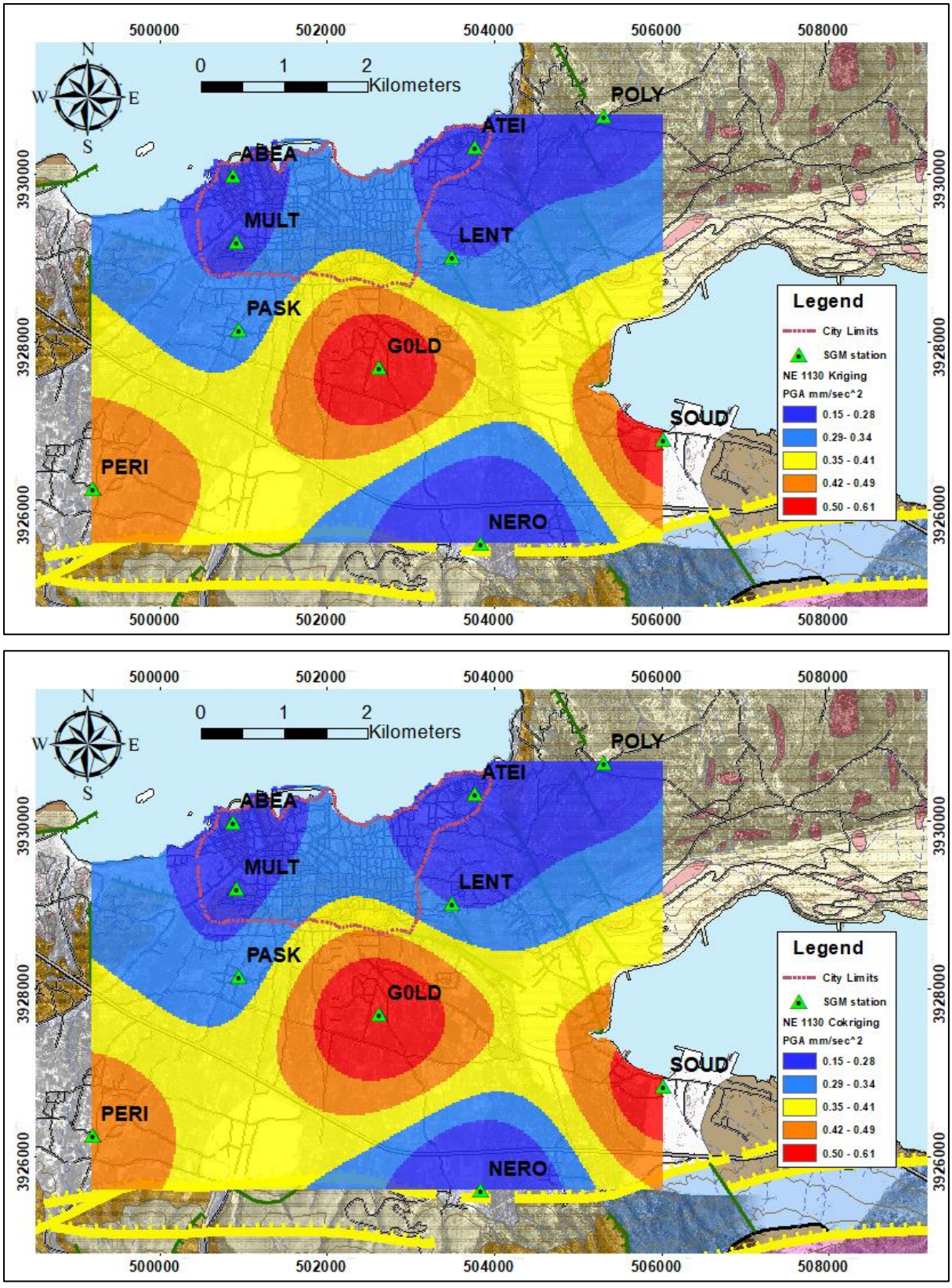

Figure 4.12 The PGA distribution as it presented from interpolation with Ordinary Kriging (up) and Ordinary Cokriging, the epicenter is 316 km away northeast of Chania with local magnitude 5.1 (17/05/2017 11:30 UTC).

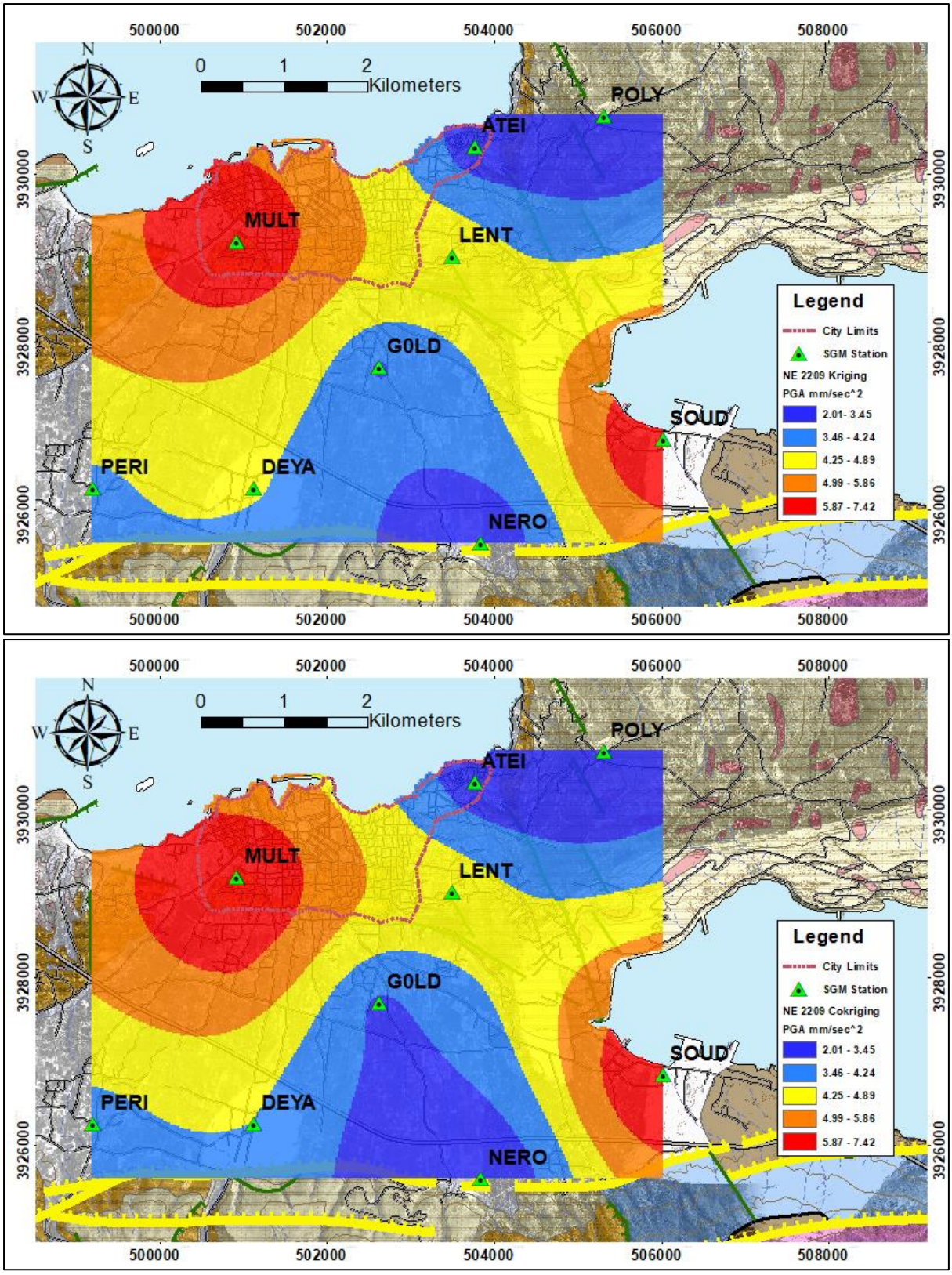

Figure 4.13 The PGA distribution as it presented from interpolation with Ordinary Kriging (up) and Ordinary Cokriging, the epicenter is 64 km away northeast of Chania with local magnitude 4.1 (26/01/2018 22:09 UTC).

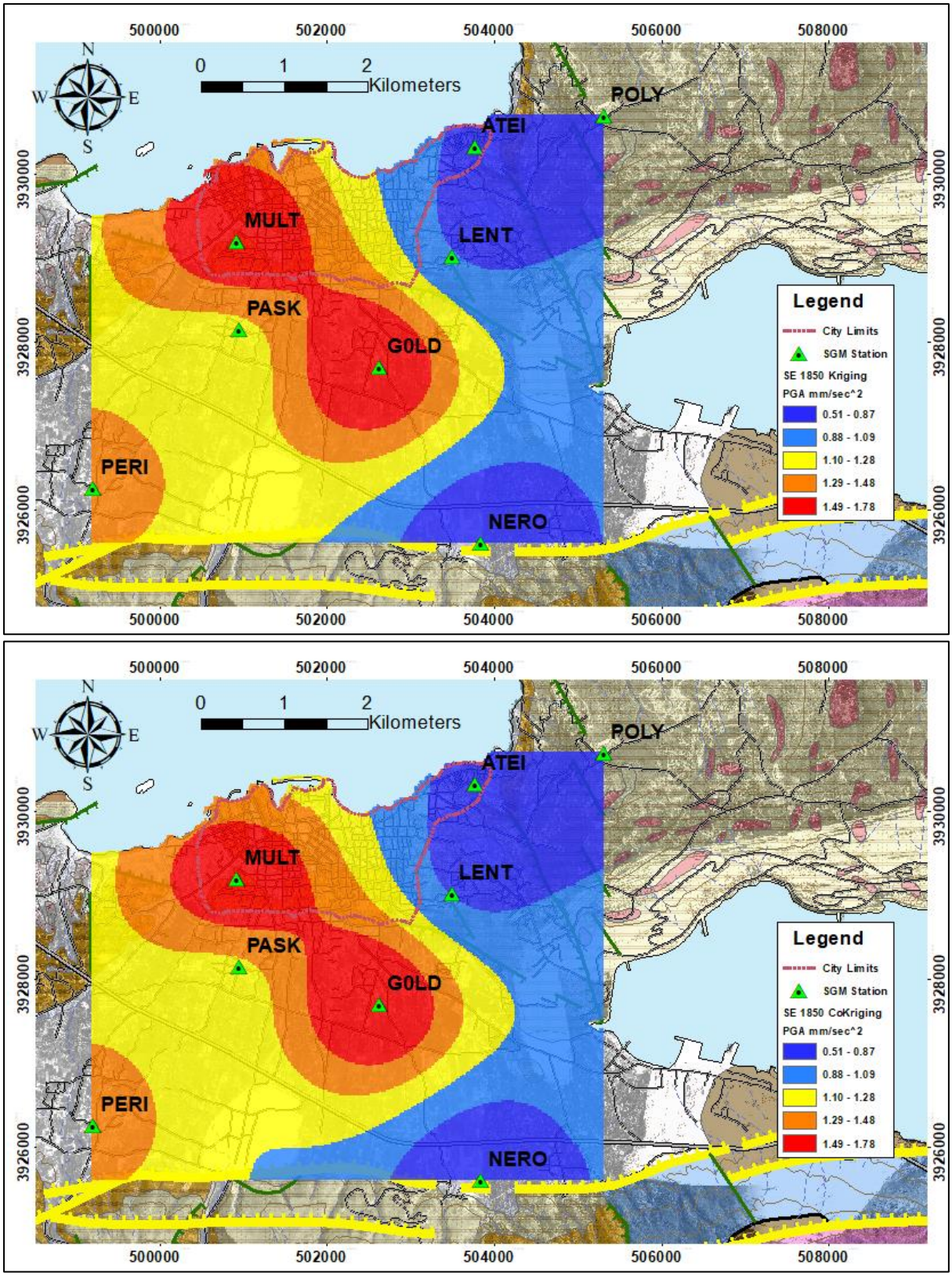

Figure 4.14 The PGA distribution as it presented from interpolation with Ordinary Kriging (up) and Ordinary Cokriging, the epicenter is 220 km away southeast of Chania with local magnitude 5.4 (25/01/2017 18:50 UTC).

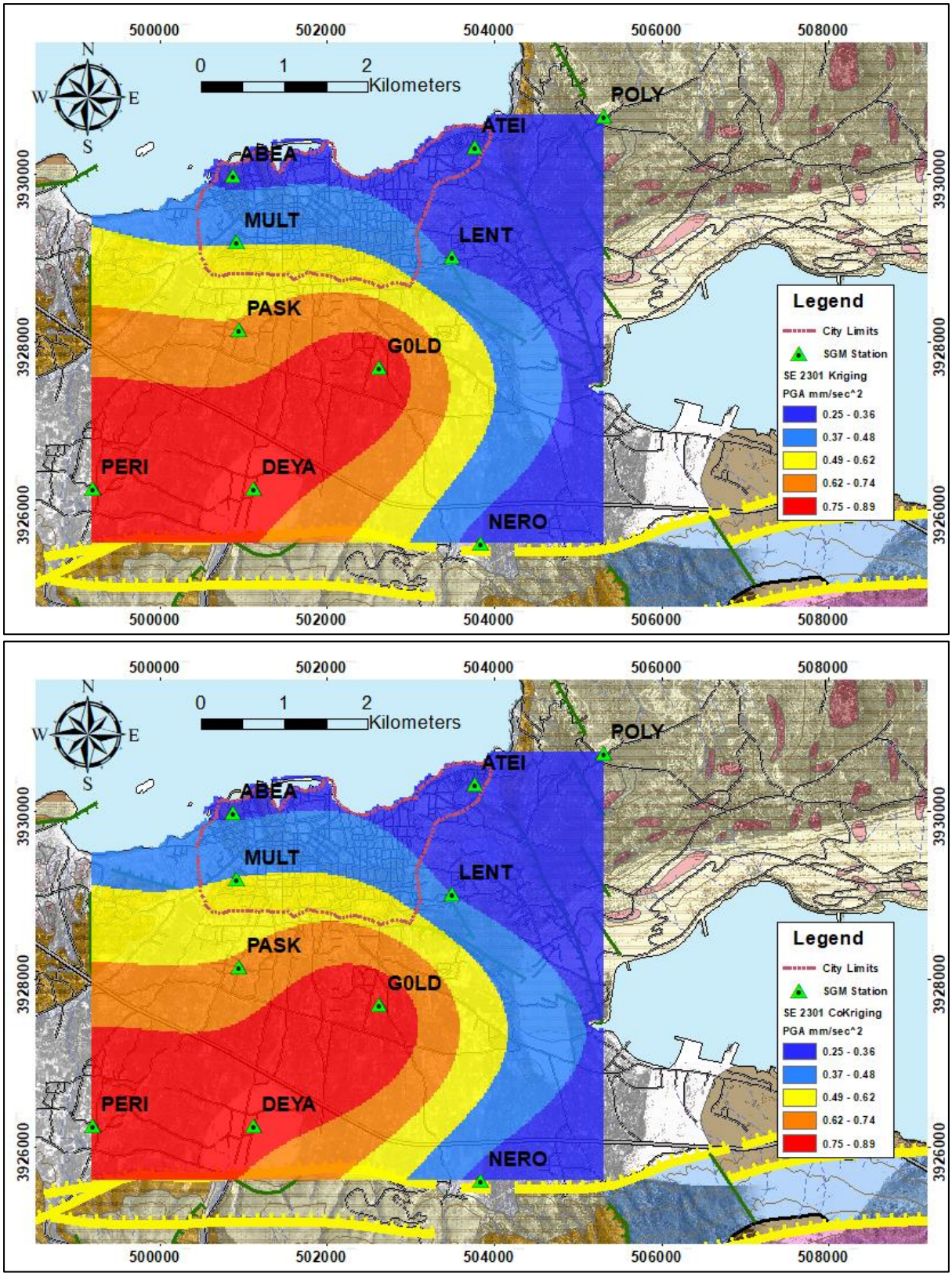

Figure 4.15 The PGA distribution as it presented from interpolation with Ordinary Kriging (up) and Ordinary Cokriging, the epicenter is 117km away southeast of Chania with local magnitude 4.5 (15/02/2017 23:01UTC).

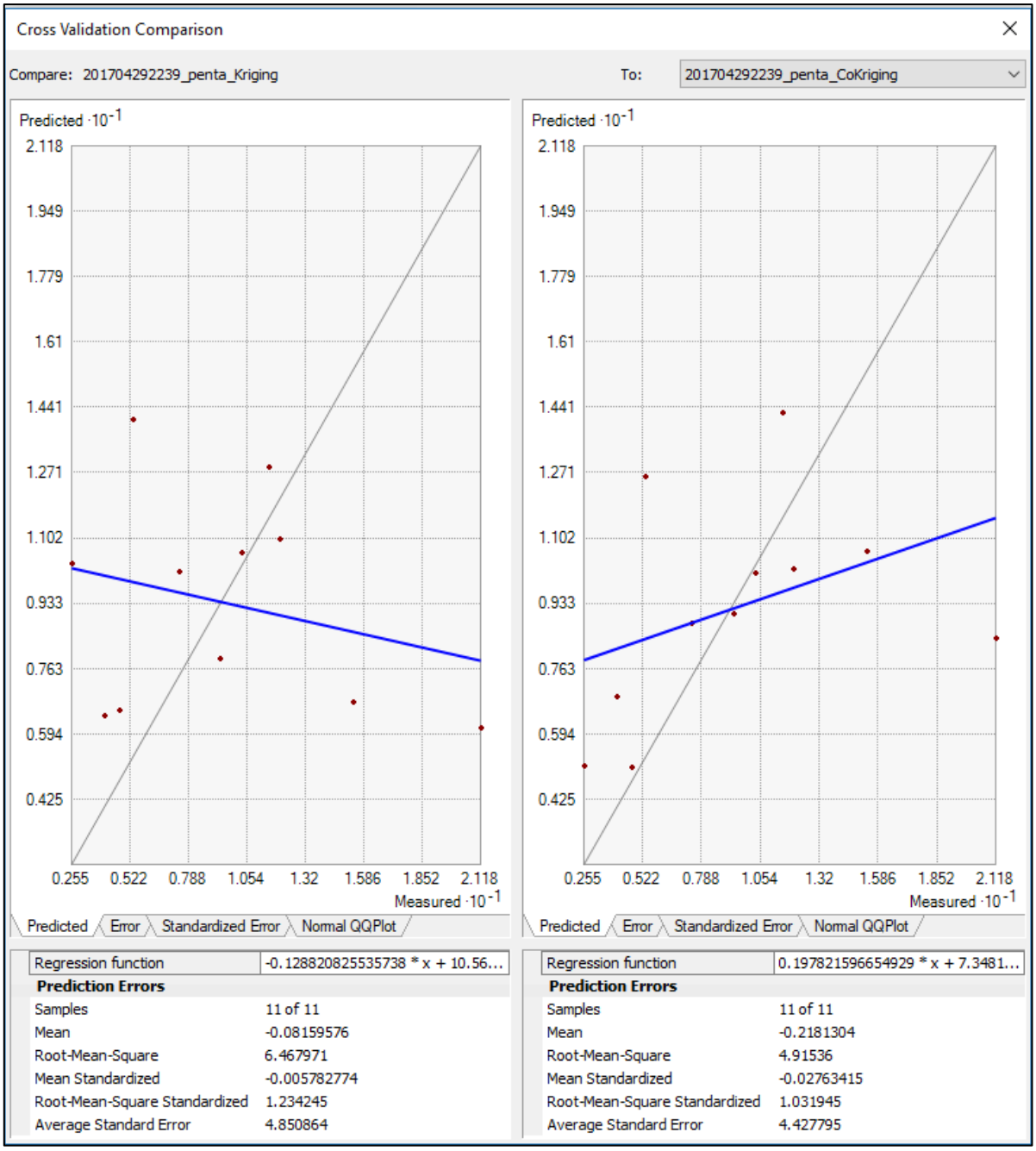

Figure 4.16 The numerical example for a northwest direction event (2017/04/29 22:39 UTC) that supports the idea of using f_0 and A_0 values, obtained from H/V analysis as parameters to control the interpolation output. In this cross-validation analysis, the left diagram presents in a least squares sense the regression of the predicted values from Ordinary Kriging interpolation against the measured ones. In the other diagram, the illustrated regression has depended variable the predicted values from Ordinary Cokriging.

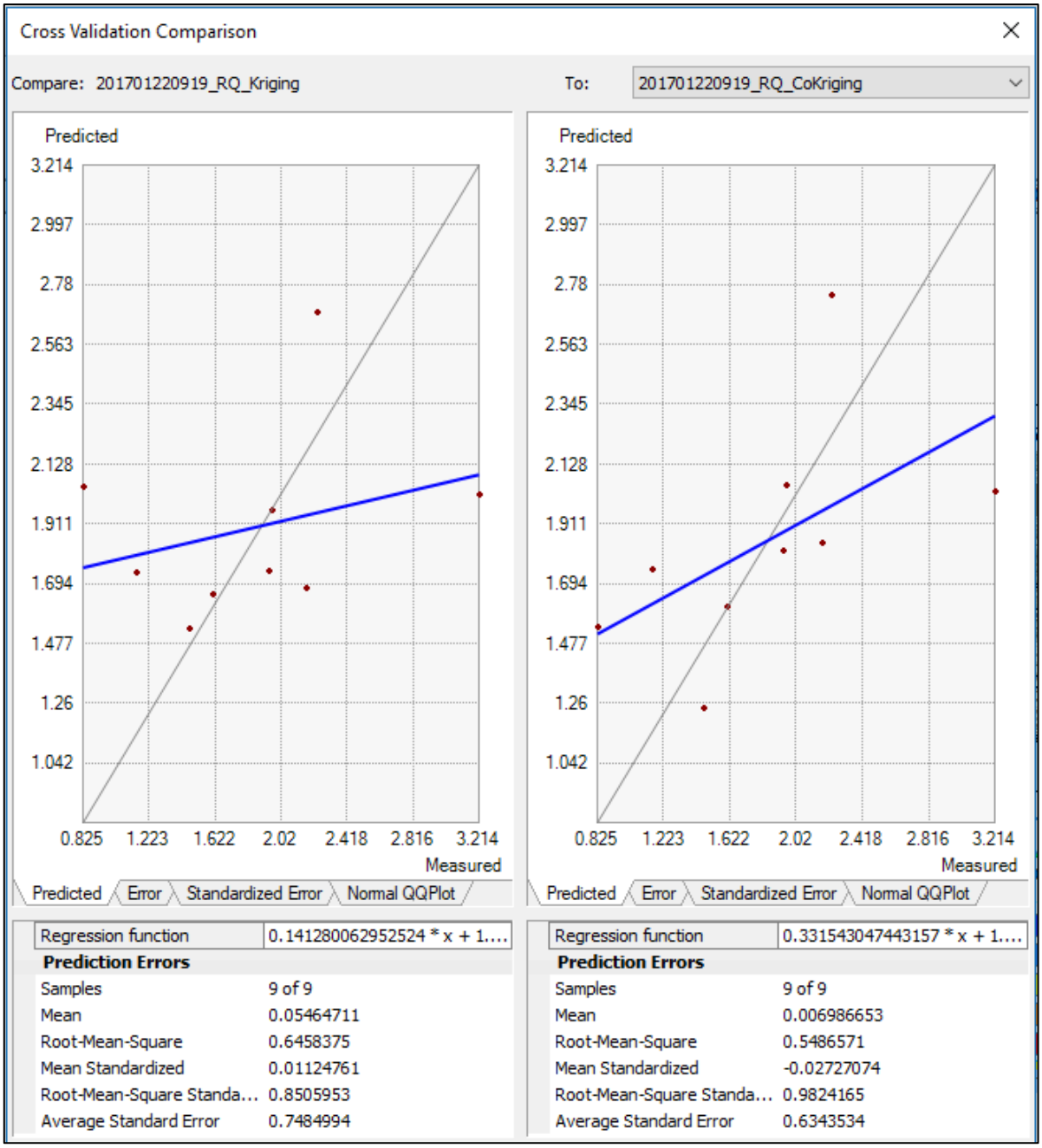

Figure 4.17 The numerical example for a northwest direction event (2017/01/22 09:19 UTC) that supports the idea of using f_0 and A_0 values, obtained from H/V analysis as parameters to control the interpolation output. In this cross-validation analysis, the left diagram presents in a least squares sense the regression of the predicted values from Ordinary Kriging interpolation against the measured ones. In the other diagram, the illustrated regression has depended variable the predicted values from Ordinary Cokriging.

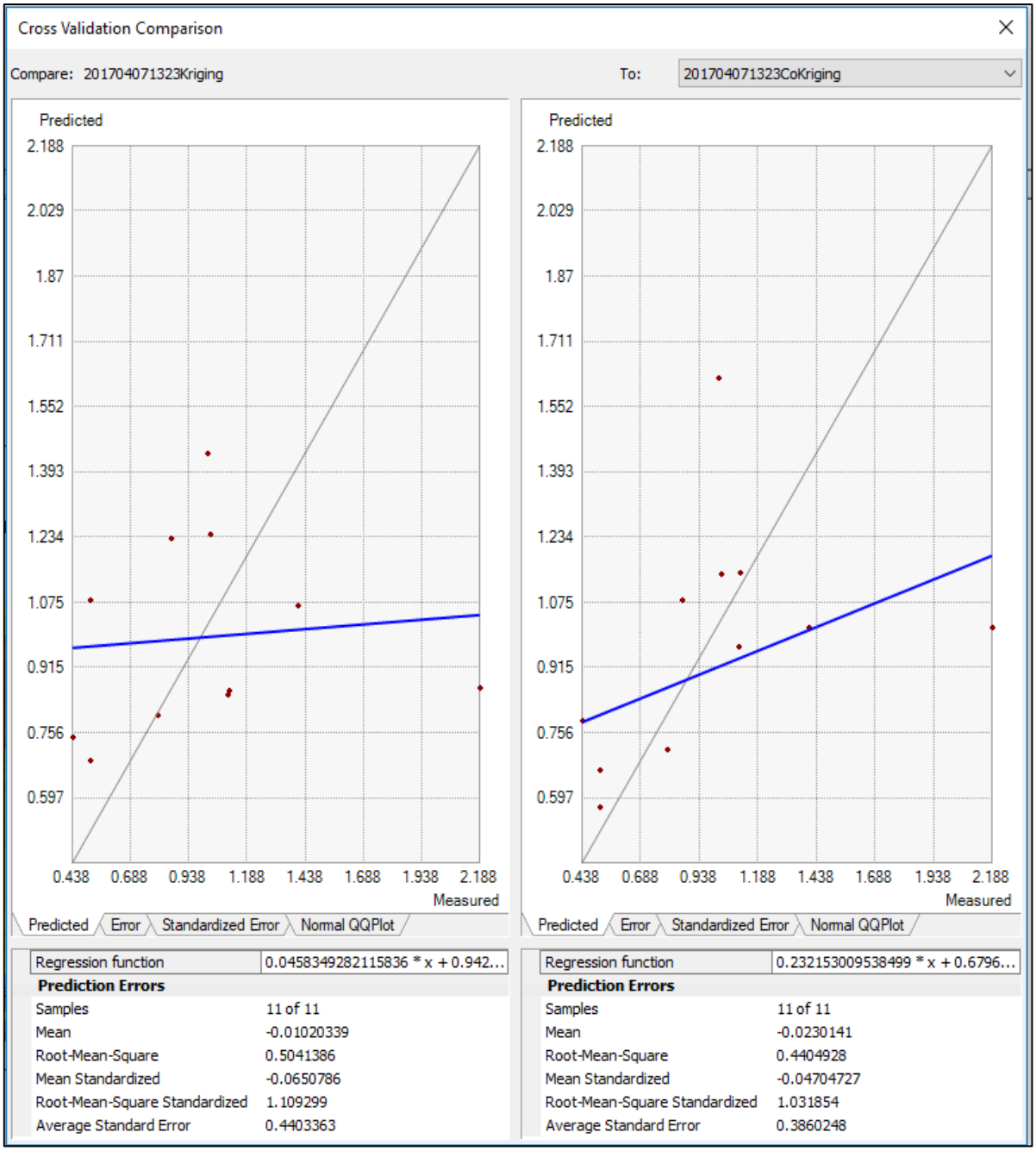

Figure 4.18 The numerical example for a southwest direction event (2017/04/07 13:23 UTC) that supports the idea of using f_0 and values, obtained from H/V analysis as parameters to control the interpolation output. In this cross-validation analysis, the left diagram presents in a least squares sense the regression of the predicted values from Ordinary Kriging interpolation against the measured ones. In the other diagram, the illustrated regression has depended variable the predicted values from Ordinary Cokriging.

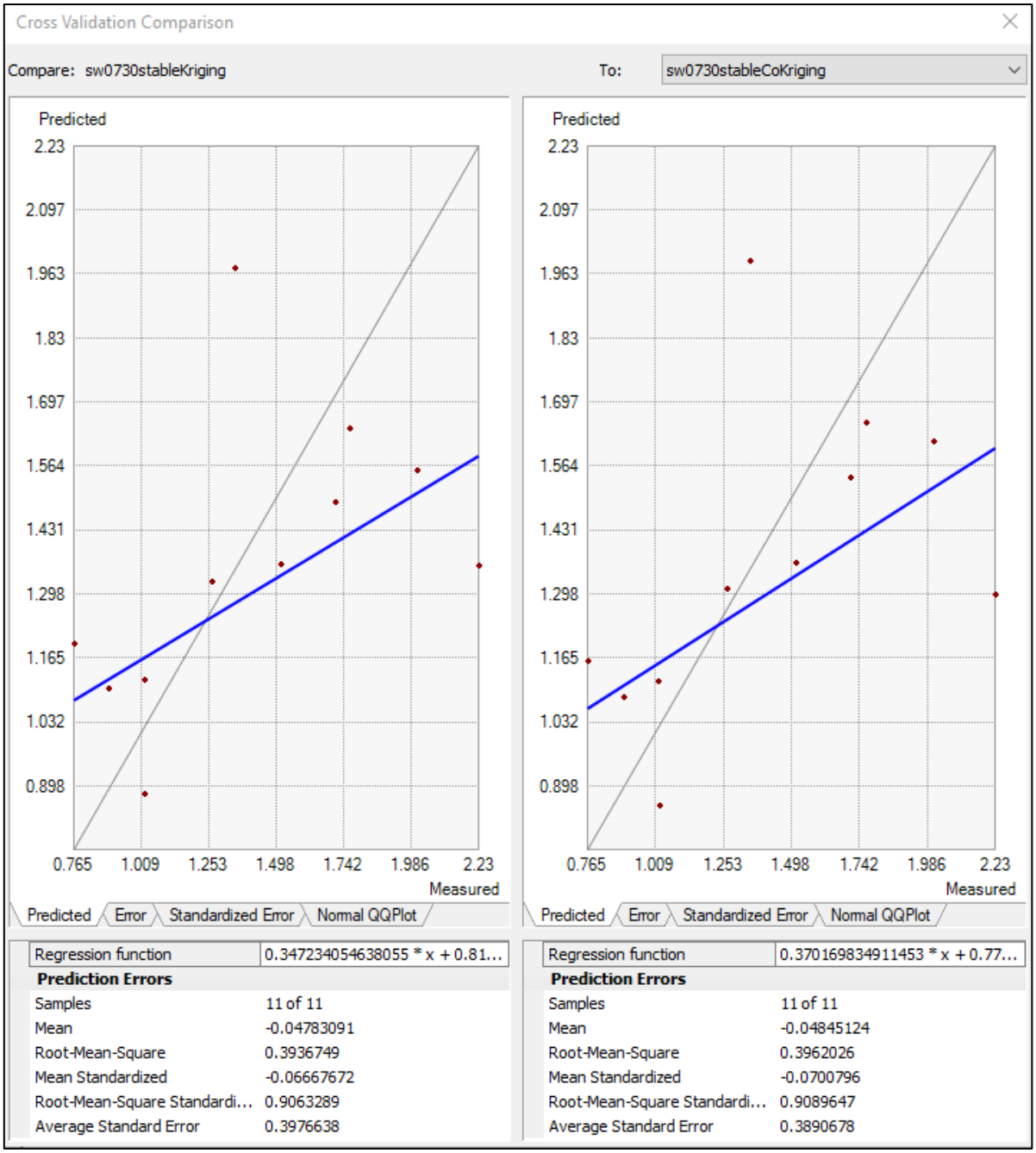

Figure 4.19 The numerical example for a southwest direction event (2017/12/13 07:30 UTC) that supports the idea of using f_0 and A_0 values, obtained from H/V analysis as parameters to control the interpolation output. In this cross-validation analysis, the left diagram presents in a least squares sense the regression of the predicted values from Ordinary Kriging interpolation against the measured ones. In the other diagram, the illustrated regression has depended variable the predicted values from Ordinary Cokriging.

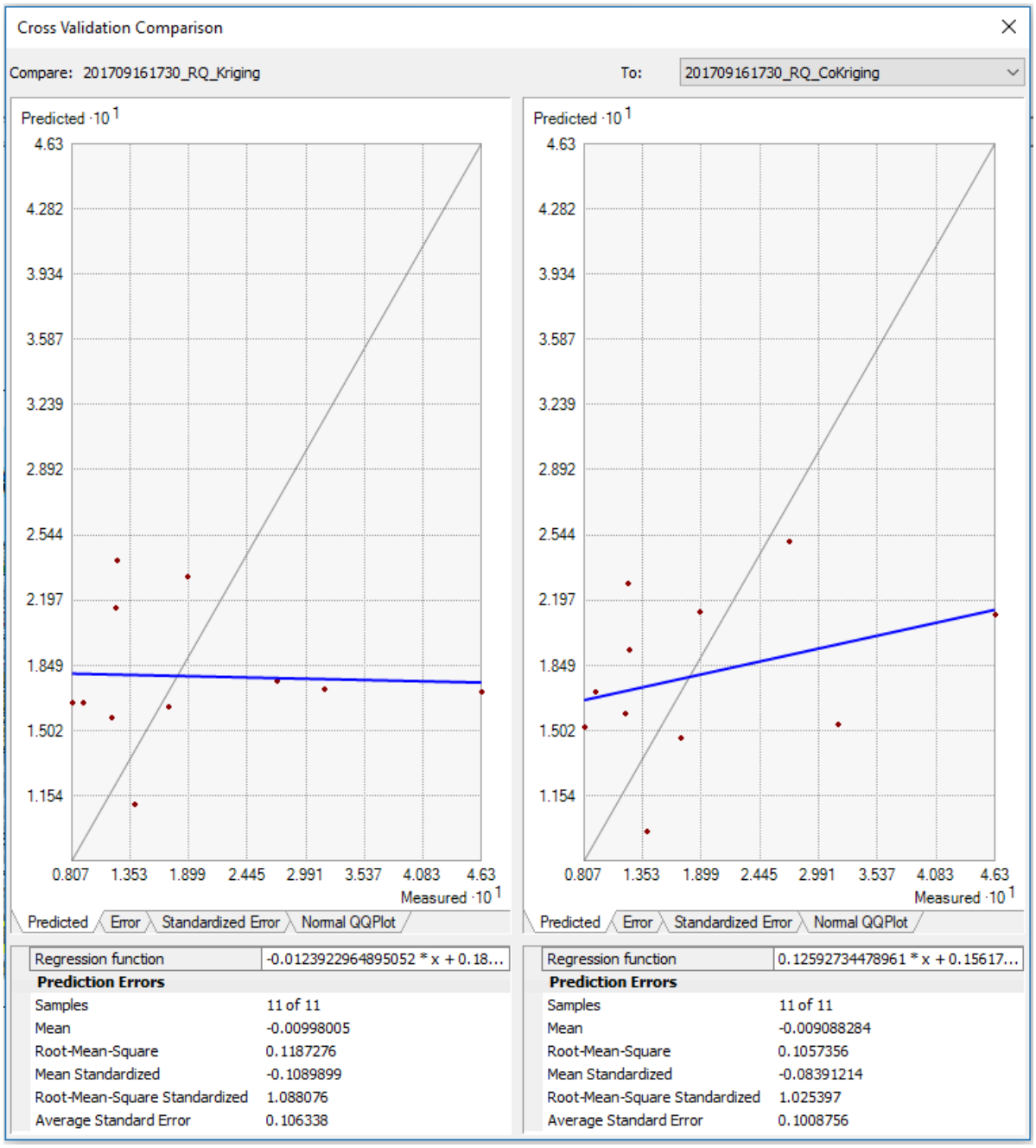

Figure 4.20 The numerical example for a northeast direction event (2017/09/16 17:30 UTC) that supports the idea of using f_0 and A_0 values, obtained from H/V analysis as parameters to control the interpolation output. In this cross-validation analysis, the left diagram presents in a least squares sense the regression of the predicted values from Ordinary Kriging interpolation against the measured ones. In the other diagram, the illustrated regression has depended variable the predicted values from Ordinary Cokriging.

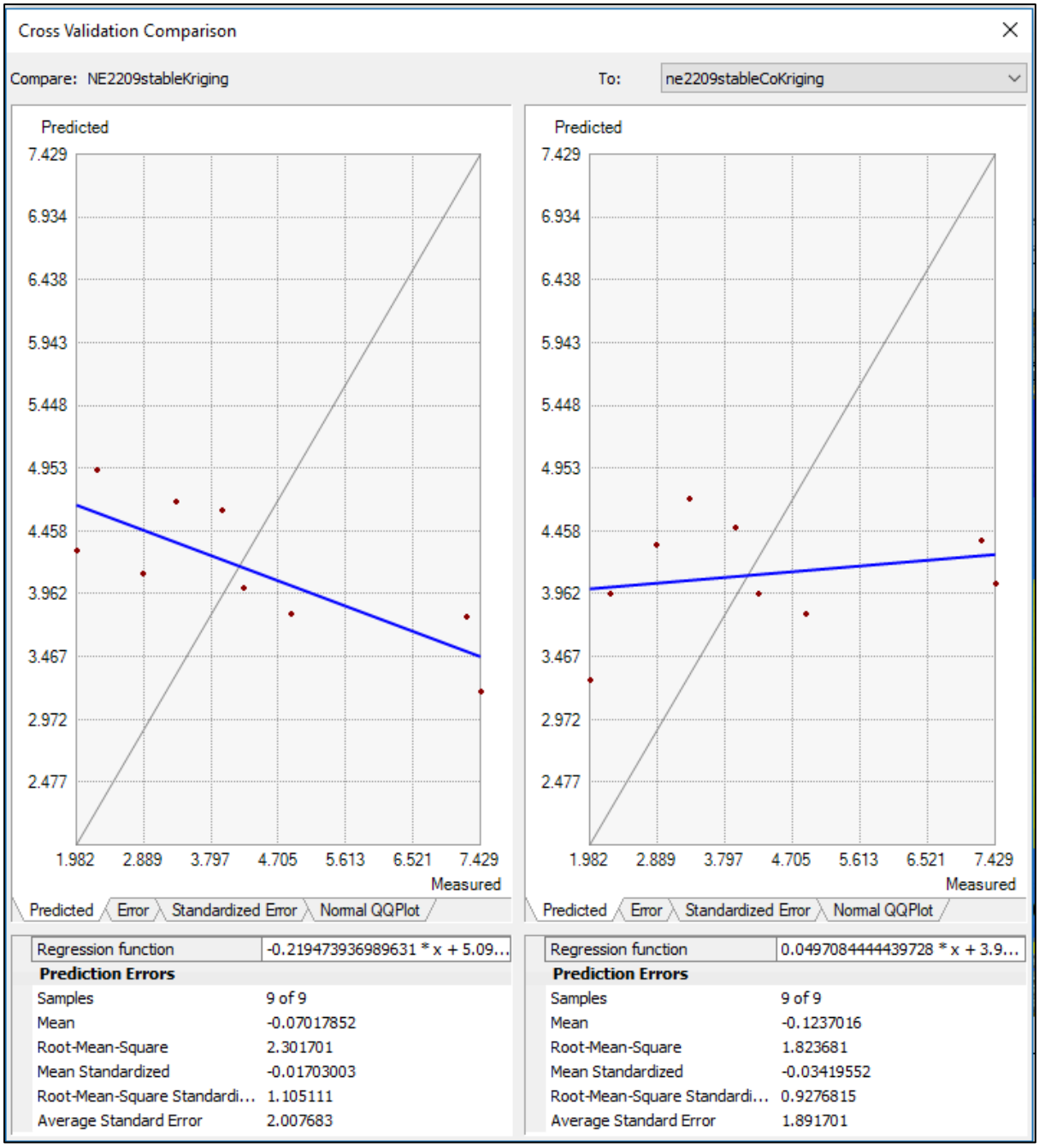

Figure 4.21 The numerical example for a northeast direction event (2018/01/26 22:09 UTC) that supports the idea of using f_0 and A_0 values, obtained from H/V analysis as parameters to control the interpolation output. In this cross-validation analysis, the left diagram presents in a least squares sense the regression of the predicted values from Ordinary Kriging interpolation against the measured ones. In the other diagram, the illustrated regression has depended variable the predicted values from Ordinary Cokriging.

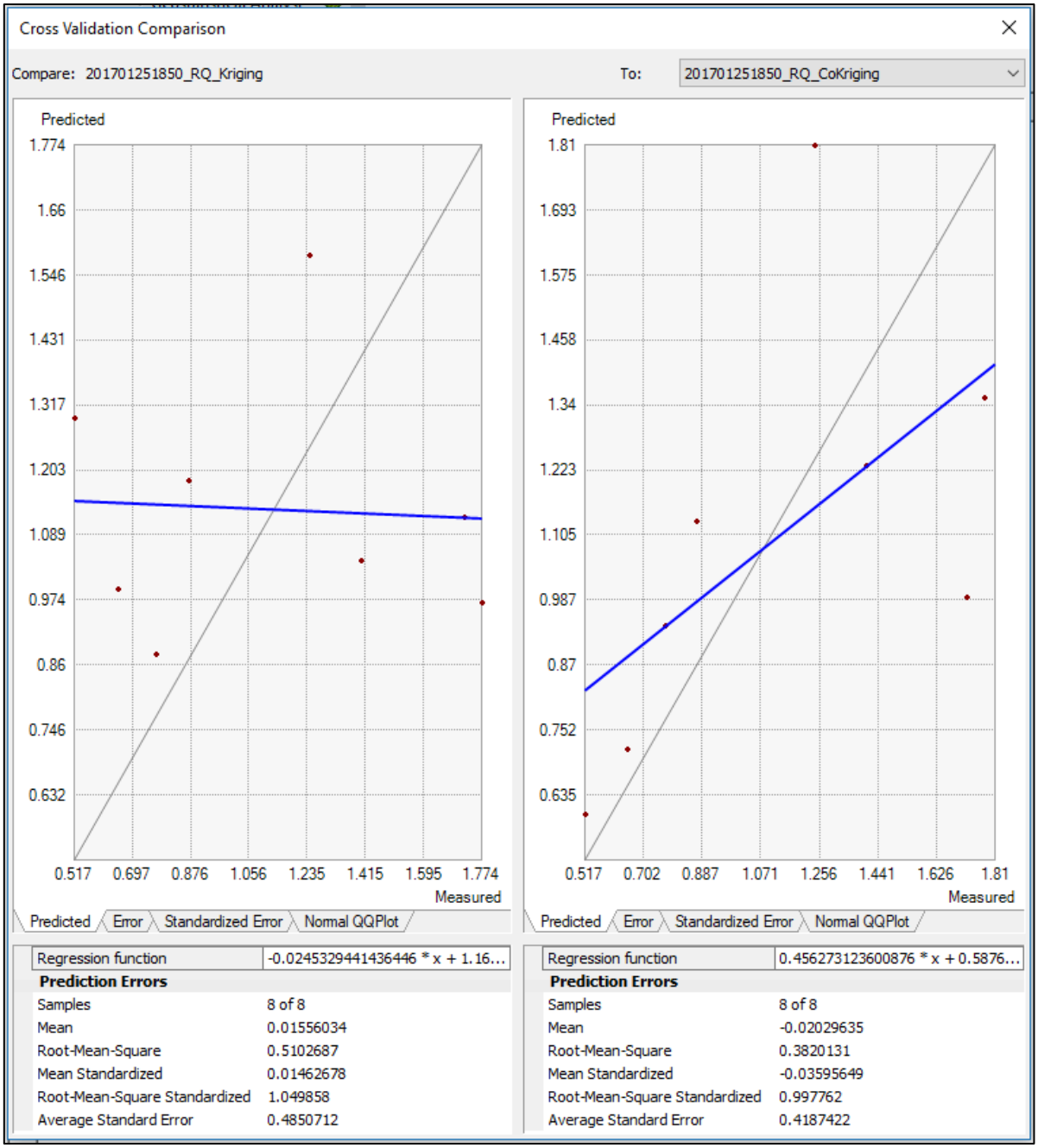

Figure 4.22 The numerical example for a southeast direction event (2017/01/25 18:50 UTC) that supports the idea of using f_0 and A_0 values, obtained from H/V analysis as parameters to control the interpolation output. In this cross-validation analysis, the left diagram presents in a least squares sense the regression of the predicted values from Ordinary Kriging interpolation against the measured ones. In the other diagram, the illustrated regression has depended variable the predicted values from Ordinary Cokriging.

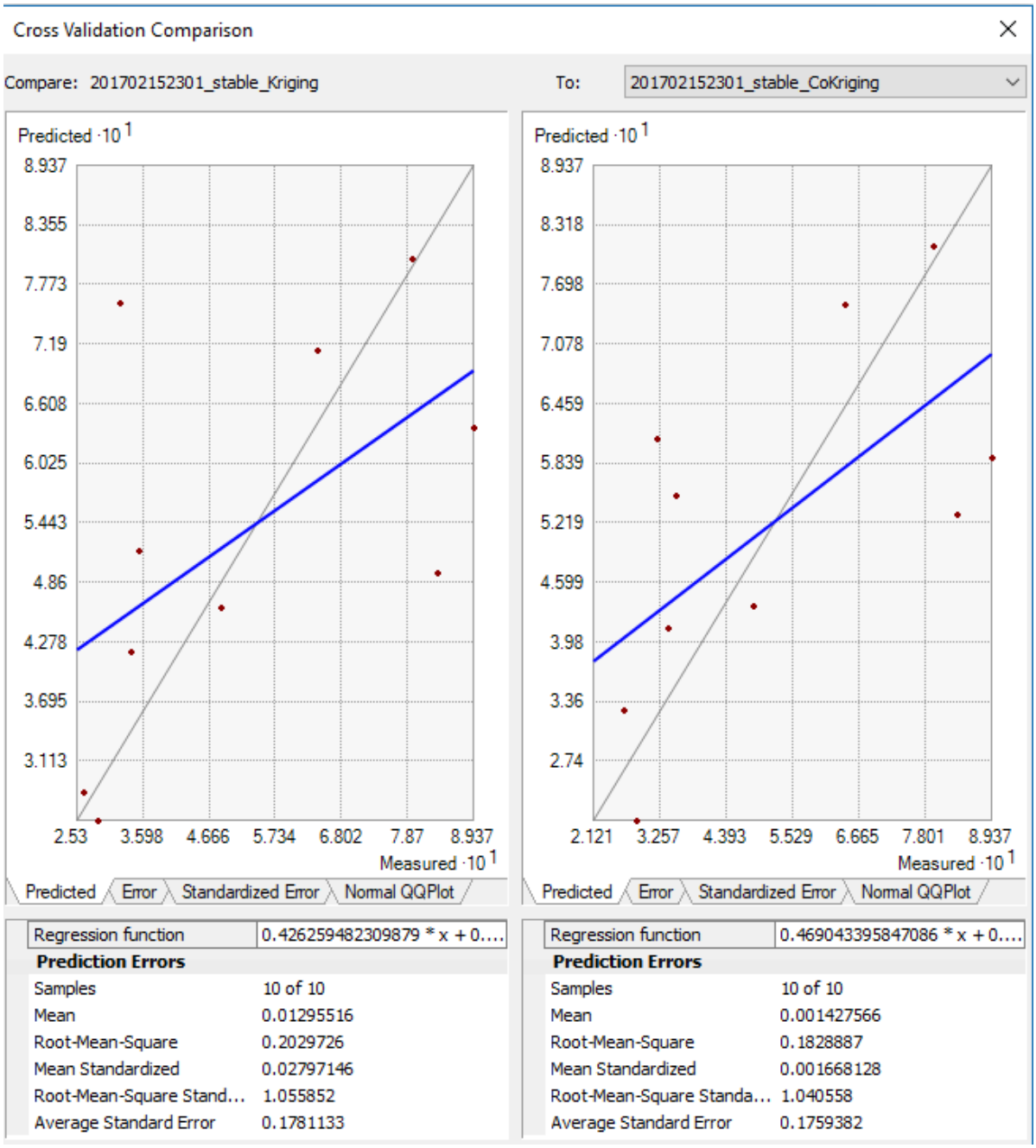

Figure 4.23 The numerical example for a southeast direction event (2017/02/15 23:01 UTC) that supports the idea of using f_0 and A_0 values, obtained from H/V analysis as parameters to control the interpolation output. In this cross-validation analysis, the left diagram presents in a least squares sense the regression of the predicted values from Ordinary Kriging interpolation against the measured ones. In the other diagram, the illustrated regression has depended variable the predicted values from Ordinary Cokriging.

5 Results

The installation of the initial first 6 stations since 2015 in the experimental phase, produced some interesting results that suggest the continuity of this project. Gradually more stations were added to cover the wide area of Chania city and its southern basin. The successful set up of the 14 SGM station to the broader area, allowed the creation of more detailed PGA maps and at the same time it was possible to study various parameters related to the acceleration distribution in the different geological formations. All the available instruments are constantly recording the ground motions and the metadata are stored to the HSNC servers. Examining the various recordings from the two years of the SGM network operation the 24bit accelerometers capabilities permit to accurately examine events with acceleration values down to 0.5 mm/sec^2 while the 16bit sensors can provide data from two orders of magnitude above the Ref Tek ones. The choice to install instruments in the urban environment in the municipality of Chania and other similar type of buildings was cost effective solution.

The new H/V microtremor measurements on the SGM station location are in good agreement with the previous investigations in the research area. Every station was considered as a single point and three measurements near the SGM sensor have been carried out. The results from all the examined locations present one peak in low frequencies between 0.33 and 0.63 Hz with an exception the DEYA station which has a second low frequency peak at 0.92 Hz. In six stations (ABEA, ARSN, ATIK, MULT, PASK and SOUD), there is a second peak f_1 in the high frequencies (1.78 to 3.92) which can be attributed to the seismic wave velocities contrast between Quaternary and Neogene sediments. The resonance amplitude presents significant larger values for the thick part of Quaternary deposits with a maximum value slightly above 4.0. The H/V results have been separated in 4 groups according to the geological formation and their spectral ratio curve similarity (figure 5.1). The first case has four SGM stations (ATEI, LENT, MAIC and POLY) installed in municipality buildings located on the early Neogene limestone. The H/V results in these locations presents one small amplitude peak in the low frequencies 0.35-0.55Hz. This kind of peak shows that there are two formations with different seismic wave velocities, the one above (Neogene limestone) has materials less stiff than the layer bellow which is considered to be the bedrock. The second group based on the microtremors survey results on the SGM station locations (G0LD and PERI) presents similar low frequency peaks but with significant higher amplitudes which means the upper layer (Quaternary) has very loose material and its stiffness is considerably smaller than the bedrock's. In the third category there are the four stations (ABEA, ATIK, ARSN and MULT)

located on formations with materials such as late Neogene marles – marles with sandstone intercalations. The lower stiffness marle-type materials have been deposited on the relatively stiff early Neogene limestone which makes an additional seismic velocity contrast that is presented as a second low amplitude peak at the high frequencies. The last group has three cases (DEYA, PASK and SOUD) on the Quaternary deposits that present a second equal or higher amplitude peak in a higher frequency. This type of image shows that between the Quaternary and the bedrock there is another formation with loose material. The NERO station according to the geologic maps is installed on the Quaternary deposits and it should be in the second group. By taking into account the limestone outcrops in the station's location as well as the H/V results which suggest that there is a small thickness stiff material above the bedrock, the station NERO has been added to the first group. It seems that the Neogene limestone covered with very thin layer, few meters of alluvial sediments which are not producing an additional peak in H/V curves.

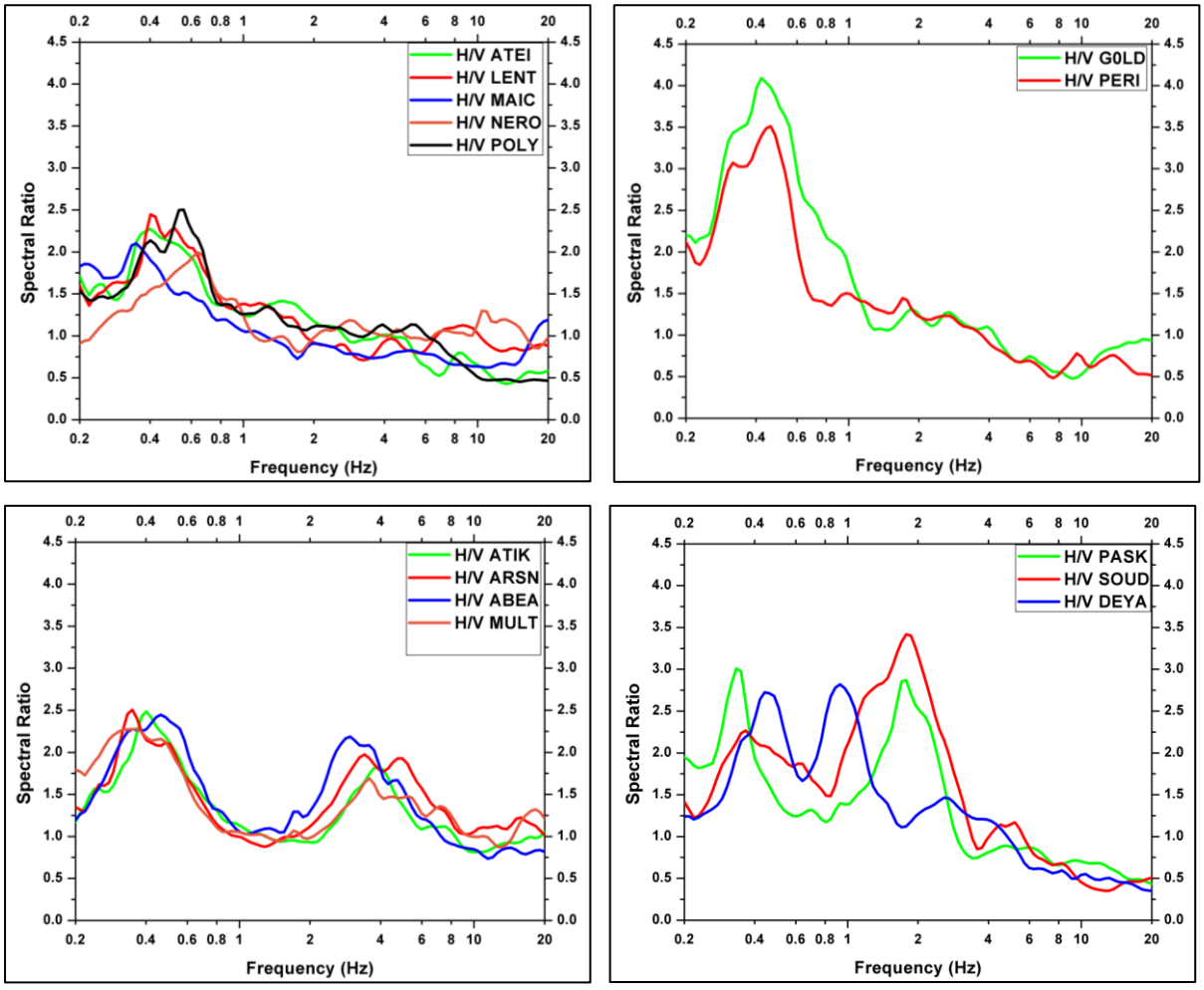

Figure 5.1 The four groups based on the geology and the similarity of the HVSR results

The events collected from the first two years of SGM stations operation brought about a decent number of recordings to apply spectral ratio techniques in seismic events in station locations. The RF spectral ratio techniques have been applied only for station that are equipped with 24bit SGM sensors. Although the research area presents predominant amplitude peaks in low frequencies (<1 Hz) and the installed instruments are designed to provide reliable data for higher frequencies (>1 Hz), an effort to examine the frequency band (0.9 – 20Hz) has been made, aiming to identify the possible changes in the spectral ratio curves, especially in the areas that present a second peak (f_1, A_1). During an earthquake, the structure stability is controlled by the intensity of ground shaking and the quality of the building, the relationship between them is provided by The International Building Code (2012): natural period $T = CH^x$ where C and x are related with the building's materials and H with the structure height (in meters). The under-investigation area, the Chania city and its southern basin has mostly low height structures (less than 20 meters according to building regulations) with concrete materials ($C \approx 0.05, x = 0.9$). Most of the buildings in research area have typically have natural periods much less than 1. The secondary peaks (f_1, A_1) in the examining area are more likely to cause damage to the building since they are closer to the building's oscillation frequency. Comparing the earthquake data recorded on ATEI accelerometer with the closest seismometer CHAN, led to the conclusion that RF curves with good SNR from the earthquakes recorded from 24bit accelerometers can be valid for frequencies down to 0.9Hz. We proceed to make a comparison of the RF and HVSR results. For most cases the amplitudes from seismic signal has higher values than the ones obtained by the microtremor method and these results can be split in two groups based on the similarity of the curves. The first set has stations who have comparably spectral ratio values and peaks while the other group has much larger RF amplitudes and in some cases different peaks appears. It seems that for Neogene sediments, the RF values are slightly increased for most of the examined frequency band, also with very good shape similarities. On the contrary, the thick Quaternary deposits present much higher amplification values especial for stations G0LD and PERI but without having a clear peak (figure 5.2). The same time the stations DEYA and PASK presents a distinctive secondary peak in the frequencies 3.6 and 4.6 respectively that is not present on microtremors results (figure 5.2).

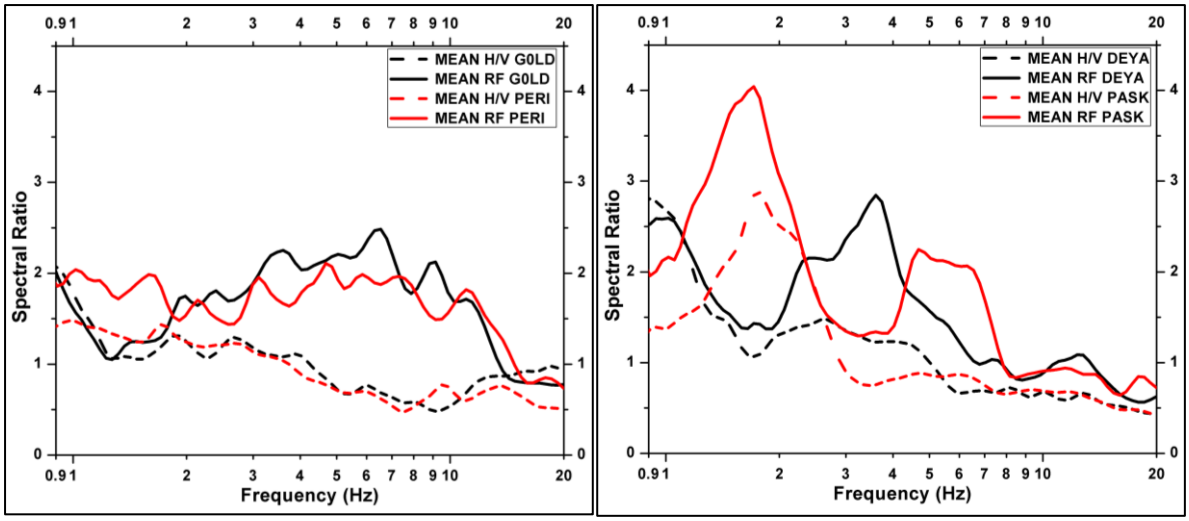

Figure 5.2 The H/V - RF method results on the Quaternary deposits. All stations have larger amplitudes with RF technique. On left diagram are the stations that don't present a clear peak with RF method while on the right diagram there are some peaks that are not noticeable with H/V method.

The first approach was to assume that the additional peaks noticed in the RF ratio method, was a product from the building harmonics. Additional measurement with the City Shark II have been carried out in the interior of the buildings next to accelerometer proving that there are no possible harmonic frequencies explaining the RF results. An alternative approach was to assume that the spectral ratio curve was amplified by dominant surface waves from short distance events but the secondary peaks remained even after removing the closest events. It seems that there are two different types of local site condition on the quaternary basin, on the stations G0LD and PERI there is an increase in amplitudes in the whole frequency range from 2 to 14Hz, which is caused by continues lateral refractions and reflections of trapped waves inside the quaternary basin. The clear peak presented in frequency 4Hz in stations DEYA and PASK can be attributed to seismic wave reflections on a vertical surface which is considered that is the Therissos fault, which is assumed to continue under the Chania sedimentary basin (Papadopoulos et al. 2017).

There are various interpolation methods with different theoretical approach, the choice of the most suitable one has been made after several tests and literature checking of previous researches. In the first phase with a few stations of the HSNC SGM network, the Ordinary Kriging presented satisfactory results but after installing more SGM stations, a more sophisticated technique was needed to provide PGA maps with increased spatial resolution. The use of ground parameters related with the geology and local site effects can improve the interpolation results. The peak values from predominant frequency and amplitude (f_0, A_0)

obtained by H/V analysis have been used as variables to give a trend to the Ordinary Cokriging method. The Ordinary Kriging and Ordinary Cokriging interpolation techniques results have been tested with the cross-validation analysis. During the cross-validation analysis, consecutively a measurement at one location is removed and a prediction is carried out with the rest of the n samples. The same occurs for the next point until all points have been checked. The prediction error (x) for every point i, is calculated by subtracting the predicted from the measured values. If the prediction errors are unbiased, the mean prediction error ($\hat{x}$) which is the mean value of the prediction errors should be near zero. The average standard error ($\widehat{SE} = \frac{1}{n}\sum_{\mathrm{i}}^{\mathrm{n}} \frac{\mathrm{x}-\hat{\mathrm{x}}}{\mathrm{sd}}$ where sd is the standard deviation) and the root mean square errors ($RMS = \sqrt{\frac{1}{n}\sum_{i}^{n}(x-\hat{x})^2}$) should have the smallest possible values. However, these values depend on the scale of the data, to ensure the error values are independent from the sample, there is the mean standardized prediction error (should also be near zero) which is a product of the prediction errors divided by their prediction standard errors. Additionally, the average standard error should be similar to the root mean square error, so by dividing them the root mean squared standardized error should be close to 1. If the root mean squared standardized errors are greater than 1, the predictions are underestimated and vice versa. The conclusion after examining numerical results of the available data, is that the Ordinary Cokriging method improves the interpolation results. The slope of the regression function between predicted and measured data has higher values for the Ordinary Cokriging cases rather than Ordinary Kriging, which means that the additional variables in model explain better the acceleration distribution. At the same time all or most of the prediction errors such as the RMS, mean standardized and average standard error are presenting a noticeable decrease in values with the Ordinary Cokriging method, while the root mean square standardized is closer to 1. The main disadvantage of the Ordinary Cokriging, is that it needs an amount of time to find the optimum semivariogram fitting. Sometimes the comparison between different models' present prediction errors with very small changes and the output map haven't got enormous differences, a fact which makes the decision process difficult. Despite the few negatives, the result maps are easily obtained by a standard procedure. In addition, the illustrated data have increased spatial resolution since the interpolation method is taking the local geology into account.

6 Concluding remarks - Future work

A dense SGM network with 14 stations has been installed in the Chania city and its southern basin. The under-investigation area is covered with medium and weak in term of stiffness materials. Aiming to perform a detailed monitoring of the ground shacking, the SGM sensors have been installed in different geological formation. The estimation of the PGA values in location without sensor has been achieved with the use of interpolation techniques. The ground related parameters f_0 and A_0 obtain from spectral ratio HVSR have been used to improve the interpolation method. New microtremors measurements in the locations of the SGM stations have been carried out to provide the H/V parameters and investigate the local site effects. In two years of the SGM network operations, a considerable number of event have been recorded. The recordings have been used to the RF method to examine local site effects with a different method.

The various recordings obtained from SGM network allowed to perform an investigation with the RF technique. It will be very interesting to apply the classical spectral ratio method (SSR) but that involves having a sensor on the bedrock formation. Unfortunately, a solid rock site with no amplification has not been found yet even through several different possible locations have been tested (Pazinos, Sternes, Malaxa, Kampani and Platani area). The only possible suitable area with bedrock formation is more than 7km away (Agia Triada Monastery) from the nearest network stations and installing a sensor at this place is considered as the last option. The investigation for a suitable and close to SGM network reference station will continue in the near future.

Another aspect that needs to be done is the automation of the interpolation procedure. So far, the seismic data and the strong motion parameters can be obtained almost in real time after a seismic event with few simple Linux scripts. The PGA interpolation method is not yet an automatic process, it should be soon so the shakemaps will produced faster.

An attempt to fit the PGA value of each station, as the criterion variable, against the corresponding A_0 value, as the predictor variable, in a least squares regression sense, for 80 different case studies lead to the following results: In some cases, the PGA vs A_0 values fits in a linear regression with very good results, while in other examples the regression analysis shows that the data are scattered. There are cases where some distant earthquakes present a nice fitting (figures 6.1 and 6.5) while in other examples are not (figures 6.2 and 6.4b). At the same time, there are close distance events with good linear regression (figures 6.3 and 6.7) and

again there are events with very poor (figures 6.4a, 6.6) or not so good fitting (figure 6.8). These results don't lead to a robust conclusion. One important observation is that all the cases with good PGA vs A_0 fitting had low PGA values in all SGM stations approximately less the 2 mm/sec^2, a further study with events that are capable for higher PGA recordings is needed. Another aspect to examine is the slope of the regression line value which varies between 0 and 1 for most cases, while in few events it is slightly above 1 and the most important is that there are two cases where it took much higher values like 3 and 7. The epicenters of these two events were very close to the SGM network, the one 19 km away with local magnitude 3.3 and the other 45km away with local magnitude 4.9. The recorded PGA values were considered higher than the most of previous reports but there are also other cases with similarly high PGA values and the regression slope is again between values 0 and 1. After these notes and considerations, two new questions come up:

- Were the results of these two earthquakes a product of high directivity? or
- Is the slope and the fitting of the regression line an indicator between linear and nonlinear site effects?

A future analysis which will include more events with higher magnitudes values at short distances will probably answer all these questions and produce some interesting results.

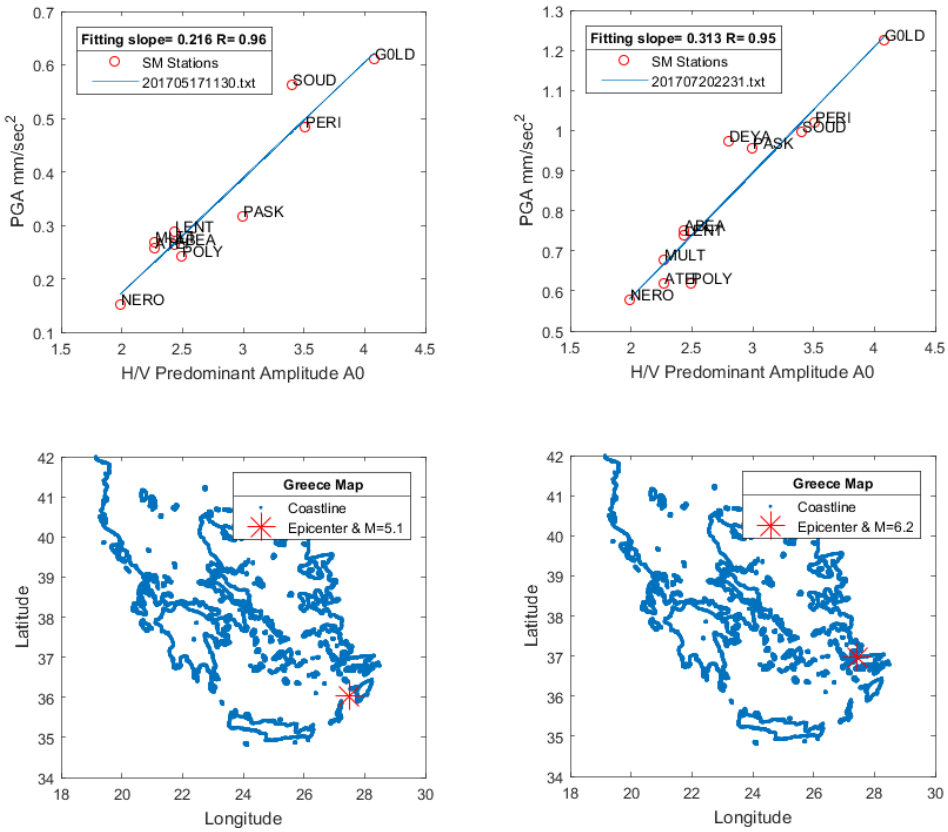

Figure 6.1 Two distant events northeast of Chania that the PGA vs A0 have a good fit (up), on the coastline image (down) with red star is denoted the epicenter of the event

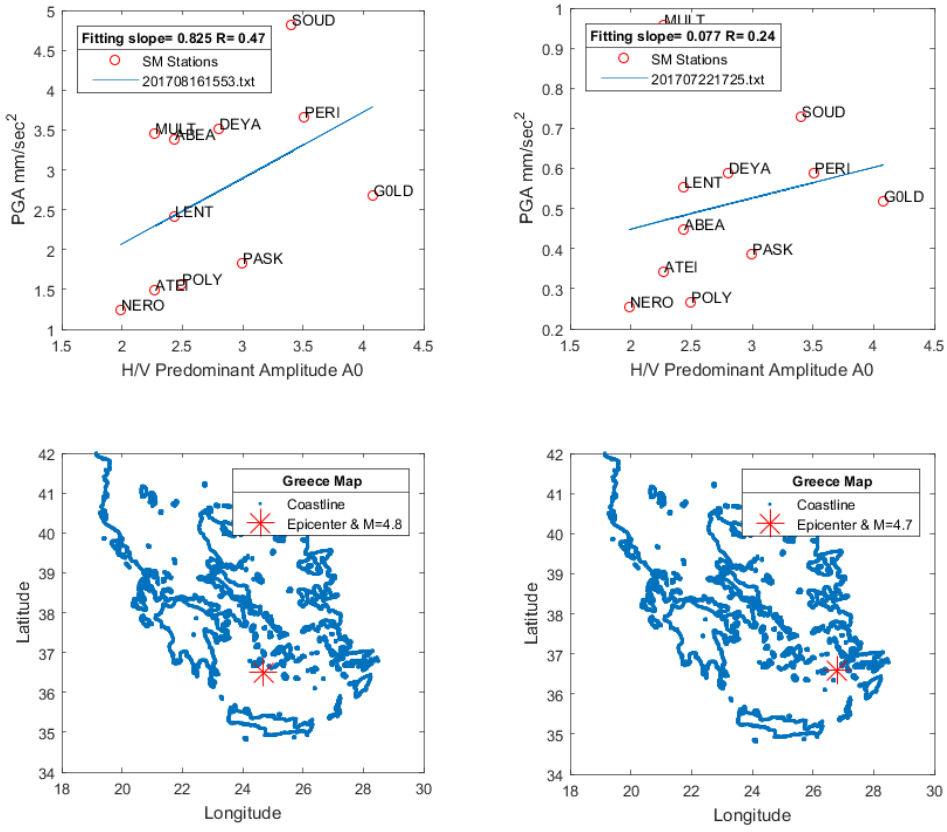

Figure 6.2 Two distant events northeast of Chania that the PGA vs A0 do not have a good fit (up), on the coastline image (down) with red star is denoted the epicenter of the event

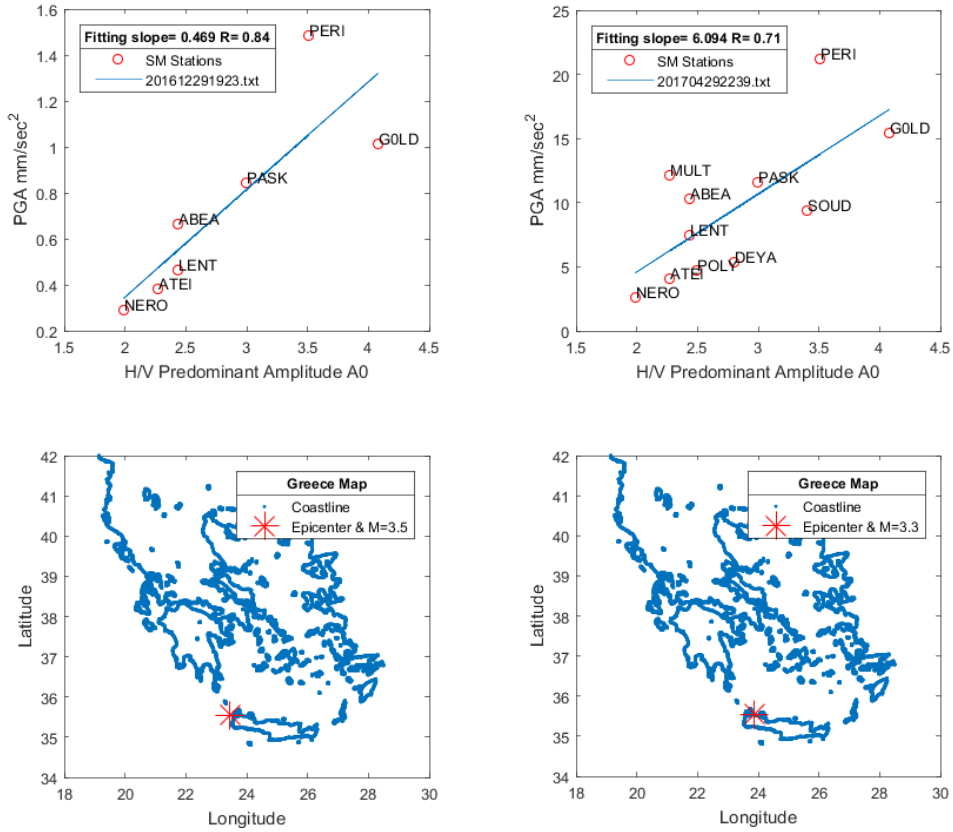

Figure 6.3 Two close distance events northwest of Chania that the PGA vs A0 have a good fit (up), on the coastline image (down) with red star is denoted the epicenter of the event

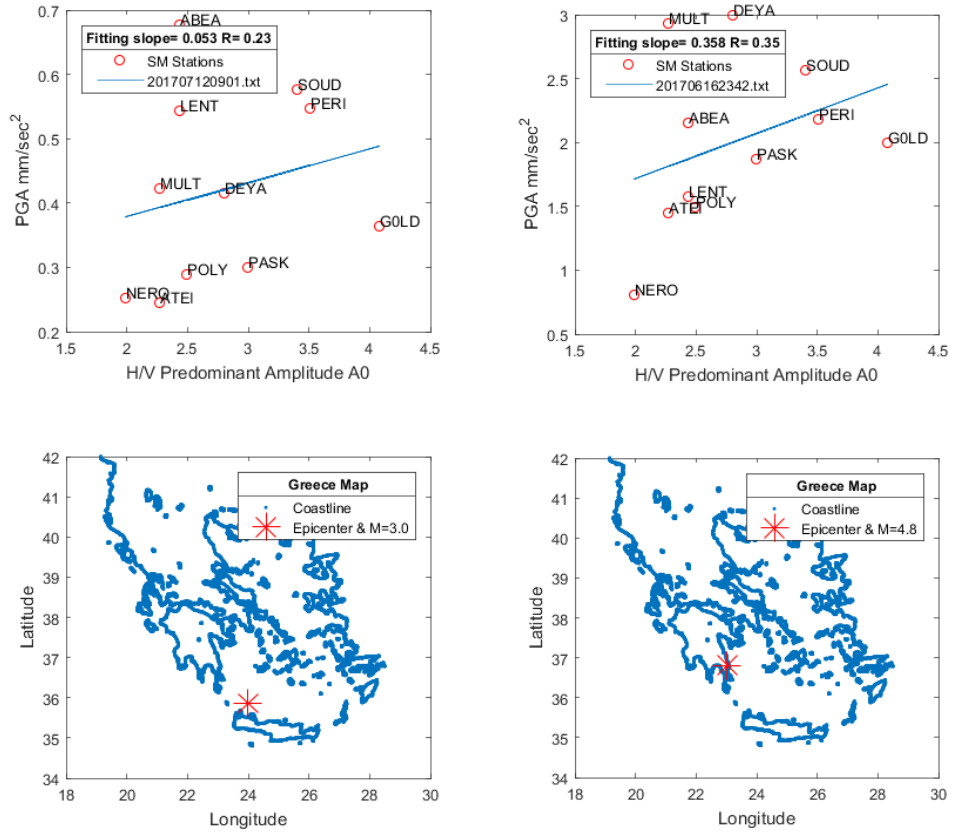

Figure 6.4 One close distance and another far away event northeast of Chania that the PGA vs A0 do not have a good fit (up), on the coastline image (down) with red star is denoted the epicenter.

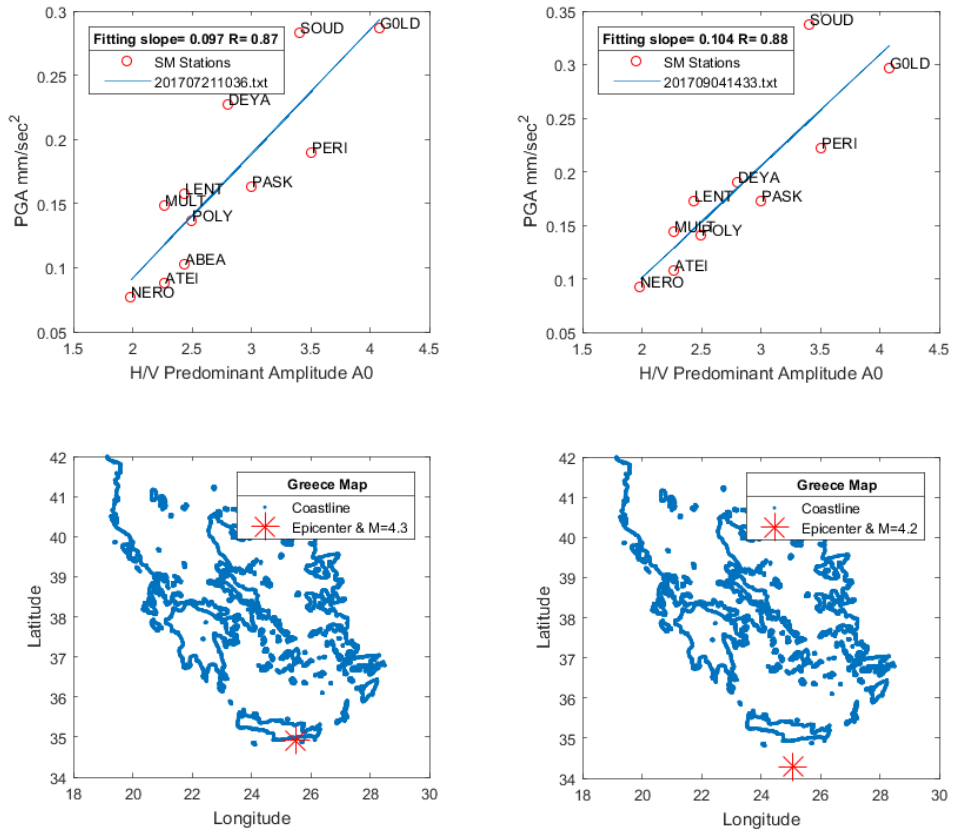

Figure 6.5 Two distant events southeast of Chania that the PGA vs A0 have a good fit (up), on the coastline image (down) with red star is denoted the epicenter of the event

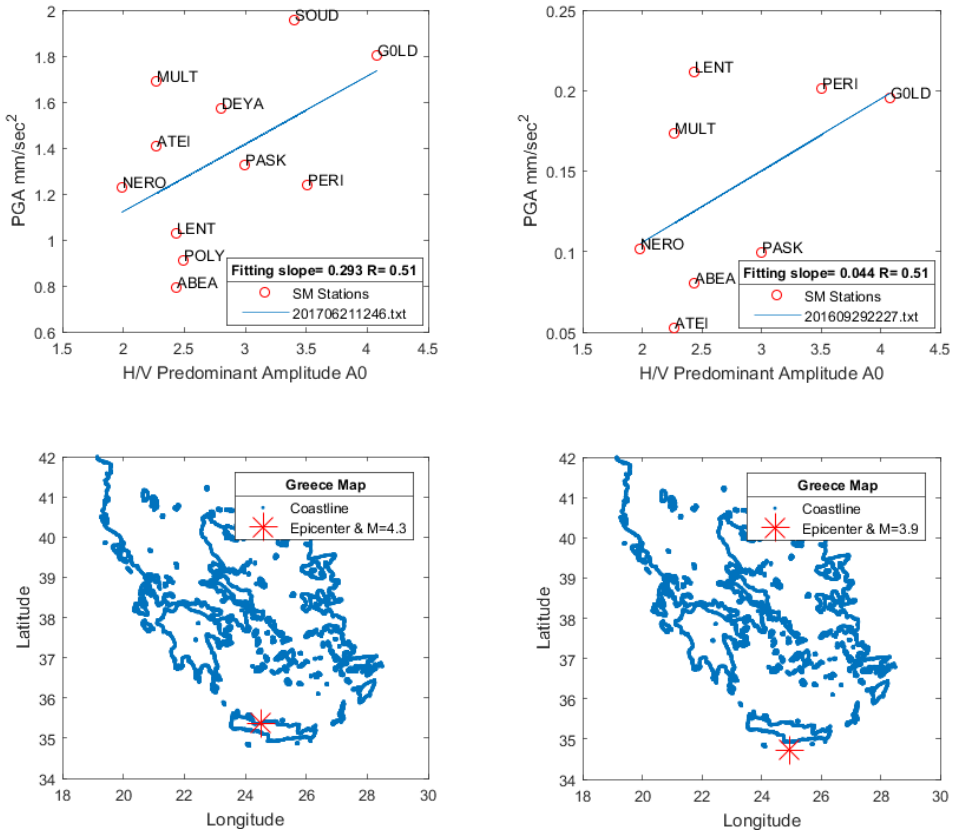

Figure 6.6 Two close distance events northeast of Chania that the PGA vs A0 do not have a good fit (up), on the coastline image (down) with red star is denoted the epicenter of the event

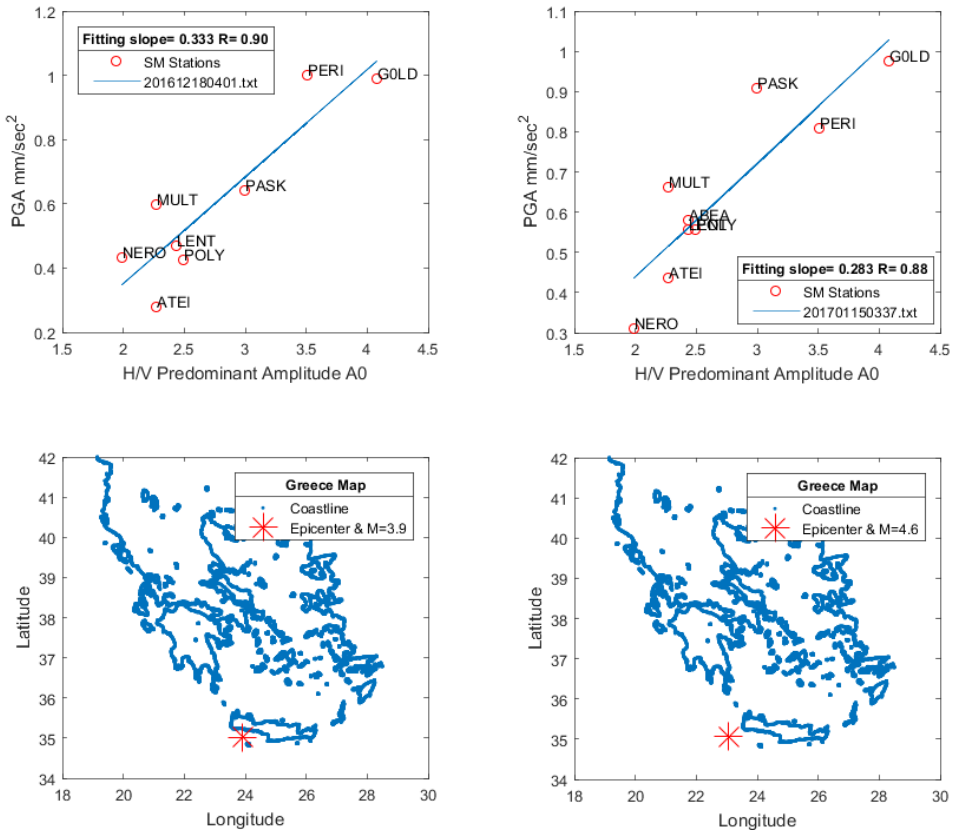

Figure 6.7 Two close distance events southwest of Chania that the PGA vs A0 have a good fit (up), on the coastline image (down) with red star is denoted the epicenter of the event

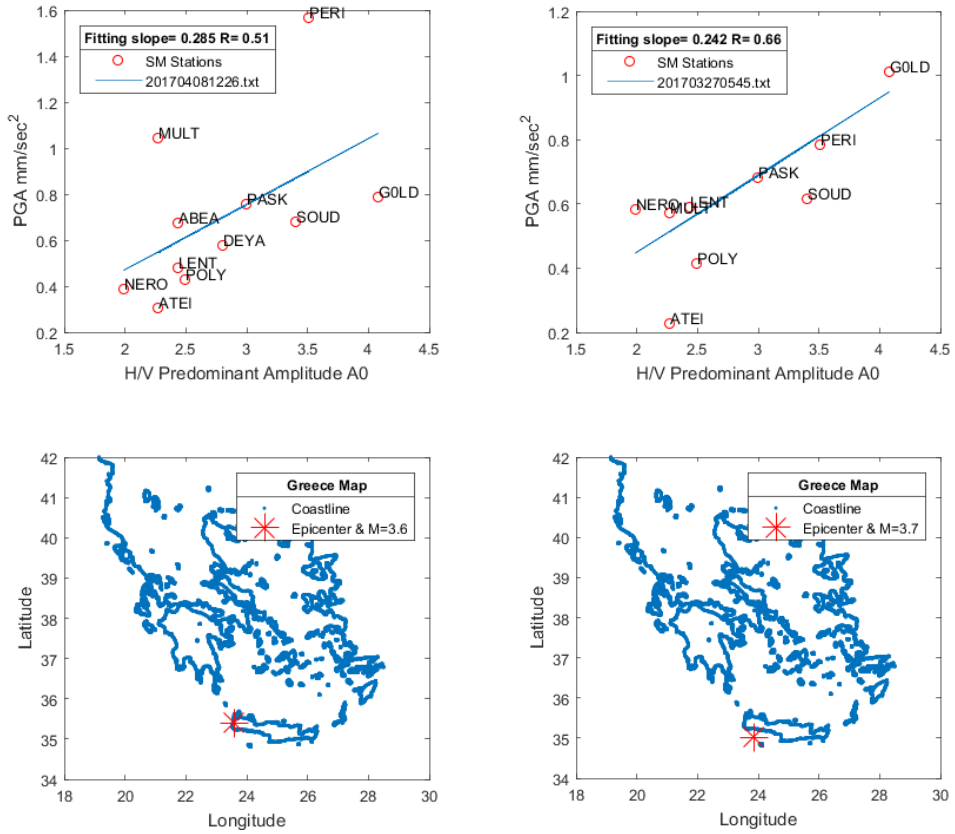

Figure 6.8 Two close distance events southwest of Chania that the PGA vs A0 do not have a good fit (up), on the coastline image (down) with red star is denoted the epicenter of the event

References

Akamatsu K, 1961. On microseisms in frequency range from 1 c/s to 200 c/s, Bull. Earthq. Res. Inst., Tokyo University, Vol.39, pp. 23-75.

Aki K, 1957. Space and time spectra of stationary stochastic waves, with special reference to microtremors, Bull. Earthquake. Res. Inst. Tokyo, 35, 415-457.

Athanasopoulos G A and Pelekis P C, 2000. Site Effects on the Seismic Ground Response of the City of CHANIA, GREECE, Report prepared for the E.C. project SEISMOCARE (Computer Aided Reduction of Seismic Risk with Application in Existing Cities, Town Planning and Construction).

Arias A, 1970. A measure of earthquake intensity. – In: R.J. HANSEN (Ed.): Seismic Design for Nuclear Power Plants, The M.I.T. Press, 438–483.

Aristotle University of Thessaloniki Seismological Network, International Federation of Digital Seismograph Networks (HT), https://doi.org/10.7914/SN/HT.

Bard P Y, Duval A M, Lebrun B, Lachet C, Riepl J, Hatzfeld D, 1997. Reliability of the H/V technique for site effects measurement: an experimental assessment. Instabul, Proc. 8th Int. Conf. Soil Dyn. Earthq. Engrg.

Bastelli G, 2002. Microzonazione di Chania (Creta). Tesi di laurea. Universita degli Studi della Basilicata (in Italian)

Bonneau M and Fleury J J,1971 Preisions sur la serie d'Ethia (Crete,Grece): Existence d'un premier flysch mesocretace CR Acad Sci Paris 272: 1840-1842

Bonneau M and Lys M, 1978 sur la presence de Permien fossilifere dans l'unite de Vatos (Crete): sa nature interne et 1' ampleur des charriages dans l'arc egeen. CR Acad Sci Paris 287:423--426

Bonneau M, Beauvais L and Middlemiss F A, 1974 L'unit6 de Miamou (Crete, Greece) et sa macrofaune d'age Jurassique superieur (Brachiopods, Madreporaires). Ann Soc Grol Nord 94:71-85

Bonilla L F, Steidl J H, Lindley G T, Tumarkin A G, and Archuleta R J, 1997. Site amplification in the San Fernando Valley, California: variability of site-effect estimation using the S-wave, coda,and H/V methods,Bull. Seism. Soc. Am .87, 710–730

Borcherdt R D and Glassmoyer G, 1992. On the characteristics of local geology and their influence on ground motions generated by the Loma Prieta earthquake in the San Francisco Bay region, California. Bull Seismol Soc Am 82(2): 603–641

Chávez-García F J, Sanchez L R and Hatzfeld D, 1996. Topographic site effects and HNSR. A comparison between observations and theory, Bull. Seism. Soc. Am., 86, 1559-1573.

Childs C,2004. Interpolation surfaces in ArcGIS spatial analyst. ESRI education services, 1-4.

Creutzburg N and Seidel E. 1975. Zum Stand der Geologie des praeneogens auf Kreta, N. Jahrb. Geol. Palaeont. Abh., 149, 363-383.

Douglas J, 2003. Earthquake ground motion estimation using strong-motion records: a review of equations for the estimation of peak ground acceleration and response spectral ordinates. Earth-Science Reviews. 61 (1–2): 43–104. doi:10.1016/S0012-8252(02)00112-5.

Epting M, Kudrass H, Schaffer A (1972) Stratigraphie et positiondes series metamorphiques aux Talea Ori. Z Dtsch Geol Ges 123:365- 370

Field E & Jacob K, 1993. The theoretical response of sedimentary layers to ambient seismic noise. Geophys. Res. Lett. 20–24, p. 2925–2928.

Fytrolakis N, 1980. The geological structure of Krete. Probleme, observations and conclusions. Habil. Thesis, Nat. Tech. Univ. Athens, 1-147 (in Greek).

Gandin, L S, 1963. Objective analysis of meteorological fields: Gidrometeorologicheskoe Izdatel'stvo (GIMIZ), Leningrad (translated by Israel Program for Scientific Translations, Jerusalem, 1965, 238 pp.)

Haghshenas E, Bard P Y, Theodulidis N, 2008. Empirical evaluation of microtremor H/V spectral ratio, Bulletin of Earthquake Engineering, 6(1): 75-108.

Hengl T, 2007. A Practical Guide to Geostatistical Mapping of Environmental Variables, European Commission, Joint Research Centre, Institute for Environment and Sustainability

Hong H P and Liu T J, 2015. Geographically Varying Ground-Motion Prediction Using Records from Historical Events, Seismological Research Letters Volume 86, Number 3: 948-967

Johnston K, Ver Hoef J, Krivioruchko K, Lucas N, 2003. ArcGIS 9, Using ArcGIS Geostatistical Analyst, Redlands California: Environmental Systems Research Institute

Irikura K and Kawanaka T, 1980. Characteristics of microtremors on ground with discontinuous underground structure. Bulletin of the Disaster Prevention Research Institute, 30(3), 81-96.

Isaaks E H, Srivastava R M, 1989. Applied Geostatistics. Oxford University Press, New York, p.542.

Ishihara K, 1996. Soil Behaviour in Earthquake Geotechnics, Oxford Engineering Science Series 46, Oxford Science Publications, 120-123.

Kamura K, 1997. On microtremors observed in Tokyo Bay area, Japanese document. In Japanese with English abstract (pp. 47-53).

Kilias A, Falalakis G and Mountrakis D, 1999. Cretaceous-Tertiary structures and kinematics of the Serbomacedonian metamorphic rocks and their relation to the exhumation of the Hellenic Hinterland (Macedonia, Greece). Intern. J. of Earth Scien., 88, pp. 513-531.

Krahl J, Kaufmann G, Kozur H, Richter D, Forster O, Heinritzi F, 1983. Neue Daten zur Biostratigraphie und zur tektonischen Lagerung der Phyllit-Gruppe und der Trypali-Gruppe auf der Insel Kreta (Griechenland). Geol Rundsch 72: 1147-1166

Konno K and Ohmachi T, 1998. Ground-motion characteristics estimated from spectral ratio between horizontal and vertical components of microtremors. Bull. Seismol. Soc. Am. 88, p. 228–241.

Kopp K. and Ott E, 1977. Spezialkartierungen in Umkreis neuer Fossilfunde im Tripali- und Tripolitsa-kalken West Kretas. N. Jahrb. Geol. Palaeontol. Mh., 1977, 217-238.

Lachet C and Bard P Y, 1994. Numerical and Theoretical Investigations on the Possibilities and Limitations of Nakamura's Technique, J. Phys. Earth., 42, 377–397.

Lachet C, Hatzfeld D, Bard P Y, Theodoulidis N, Papaioannou C, Savvaidis A, 1996. Site effects and microzonation in the City of Thessaloniki (Greece) comparison of different approaches. Bulletin of the Seismological Society of America. 86. 1692-1703

Le Pichon X and Angelier J, 1979. The Hellenic Are and Trench System: a key to the neotectonic evolution of the eastern Mediterranean area, Tectonophysics, 60, 1–42, 1979.

Lermo J and Chavez-Garcia F, 1993. Site effect evaluation on using spectral ratios with only one station, Bulletin of the Seismological Society of America, Vol 83, No. 5: 1574-1594.

Matheron, G, 1962. Traité de geostatisque appliquée, vol. I: Memoires du Bureau de Recherches Géologiques et Miniéres, no. 14, Editions Technip, Paris, 333 pp.

Marcotte D, 1991. Cokriging with Matlab. Computers & Geosciences Vol. 17, No. 9: 1265-1280

Mastrolorentzo G, 2004. Profili Di Velocita' Vs Nell'abitato Di Chania'(Creta), Msc Thesis, Universita degli Studi della Basilicata

McKenzie D, 1972: Active Tectonics of the Mediterranean Region, The Geophysical Journal of the Royal Astronomical Society, 30,109–185, 1972.

Mountrakis D, 1986. The Pelagonian zone in Greece: A polyphase deformed fragment of the Cimmerian continent and its role in the geotectonic evolution of the Eastern Mediterranean. Journal of Geology, 94, pp. 335 - 347.

Mountrakis D, Killias A, Pavlaki A, Fassoulas C, Thomaidou E, Papazachos C, Papaioannou C, Roumeliozi Z, Benetatos C, Vamvakaris D, 2012. Neotectonic study of Western Crete and implications for seismic hazard assessment, J Virtual Explor 42:19–20

Mucciarelli M, 1998. Reliability and Applicability of Nakamura's technique using Microtremors: An experimental approach, J. Earthq. Eng., 2: 625-638.

Nakamura Y, 1989. A method for dynamic characteristics estimation of subsurface using ambient noise on the ground surface, QR Railway Tech Res. Inst. 30:25–33

National Observatory of Athens Seismic Network, International Federation of Digital Seismograph Networks(HL). https://doi.org/10.7914/SN/HL.

Nogoshi M and Igarashi T, 1970. On the propagation characteristics of microtremors. J. Seism. Soc. Japan, 23, 264-280.

Nogoshi M and Igarashi T, 1971. On the Amplitude Characteristics of Microtremor (Part 2), J. Seismol. Soc. Japan, 24, 26-40.

Papadopoulos I, Papazachos C, Savvaidis A, Theodoulidis N, Vallianatos F, 2017. Seismic microzonation of the broader Chania basin area (Southern Greece) from the joint evaluation of ambient noise and earthquake recordings. Bull Earthquake Eng 15: 861–888.

Papazachos B C, 1990. Seismicity of the Aegean and surrounding area, Tectonophysics, 178, 287–308.

Papazachos C B and Nolet G P, 1997. P and S deep velocity structure of the Hellenic area obtained by robust nonlinear inversion of travel times, J. Geophys. Res., 102, 8349–8367.

Riepl J, Bard P Y, Hatzfeld D, Papaioannou Ch, and Nechtschein S, 1998. Detailed evaluation of site-response estimation methods across and along the sedimentary valley of Volvi (EURO-SEISTEST), Bull. Seism. Soc. Am., 88, 488–502.

Sarris A, Loupasakis, C, Soupios P, Trigkas V, and Vallianatos F, 2010. Earthquake vulnerability and seismic risk assessment of urban areas in high seismic regions: application to Chania City, Crete Island, Greece. Natural hazards, 54(2), 395-412.

Seidel E, 1971. Die Pindos Serie in West Kreta auf der Insel Gavdos und im Kedros Gebiet (Mittelkreta). N. Jahrb. Geol. Palaeontol. Abh., 137, 443-460.

Seidel E, 1978 Zur Petrologie der Phyllit-Quarzit-Serie Kretas. Habil Schr Tech Univ Braunschweig: 145 S

Seidel E, Schliestedt M, Kreuzer H, Harre W, 1977 Metamorphic rocks of Late Jurassic age as components of the ophiolitic mélange on Gavdos and Crete (Greece). Geol Jb B28:3-21

Seidel E, Kreuzer H and Harre W, 1981. A Late Oligocene/Early Miocene high pressure belt in the external Hellenides. Geol. Jahrb., E 23, 165-206.

Setianto A and Triandini T, 2013. Comparison of kriging and inverse distance weighted (idw) interpolation methods in lineament extraction and analysis, J. SE Asian Appl. Geol., Jan–Jun 2013, Vol. 5(1), pp. 21–29.

Seo, K. et al. 1996. Study of site effects in Kobe area using microtremors, Proc.11th World Conf.on Earthq.Eng.,Paper No.1656

Seo K, 1997. Comparison of measured microtremors with damage distribution. In JICA, Research and Development Project on Earthquake Disaster Prevention.

Seo, K, 1998. Application of microtremors as a substitute of seismic motion--reviewing the recent microtremors joint research in different sites (Special Issue: Workshop on Seismic Microzonation in Earthquake Vulnerable Countries Reports from Metro Manila, Granada, Caracas and Kobe)., 49-58.

SESAME European research project (2004). Guidelines for the implementation of the H/V spectral ratio technique on ambient vibrations, s.l.: European Commission – Research General Directorate Project No. EVG1-CT-2000-00026 SESAME.

Seismological Network of Crete (HC). International Federation of Digital Seismograph Networks, https://doi.org/10.7914/SN/HC.

Sibson R, 1981. A brief description of natural neighbor interpolation (Chapter 2). In V. Barnett. Interpreting Multivariate Data. Chichester: John Wiley. pp. 21–36.

Tiedemann H, 1992. Earthquakes and Volcanic Eruptions. A Handbook on Risk Assessment. Zurich: Swiss Reinsurance Company.

Tukey J W,1958. Bias and confidence in not quite large samples (abstract). The Annals of Mathematical Statistics. 29 (2): 614. doi:10.1214/aoms/1177706647.

Wood H O and Neumann Frank, 1931. Modified Mercalli Intensity Scale of 1931: Seismological Society of America Bulletin, v. 21, no. 4, p. 277-283.

Voronoi G, 1908. Recherches sur les paralléloèdres Primitives. J. reine angew. Math. 134, 198-287.

Richter C F, 1935. An instrumental earthquake magnitude scale. Bulletin of the Seismological Society of America, pp. 1 - 32.

Quenouille, Maurice H, 1949. Problems in Plane Sampling. The Annals of Mathematical Statistics. 20 (3): 355–375. doi:10.1214/aoms/1177729989. JSTOR 2236533.

Udwadia F and Trifunac M, 1973. Comparison of earthquake and microtremor ground motions in El Centro, California, Bull. Seismol. Soc. Am., 63, 1227-1253.

Yamazaki F and Ansary M A, 1997. Horizontal-to-vertical spectrum ratio of earthquake ground motion for site characterization. Earthquake engineering & structural dynamics, 26(7), 671-689.

Zager D (1972) Sedimentologie der Tripolitsakarbonate im nordlichen Mittelkreta. Dissertation, Univ Freiburg: 1-165

Zare M, Bard P Y and Ghafory-Ashtiany M, 1999. Site characterizations for the Iranian strong motion network, Soil Dyn. Earthquake Eng 18, 101-123